

Detection of partial discharges in stator windings of turbine generators

Citation for published version (APA):

Pemen, A. J. M. (2000). *Detection of partial discharges in stator windings of turbine generators*. [Phd Thesis 1 (Research TU/e / Graduation TU/e), Electrical Engineering]. Technische Universiteit Eindhoven.
<https://doi.org/10.6100/IR530786>

DOI:

[10.6100/IR530786](https://doi.org/10.6100/IR530786)

Document status and date:

Published: 01/01/2000

Document Version:

Publisher's PDF, also known as Version of Record (includes final page, issue and volume numbers)

Please check the document version of this publication:

- A submitted manuscript is the version of the article upon submission and before peer-review. There can be important differences between the submitted version and the official published version of record. People interested in the research are advised to contact the author for the final version of the publication, or visit the DOI to the publisher's website.
- The final author version and the galley proof are versions of the publication after peer review.
- The final published version features the final layout of the paper including the volume, issue and page numbers.

[Link to publication](#)

General rights

Copyright and moral rights for the publications made accessible in the public portal are retained by the authors and/or other copyright owners and it is a condition of accessing publications that users recognise and abide by the legal requirements associated with these rights.

- Users may download and print one copy of any publication from the public portal for the purpose of private study or research.
- You may not further distribute the material or use it for any profit-making activity or commercial gain
- You may freely distribute the URL identifying the publication in the public portal.

If the publication is distributed under the terms of Article 25fa of the Dutch Copyright Act, indicated by the "Taverne" license above, please follow below link for the End User Agreement:

www.tue.nl/taverne

Take down policy

If you believe that this document breaches copyright please contact us at:

openaccess@tue.nl

providing details and we will investigate your claim.

DETECTION OF PARTIAL DISCHARGES IN STATOR WINDINGS OF TURBINE GENERATORS

PROEFSCHRIFT

ter verkrijging van de graad van doctor aan de
Technische Universiteit Eindhoven, op gezag van de
Rector Magnificus, prof.dr. M. Rem, voor een
commissie aangewezen door het College voor
Promoties in het openbaar te verdedigen
op woensdag 23 februari 2000 om 16.00 uur

door

August Johannes Marie Pemen

geboren te Breda

Dit proefschrift is goedgekeurd door de promotoren:

prof.dr.ir. P.C.T. van der Laan

en

prof.dr.ir. A.J.A. Vandenput

These investigations have been supported by
KEMA, Arnhem, The Netherlands
and
the Dutch power utilities EPON, EPZ, EZH and UNA.

Printed by Universiteitsdrukkerij Technische Universiteit Eindhoven.

CIP-DATA LIBRARY TECHNISCHE UNIVERSITEIT EINDHOVEN

Pemen, August J.M.

Detection of partial discharges in stator windings of turbine generators /
by August J.M. Pemen. - Eindhoven : Technische Universiteit Eindhoven,
2000.

Proefschrift. - ISBN 90-386-1720-8

NUGI 832

Trefw.: hoogspanningsmeettechniek / elektrische ontladingen /
elektrische machines ; wikkelingen / synchrone generatoren /
hoogspanningsisolatie.

Subject headings: high-voltage techniques / partial discharges /
turbogenerators / insulation testing / machine insulation.

Contents

Summary	5
Samenvatting	7
1 Introduction	9
1.1 Turbine generators, our modern workhorses	9
1.2 Insulation systems for stator windings	10
1.3 Insulation quality and partial discharges	11
1.4 Overview of techniques for PD monitoring	14
1.5 PD monitoring in this thesis	16
2 Propagation of partial discharge signals in a stator winding	23
2.1 From abc-model to complex windings	23
2.2 Experimental setup	24
2.3 Experimental results	27
2.3.1 Analysis of the 'fast mode' and the 'slow mode'	27
2.3.2 The "calibration problem"	32
2.3.3 Cross-talk between the phases	34
2.4 Discussion	37
2.5 Summary and concluding remarks	41
3 Sensors for partial discharge monitoring	45
3.1 Introduction	45
3.2 Capacitive sensors	46
3.2.1 Principle	46
3.2.2 EMC-properties of capacitive sensors	47
3.2.3 Bus-support-capacitors	48
3.2.4 Ring-capacitors	49
3.2.5 Overvoltage capacitors	50
3.3 Toroidal single-turn inductive current sensor	51
3.3.1 Introduction	51
3.3.2 Single-turn loops	52
3.3.3 The toroidal single-turn current sensor	54
3.4 Pick-up loops	63

4	Measuring techniques and signal handling	65
4.1	Introduction	65
4.2	Time domain measurements	66
4.2.1	Measuring system and procedure	66
4.2.2	Measurements on generator Hemweg-6	68
4.2.3	Procedure for the signal processing	70
4.3	A tunable narrow-bandwidth detector	73
4.3.1	General	73
4.3.2	Measurements on generator Hemweg-8	73
4.4	Concluding remarks	77
5	Measurements on turbine generator Hemweg-6	79
5.1	Introduction	79
5.2	External propagation of PD-signals	80
5.3	Comparison of inductive and capacitive sensors	84
5.4	Partial discharge patterns	84
5.5	Measurements with pick-up loops	87
5.6	Conclusions	89
6	Measurements on turbine generator Amer-9	91
6.1	Introduction	91
6.2	Time domain measurements	91
6.2.1	Measured waveshapes	91
6.2.2	Partial discharge patterns	96
6.3	Additional measurements	99
6.3.1	Simultaneous measurements at each of the four sensor terminals	99
6.3.2	Zero-span measurements with a spectrum analyzer	100
6.3.3	Measurements with pick-up loops	100
6.4	Conclusions	103
7	Measurements on turbine generator Hemweg-8	105
7.1	Introduction	105
7.2	Time domain measurements	105
7.2.1	Measured waveshapes	105
7.2.2	Partial discharge patterns	110
7.3	Measurements with the tunable narrow-bandwidth detector	112
7.4	Localization of two discharge sources	114

7.4.1 Sparking near the current sensor in phase U	114
7.4.2 Sparking inside the step-up transformer	116
7.5 Conclusions	119
8 Measurements on gasturbine generator Roca-3	121
8.1 Introduction	121
8.2 Time domain measurements	121
8.3 Measurements with the tunable narrow-bandwidth detector	128
8.4 Conclusions	130
9 Localization of discharges in the Maasvlakte power plant	131
9.1 Introduction	131
9.2 Localization of a PD source at generator Maasvlakte-1	131
9.3 Localization of a PD source at generator Maasvlakte-2	134
10 Conclusions	139
Bibliography	143
Appendix A Overview of generators used for the measurements in this thesis	155
Appendix B Construction of bus-support-capacitors	157
B.1 General	157
B.2 Specifications and commissioning testing	157
Appendix C The balun transformer	161
Appendix D Sheath currents in an isolated-phase-bus	165
D.1 General	165
D.2 Model to calculate sheath currents	166
D.3 Measurements at the IPB of the Hemweg-6 power plant	168
D.4 Calculations and discussion	170
Dankwoord	173
Curriculum vitae	175

Summary

Power utilities aim at the production of electrical energy at low cost and with a high availability. To achieve this for crucial components as turbine generators, two aspects are of major importance: (i) minimal costs for maintenance, and (ii) reduction of in-service failures. This can only be realized when effective tools are available to assess the condition of a generator. Partial discharge measurements on the quality of stator windings have been in use for already more than 35 years. In general, these partial discharge measurements are carried out on stand-still generators. However measurements should preferably be done on-line during regular operation.

This thesis describes methods to monitor partial discharges in stator windings during regular operation. Present methods may easily give false indications as a result of the high levels of interference in a power plant. Two new methods, both employing specially developed sensors, were evaluated under practical conditions in six power plants.

We have succeeded in obtaining interference-free partial discharge patterns. Interference is rejected to a large extent by applying consistent EMC-methods and by using measuring frequencies above 5 MHz. Remaining interference can be rejected by using an appropriate measuring technique. Two methods have been successfully evaluated: (i) time-domain measurements followed by signal-processing to discriminate between partial discharges and interference, and (ii) a tunable narrow-bandwidth filter which can be tuned to a frequency where partial discharges are strong and interference is weak. In addition, both techniques enable a good discrimination between partial discharges and signals caused by cross-talk. This cross-talk between the phases is caused by capacitive and inductive couplings between the stator windings.

Various sensors have been developed and permanently installed at several generators: (i) bus-support-capacitors (capacitor inside a support insulator of the isolated-phase-bus), (ii) ring capacitors inside the isolated-phase-bus, (iii) overvoltage capacitors of a generator circuit-breaker, (iv) a single-turn current sensor around the high-voltage terminals of the generator, and (v) a pick-up loop to locate a discharge source. A direct comparison of the sensors has been made at two generators. It was found that: (i) all sensor types give good and comparable results, (ii) the best sensitivity is obtained with bus-support capacitors.

For several generators, abnormal partial discharge activity was observed. In all cases, the source of these partial discharges could be located: (i) sparking inside a step-up transformer, (ii) an improperly installed bleeding-resistor in a generator circuit-

breaker, (iii) sparking near a current-sensor, and (iv) discharges in a slightly damaged bus-support-capacitor. The transit-time between various sensors and reflections of the discharge signal can be used to verify whether discharge activity takes place in the generator or for instance near the step-up transformer. Pick-up loops can be used as additional sensors to locate abnormal partial discharge activity.

By means of measurements on a dismantled 35 MW stator, we studied the propagation of partial discharge pulses in a stator winding and found that a stator winding acts as a transmission line. Therefore a partial discharge signal manifests itself at the generator terminals after a transit time that depends on the origin of the discharge. Due to capacitive and inductive couplings in the end-winding region, a second propagation mode is present for higher frequencies. This 'fast mode' manifests itself at the terminals without appreciable time delay. The capacitive and inductive couplings also cause cross-talk between the phases. As a consequence, a signal measured in one phase does not necessarily originate from a discharge in that phase. The amplitudes of the fast mode and, to a lesser extent, the slow mode (or transmission line mode) are heavily damped when the discharge occurs further away of the measuring terminal. The consequence is that only discharges close to the measuring terminal can be observed. In practice most partial discharges are expected close to measuring terminals. The total charge at the terminals is only weakly dependent on the origin of the discharge. The propagation of a partial discharge signal is not only influenced by the construction of the generator but also by its external connections.

In general, the tunable narrow-bandwidth detector is most suitable for continuous and periodic on-line measurements on a generator. In special cases, when abnormal partial discharge patterns are recorded, the time-domain measurements give more information. For practical partial discharge monitoring to assess the condition of generators, we suggest the following strategy:

- continuous monitoring of the partial discharge level by means of a tunable narrow-bandwidth detector, tuned to the 'best' tuning frequency
- recording at regular intervals of the partial discharge patterns by means of a tunable narrow-bandwidth detector and, to verify the choice of the best tuning frequency, at 30 different tuning frequencies
- in case of abnormal patterns, the results must be verified by means of time-domain measurements. These measurements require the presence of experienced personnel. Extra information about the discharge source can then be obtained by means of transit-time measurements between different sensors.

Samenvatting

Elektriciteitsbedrijven wekken hun elektrische energie op tegen zo laag mogelijke kosten en met hoge betrouwbaarheid. Voor de generatoren in elektriciteitscentrales betekent dit: (i) het laag houden van kosten voor onderhoud, en (ii) het beperken van storingen. Om dit te realiseren zijn technieken nodig waarmee de conditie van een generator kan worden bepaald. Al meer dan 35 jaar worden partiële ontladingsmetingen gebruikt om de kwaliteit van statorwikkelingen te meten. Tot op heden werden deze metingen tijdens stilstand uitgevoerd. Het verdient echter de voorkeur om deze metingen tijdens regulier bedrijf van de generator uit te voeren.

Dit proefschrift beschrijft methoden waarmee partiële ontladingsmetingen aan een generator tijdens normaal bedrijf zijn uitgevoerd. Als gevolg van het hoge niveau van allerhande stoorsignalen zijn bestaande methoden niet erg betrouwbaar. In dit proefschrift worden twee nieuwe methoden getest onder praktische omstandigheden in zes elektriciteitscentrales. Hierbij wordt gebruik gemaakt van speciaal ontwikkelde sensoren.

Het blijkt dat storingsvrije ontladingsmetingen goed mogelijk zijn. Door het toepassen van goede EMC-methoden en het kiezen van meetfrequenties boven 5 MHz wordt interferentie aanzienlijk onderdrukt. Resterende interferentie kan worden geëlimineerd met behulp van een geschikte meetmethode. Twee methoden zijn met succes toegepast: (i) metingen in het tijdsdomein gevolgd door signaal processing om ontladingen en stoorsignalen van elkaar te onderscheiden, en (ii) een afstembaar smalbandig filter wat wordt afgestemd op een frequentie waar signalen van partiële ontladingen veel sterker zijn dan stoorsignalen. Ook overspraak tussen de fasen, een gevolg van capacatieve en inductieve koppelingen bij de wikkelkoppelen, wordt met beide methoden effectief onderdrukt.

Diverse sensoren zijn ontwikkeld en permanent geïnstalleerd bij generatoren: (i) bus-support-capacitors (een capacatieve sensor in een steunisolator van het railkokersysteem), (ii) een ring sensor in het railkokersysteem, (iii) overspanningscondensatoren van een generator schakelaar, (iv) een één-winding inductieve stroomsensor om een aansluitklem van de generator, en (v) een meetlus. De diverse sensoren zijn bij twee generatoren vergeleken. Alle sensoren gaven goede en vergelijkbare resultaten. De hoogste gevoeligheid wordt verkregen met bus-support-capacitors.

Bij diverse generatoren werden afwijkende ontladingspatronen waargenomen. In alle gevallen kon de bron van deze ontladingen worden gelokaliseerd: (i) vonken in een step-up transformator, (ii) een foutief gemonteerde dempweerstand in een generator

schakelaar, (iii) vonken bij een stroomsensor, en (iv) ontladingen in een licht beschadigde bus-support-capacitor. Lokalisatie van een ontladingsbron buiten de generator is mogelijk met behulp van looptijdverschillen tussen de diverse sensoren en reflectietijden van het ontladingssignaal. Meetlussen kunnen hierbij worden gebruikt als een handige, additionele sensor.

Met behulp van metingen aan een ontmantelde 35 MW stator is de propagatie van ontladingssignalen in een statorwikkeling bestudeerd. Het blijkt dat een statorwikkeling kan worden beschouwd als een transmissielijn. Een partiële ontladingssignaal manifesteert zich aan de klemmen van een generator na een looptijd die afhankelijk is van de plaats van de ontlading (de zogenaamde 'langzame mode'). Als gevolg van capacitieve en inductieve koppelingen bij de wikkelpennen bestaat een tweede propagatie-mode voor de hogere frequenties. Deze 'snelle mode' arriveert aan de klemmen zonder noemenswaardige tijdsvertraging. Daarnaast vindt overspraak plaats tussen de fasen als gevolg van de capacitieve en inductieve koppelingen in de wikkelpennen. Een gevolg hiervan is dat een ontladingssignaal in een bepaalde fase niet per se afkomstig hoeft te zijn van een ontlading in deze fase. De amplitudes van de 'snelle mode' en, in iets mindere mate, de 'langzame mode' worden sterk gedempt naarmate de ontlading dieper in de wikkeling optreedt. Hierdoor kunnen alleen ontladingen dicht bij de aansluitklemmen worden gedetecteerd. In de praktijk zullen de meeste ontladingen hier ook optreden. De totale lading aan de aansluitklemmen is nauwelijks afhankelijk van de plaats waar een ontlading optreedt. De propagatie van een ontladingssignaal wordt ook bepaald door het externe circuit van de generator.

In de praktijk is de afstembare smalbandige detector het meest geschikt voor continue of periodieke on-line metingen aan een generator. Tijdsdomein-metingen geven meer informatie wanneer afwijkende ontladingspatronen worden waargenomen. Voor een effectieve conditie bewaking van een generator wordt de volgende strategie aanbevolen:

- continue monitoring van het ontladingsniveau met behulp van een afstembare smalbandige detector, afgestemd op de 'beste' afstemfrequentie
- periodiek (bijvoorbeeld jaarlijks) vastleggen van de partiële ontladingspatronen met behulp van een afstembare smalbandige detector. Om de juiste keuze van de 'beste' frequentie te controleren worden metingen uitgevoerd bij 30 verschillende afstemfrequenties
- in het geval van afwijkende ontladingspatronen moeten tijdsdomein metingen worden uitgevoerd door gespecialiseerd personeel. Extra informatie over de plaats van een ontlading kan worden gehaald uit de looptijden tussen verschillende sensoren.

Chapter 1

INTRODUCTION

1.1 Turbine generators, our modern workhorses

The goal of power utilities is to produce electrical energy with a high availability, at low cost and with minimal environmental impact [Sep96]. This can only be achieved by means of a well balanced integration of many technological disciplines, one of which is electrotechnical engineering. A good example is the operation of a turbine generator¹, where the stator winding experiences large electrical, mechanical and thermal stresses during operation. In the long run these stresses may reduce the quality of the insulation. For operators of generators, two aspects are of major importance [Pem97a]:

- reduction of in-service failures by early detection of possible failures. Although generators have a high reliability, in-service failures do occur. Failure statistics for The Netherlands show 698 generator failures during the last 17 years [Moo93]. Although this number of failures is relatively low, the average non-available energy caused by these failures is large: 703 GWh/year. This is about 1 % of the total electrical energy consumption in The Netherlands in 1996. An appreciable fraction, about 33 %, of in-service failures is related to stator windings. A description of several fatal winding failures that happened in The Netherlands during the last 17 years is given in [Moo93]
- minimal costs for maintenance, e.g. by condition-based maintenance and, when possible, by increasing maintenance intervals [Tav87].

This can only be realized when effective tools are available to assess the condition of a generator. Partial discharge (PD) measurements are in use for already more than 35 years to measure the quality of stator windings [Tem62]. In general PD measurements are carried out on stand-still generators during maintenance periods; however PD measurements should preferably be done on-line during regular operation. The advantages of on-line measurements are: (i) condition assessment is possible at every moment, (ii) they take place under realistic stresses, (iii) early detection of possible failures, and (iv) permanent condition monitoring is possible. In addition, no external test-transformer is needed, which would stress the entire winding whereas during regular operation the electrical stress increases linearly along the winding.

¹from now on we write 'generator' instead of 'turbine generator'

For the monitoring of PD's during regular operation, the standard technique according to the IEC-standard 270 [IEC81] cannot be used. Due to the high electrical interference levels in power plants, improvements are needed in: (i) electromagnetic compatibility (EMC) to suppress interference, (ii) sensors (particularly their bandwidth), and (iii) measuring methods. This thesis describes two methods to monitor partial discharges in stator windings during regular operation. Both methods employ specially developed capacitive and inductive sensors. The first technique measures PD signals in the time-domain on a pulse-by-pulse basis. By means of signal processing remaining interference pulses are rejected. For the second technique, a tunable narrow-bandwidth filter is tuned to a frequency where PD's are strong and interference is low. A detailed outline of this thesis is given in Section 1.5. First this chapter gives an introduction to insulation systems for stator windings (Section 1.2), insulation quality and partial discharges (Section 1.3), and an overview of techniques for PD monitoring (Section 1.4).

1.2 Insulation systems for stator windings

Formerly most rotating machines were insulated with asphalt-bonded mica tapes, which contain mica in the form of large flakes or splittings. This thermoplastic insulation was vulnerable to delamination after repeated thermal cycling. The delamination results in very large partial discharges, but nevertheless this insulation was used successfully for decades. Some generators were in operation for more than 40 years, without serious problems [Mie92].

Today epoxy-bonded (or sometimes polyester-bonded) mica tapes are used [Dol60], [Bri67], [Wic81]. The introduction of these tapes in the 1960's caused a revolution in the generator world. Due to the better properties of the insulation, ratings could soon be doubled from 150 to 300 MW. Within one decade ratings of over 1000 MW were possible, thanks to improved insulation and cooling techniques [Sch94a].

The thickness of the insulation is always a compromise between the allowed electrical stress and the thermal conductance. Much research is done on increasing the allowed electrical stress (now 2-3 kV/mm, future 3-5 kV/mm) [Qui94]. Also much effort is put in improving the thermal conductivity, for instance by the use of Al_2O_3 powder as filler material for the epoxy-resin [Ste94], [Bra94]. These improvements are important because they may lead to air-cooled generators with ratings that can now only be achieved with hydrogen cooling.

A semi-conducting coating (usually a graphite tape) is used on the surface of

the insulation in the slot-section of the bar, to prevent partial discharges in the unavoidable gaps between insulation and stator iron (slot-discharges). To prevent large partial discharges at the ends of the slots, a stress control (usually a silicon carbide coating) is applied to the end-arms of the bar. An important part of the insulation system is the slot-tightening system and the end-winding support. Vibration of the bar causes erosion of the insulation, and thus should be prevented. On the other hand, to allow thermal expansion some movement must be possible. For a good tightening hard wedges are used, in combination with semi-conductive side and wedge packings or ripple springs [Vak94].



Figure 1.1 *Statorbar of a 22 MW air-cooled generator, damaged by slot-discharges.*

1.3 Insulation quality and partial discharges

Partial discharges are both a symptom and a cause of deterioration. An example is given in Fig. 1.1, which shows a stator bar of a 22 MW air-cooled generator that is damaged by slot-discharges. In this case this resulted in a breakdown. Slot-discharges occur due to damage to the semi-conducting coating related to vibrations of the bars in the slots [Jac82], [Wil91]. Very intense slot-discharges can lead to a breakdown within one year. That slot-discharges must be taken seriously is shown in [Bin87], where it is reported that 20 % out of 479 inspected generators showed signs of slot-discharges.

An overview of important failure mechanisms of stator windings and characteristics of partial discharge patterns is given in Table I. All of these failure mechanisms can lead to a breakdown of the stator insulation, but generally they only manifest themselves when extra stress is caused by 'external events'. Examples are lightning

Table I *Most important failure mechanisms of stator windings and the corresponding characteristics of PD patterns [Fru90], [Sto95], [Sto97], [Sed97], [Bin98].*

failure mechanism	position of PD's on 50 Hz voltage	asymmetry between negative and positive cycle of 50 Hz voltage	load dependent	temperature dependent
internal discharges in voids in the insulation	between 0°-90° and 180°-270°	no	no	yes
loose windings (slot discharges)	between 0°-90° and 180°-270°	much larger magnitudes at negative cycle	yes	little
loose bond between insulation and copper conductor (thermal cycle deterioration)		much larger magnitudes at positive cycle	little	yes
end-winding discharges between two phases	concentrated near 100° and 280°	no	no	no
end-winding deterioration or contamination		much larger magnitudes at negative cycle	no or little	yes

strikes, power system disturbances, operator errors (fault synchronization) or poor maintenance (loose wedges lead to slot discharges). Nevertheless, continuous gradual deterioration will occur for each generator, which can lead to reduced reliability of older generators. The possible deterioration processes are summarized in Fig. 1.2.

Mechanical stress is recognized as the parameter with the strongest influence on the life of a generator [Kim93]. It results from thermomechanical cycles at start/stop operations or load cycles, and from electromagnetic forces at twice the system frequency. In [Kim95], a scanning electrode microscope is used to observe the generation and development of defects under mechanical stress. Initially, isolated delamination occurs in mica crystals and at the interface between mica and epoxy. Gradually these laminations are connected by cracks, often perpendicular to the mica surface so they can lower the breakdown voltage.

Thermal aging causes molecular decomposition and oxidation of the organic material [Kim97]. As a result the adhesive strength between the epoxy and mica decreases, leading to delamination at the interface between epoxy and mica. Although thermal aging in itself has less impact on the breakdown voltage, it accelerates erosion of the insulation when it is combined with mechanical stress and partial discharges [Kim91], [Ren85]. A second type of thermal aging is caused by the different thermal expansion coefficients for copper and the insulation. Along the length of the bar a

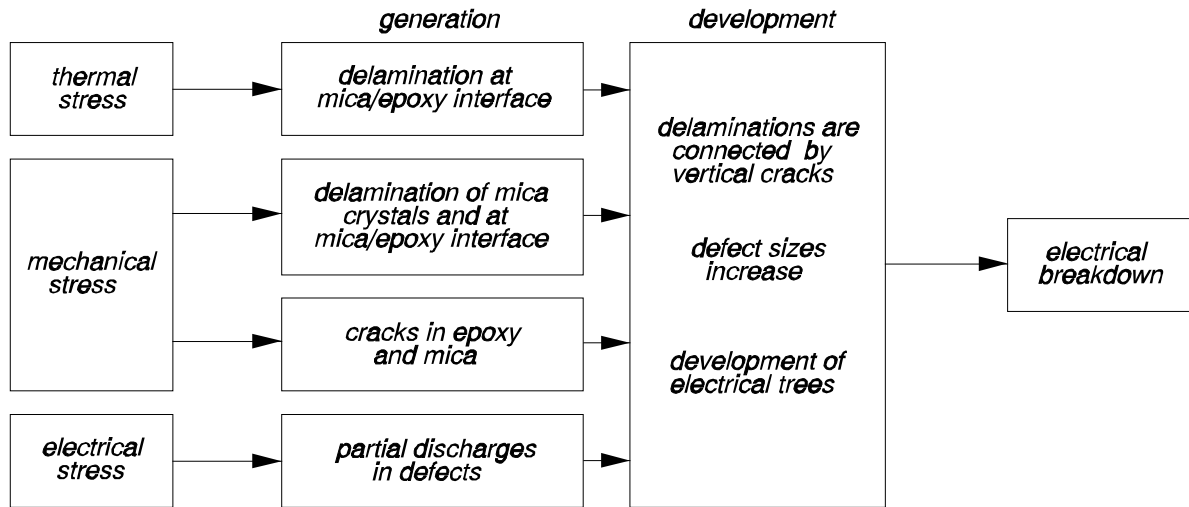


Figure 1.2 Schematic representation of deterioration mechanisms

considerable shear stress between the conductor and the insulation can occur during thermal cycles [Sed94]. The bond between conductor and insulation may break or wrinkles in the insulation can be formed [Wic81], leading to increased partial discharge activity and rapid deterioration.

Electrical stress causes partial discharges in defects that are caused by thermal and mechanical stresses. Partial discharges cause erosion and treeing in insulation materials, but for micaceous insulation this erosion is often suppressed by the high discharge resistance of mica crystals [Kim93]. Therefore large partial discharge levels can be allowed in this type of insulation compared to what is permissible in other high-voltage insulation systems, as can be seen in Table II. Nevertheless, over a 25 year period, partial discharges contribute to severe deterioration of the insulation.

Table II Maximum acceptable PD levels for several HV insulation systems [Woo93]

GIS	2-5 pC
XLPE cables	5 pC at $1.5 \cdot U_{\text{nom}}$
transformers	300 pC at $1.3 \cdot U_{\text{nom}}$, 500 pC at $1.6 \cdot U_{\text{nom}}$
generators	>1000 pC can be tolerated for over 25 years

From the above description of the deterioration process it is clear that internal defects in the insulation play an important role. Generally these internal defects are accompanied by partial discharges, which can be detected by chemical, acoustic or optic techniques, however electrical measuring techniques are far more sensitive. A

often used technique are loss tangent measurements, which can only be done off-line. The loss tangent $\tan \delta$ is a "bulk" parameter, which can be used in the assessment of the condition of the entire winding. Single weak points however are difficult to detect with $\tan \delta$ measurements [Cul89]. Partial discharge measurements enable the detection of individual defect-sites. Several on-line PD tests have been developed. An overview is given in the next section. It will be shown that available methods may easily give false indications as a result of the high levels of electrical interference in a power plant. The main goal of the work in this thesis was the development of interference-free and therefore reliable PD measuring methods.

1.4 Overview of techniques for PD monitoring

The most common way to plot results from partial discharge measurements is the so called phase-resolved partial discharge pattern [Gul95]. The magnitude of each partial discharge is plotted with respect to its position on the 50 Hz voltage. In addition the number of partial discharge pulses with respect to the 50 Hz voltage is plotted. Results can be plotted either in 2-D diagrams or in a 3-D diagram. Examples of on-line measured 2-D and 3-D partial discharge patterns are given in Fig. 1.3. Phase-resolved partial discharge patterns are useful in identifying the most important failure mechanisms of stator windings.

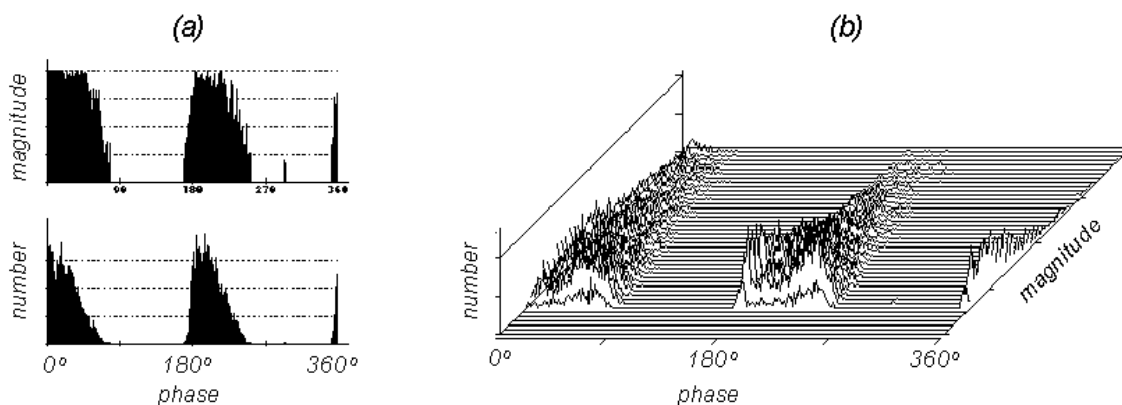


Figure 1.3 Examples of (a) 2-D and (b) 3-D phase-resolved partial discharge patterns for the 169 MW gasturbine generator Roca-3. Both patterns are recorded during regular operation (see also Chapter 8).

The first systems to monitor partial discharges during regular operation were developed in the early 1970's by Westinghouse in the USA [Har79] and Ontario Hydro in Canada [Kur79]. The stimulus for this development were problems, at that time, with broken subconductors in the Roebel-bars of large turbine generators and slot-discharges in the windings of hydro generators.

For the Westinghouse method, PD currents are detected in the neutral grounding connection of the generator by means of a hf current transformer [Eme81], [Tim83]. The currents are recorded via a spectrum analyzer, which is used as a tunable narrow-bandwidth filter. The analyzer is tuned to a well-chosen frequency where partial discharge signals dominate. Disadvantages of this method are (i) the low sensitivity, (ii) it is difficult to determine the phase where a discharge takes place, (iii) due to the large self-inductance, only a small fraction of the PD current will flow through the grounding connection (see Section 5.2), and (iv) interference currents can easily be induced into the large loops that are formed by the grounding system. Nevertheless, the method is still widely used [Tim92], [Hut92].

The partial discharge analyzer (PDA) developed by Ontario Hydro found worldwide application for hydro generators [Kur84]. Cable-couplers are used as capacitive sensors (80 pF). To discriminate between partial discharges and interference, for each phase two cable-couplers are installed in the circuit-ring-bus. Due to the large dimensions of a hydro-generator circuit-ring-bus, partial discharges arrive at different times at the cable-couplers, while interference signals arrive at the same time. The system is installed in hundreds of hydro-generators, and valuable experience for the users has been built up [Ly187], [Col90].

Application of the PDA system for turbine generators has not been so successful [Cam93]. Now for each phase, one 80 pF capacitive sensor is installed at the generator terminal and one at the terminal of the step-up transformer. Elimination of interference is based on the assumption that interference signals arrive simultaneously at both sensors or come from the direction of the step-up transformer. Signals detected first by the sensor closest to the generator are regarded as partial discharges. Nevertheless, many problems with interference are reported. Apparently interference couples into the generator and arrives at the sensors as 'legitimate' signals. In addition, problems with interference can occur due to improper grounding of the sensor [Mcd99].

The problems with interference stimulated the Canadians to develop a new approach; an ultra-wide bandwidth system. Microstrip antennas (stator-slot-couplers or SSC's) with a bandwidth from 10 MHz to more than 1 GHz are installed inside the generator, next to a stator bar in a slot [Sed91], [Sto92]. This approach has proven to be very efficient in discriminating between interference and partial discharges.

Experience indicates that partial discharges are detected as pulses which are less than 6 ns wide. In contrast, all types of interference were found to have pulse-widths of at least 20 ns. The system provides an excellent localization, it can even determine whether a discharge takes place in the slot-section of a bar or in the end-winding region. An important disadvantage is that a stator-slot-coupler detects only discharges from the bar where it is installed. Also manufacturers and utilities often hesitate to install SSC's inside a generator.

A German system uses the protective snubber capacitors, that are sometimes installed to protect the generator against switching surges [Wic85], [Gru94]. The sensitivity of the system is large, unfortunately not only for partial discharges but also for interference signals. The capacitors are installed some distance away from the generator, and long leads are needed for connections. As a result, large loops are formed which act as antennas for the various interference sources that are present in a power plant. The system uses digital signal processing to reduce the sensitivity for interference.

1.5 PD monitoring in this thesis

Practical on-line partial discharge measurements take place in an industrial environment, where many sources of interference are present. As we saw in the previous section, available methods all have problems with this interference. In this thesis we have chosen to:

- concentrate on interference-free measurements by: (i) electromagnetic compatibility (EMC) methods to suppress interference, (ii) external sensors with a bandwidth which is much higher than the common 5 MHz, and (iii) measuring methods to suppress remaining interference
- locate abnormal partial discharge activity by means of additional sensors
- test the developed methods under real conditions in several power plants.

Interference-free measurements:

Especially at frequencies up to 5 MHz, intense interference is caused by e.g. the rotor excitation system. As a consequence, the question - *What can be observed under realistic conditions ?* - has to be answered. In fact we have two options:

- **measurements that provide correct pC values.** In Chapter 2 we will see that the lower frequency components of the PD signal contribute most strongly to the

apparent charge. Unfortunately, within this frequency range of interest, interference will be much stronger than the PD signal. Only under specific circumstances valuable measurements are possible by means of complex measuring procedures and signal processing [Nag93], [Köp95]. When these circumstances change (e.g. when new, 'interfering' equipment is installed in the power plant) or when unforeseen interference sources are present, these techniques do not work. Consequently, there is a high risk for false alarms, leading to a reduced credibility of PD measurements

- we give priority to **inherent interference-free measurements**. This means that interference must be suppressed thus minimizing the risk for false alarms. Since at lower frequencies more interference is present, we prefer measurements at frequencies >5 MHz. As a consequence (see Chapter 2):
 - (i) no calibration is possible and measured PD-magnitudes must be given in mV's or mA's and not in pC. Consequently, a direct comparison with measurements on other generators is difficult. However a comparison with earlier measurements on the same generator, or on the same type of generator, remain valuable
 - (ii) only discharges close to the measuring terminals can be observed. In practice this is not a serious disadvantage, since most discharges will take place in the high-voltage part of the winding.

Disturbances due to interference in power plants:

In power stations, several sources of interference are present, which may hamper PD measurements. Examples are: (i) switching pulses of the rotor excitation system, (ii) sparking brushes of the shaft-grounding, of the rotor excitation or of nearby rotating machines, (iii) local transmitters, e.g. for the control of cranes, and (iv) the power electronics and control systems of large motors, e.g. of feeding water pumps. These sources can interfere with partial discharge measurements in two ways: (i) by coupling into the measuring system, or (ii) by coupling into the stator winding or into the IPB².

Even when the measuring system itself does not pick up interference, interference can already couple into the stator winding or into the IPB and cause 'legitimate' signals at the sensors [Ito93]. Note that coupling by external fields into the generator is unlikely, since the metal enclosure forms an almost perfect 'Faraday-cage'. Nevertheless interference can enter a generator in various ways (see Fig. 1.4):

- via the rotor; the power electronics of the rotor excitation system cause transient interference pulses in the rotor winding. Via capacitive and inductive couplings,

²IPB; Isolated-Phase-Bus which connects a generator to a step-up transformer, see Appendix D

- especially in the end-winding regions, these pulses will also show up in the stator - winding. Rotor excitation pulses contain relatively low frequencies (<5 MHz) and appear at 6 or 12 fixed positions with respect to the 50 Hz voltage waveform
- via the six connections to the three phase stator windings
 - generators are fitted with several sensors, e.g. thermocouples into each slot of the stator winding. Disturbances can enter a generator via the wiring of these sensors. As a test we measured the common-mode currents of all signal cables of the 650 MW generator in the Hemweg-8 power plant. No significant currents were observed, which is an indication that this interference source can be ignored
 - any changing magnetic flux, present in the regions near the neutral or the high-voltage terminals, may result in an interference voltage.

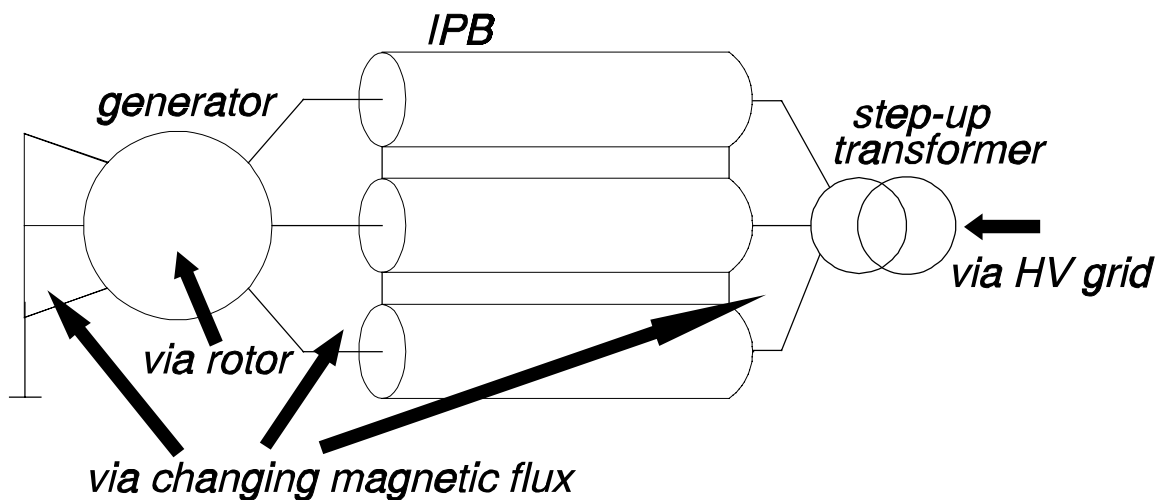


Figure 1.4 *Interference may enter a generator via various paths*

Coupling of interference into the measuring system can be avoided by state-of-the-art EMC measures [Laa97], [Deu93]. Disturbances often reach the measuring equipment via measuring or power cables. In addition to the signal currents, these cables may carry a net common-mode (CM) current. Interference due to these CM-currents can be strongly reduced by: (i) the use of measuring cables and connectors with a low transfer impedance (we used RG223 cable with N-type connectors) [Hor98], (ii) keeping CM-currents away from the measuring equipment by means of an EMC-cabinet, (iii) filtering of the power line which enters the cabinet, and (iv) keeping CM-currents away from the sensors. In addition, a good choice of measuring frequency and bandwidth must be made. Standard available sensors for on-line PD measurements

have bandwidths up to about 5 MHz³. We prefer measuring frequencies above 5 MHz, thus new sensors with bandwidths up to about 100 MHz have been developed.

By applying these EMC-techniques, interference can be rejected to a large extent. However, one must realize that, even when the measuring system itself is fully protected against interference, disturbances can still couple into the stator winding and cause undesirable but 'legitimate' signals at the sensors.

This remaining amount of interference, which is still present after the above mentioned EMC-methods have been applied, has to be rejected by a proper refinement of the measuring process. We developed two alternatives. In the first alternative PD pulses are measured in the time-domain on a pulse-by-pulse basis. By means of signal processing, remaining interference pulses are rejected. For the second alternative, a tunable narrow-bandwidth filter is used, which is tuned to a frequency where PD's are strong and interference is weak.

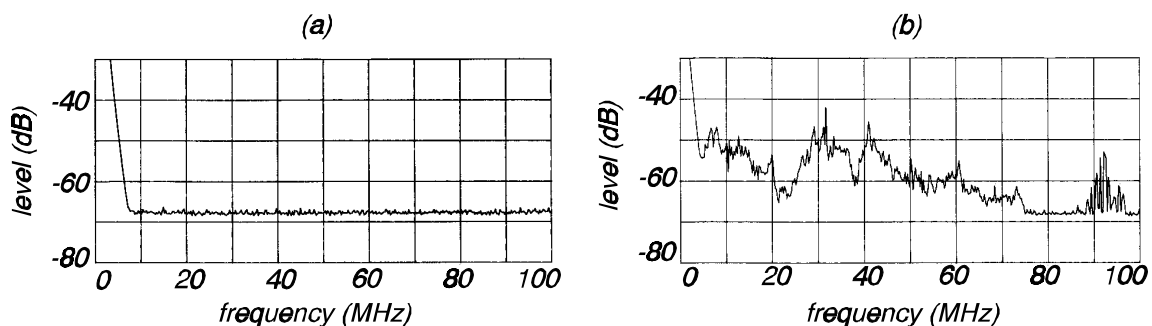


Figure 1.5 *Measured frequency-spectra at the Roca-3 gasturbine generator, (a) with and (b) without correct EMC-measures. In both cases the cable is shorted at the capacitive sensor side. In (a) N-connectors were used, while in (b) BNC-connectors, which have a larger transfer impedance, were used (note: the activity below 7 MHz is caused by an offset of the spectrum analyzer)*

Examples of good and bad EMC:

A good test to assess the EMC-quality of the measuring system is to short-circuit the measuring cable at the sensor side. An example of such a measurement in the Roca-3 power plant is given in Fig. 1.5. In case of good EMC-measures, nothing will be measured by the connected spectrum analyzer (Fig. 1.5a). In Fig. 1.5b we used

³except for stator-slot-couplers. However, Dutch power utilities do not allow the installation of sensors inside the generator but prefer external sensors. In this thesis we concentrate on external sensors.

BNC-connectors instead of N-connectors. Now interference signals couple in via the transfer impedance of the BNC-connector, resulting in an illegal signal at the spectrum analyzer.

Localization in the case of abnormal or unexpected PD activity:

When abnormal PD patterns are recorded, one has to verify that: (i) the recorded signals are indeed caused by discharges, and (ii) whether the discharges come from the generator or from other high-voltage equipment. Valuable information can be obtained when two or more sensors are used in each phase (for instance a pick-up loop can be used as an extra sensor). Now, if we measure the transit-times between the sensors, the signal-source can often be localized. Table V gives an overview of abnormal or unexpected results of on-line measurements on generators. In all cases, a pick-up loop was used to locate the source of the discharges.

Outline of this thesis:

Chapter 2 describes experiments to study the propagation of partial discharge pulses in a stator winding. Also the resulting consequences for partial discharges will be evaluated.

In Chapter 3 we describe the various sensors which have been developed for on-line measurements: (i) bus-support-capacitors, (ii) ring capacitors, (iii) overvoltage capacitors of a generator circuit-breaker, (iv) single-turn inductive current sensors, and (v) a pick-up loop.

The two measuring techniques that will be used throughout this thesis are described in Chapter 4. Both techniques are illustrated by on-line measurements on two generators. The first technique is illustrated by measurements on generator Hemweg-6. PD pulses are measured in the time-domain on a pulse-by-pulse basis, and remaining interference is rejected by means of signal processing. For generator Hemweg-8, a tunable narrow-bandwidth filter is used, which is tuned to a frequency where PD's dominate.

The various sensor types and measuring techniques have been evaluated during on-line measurements in several old and new power plants. Special emphasis has been drawn to: (i) comparison of the various sensors (See Table III), (ii) comparison of both measuring techniques (see Table IV), and (iii) localization of unexpected PD activity (see Table V). The measurements on six generators are reported in Chapter 5 (Hemweg-6), Chapter 6 (Amer-9), Chapter 7 (Hemweg-8), Chapter 8 (gasturbine generator

Roca-3) and Chapter 9 (two generators in the Maasvlakte power-plant). Conclusions are described in Chapter 10.

Table III *Overview of the various sensors, installed at generators*

	bus-support-capacitor	ring-capacitor	overvoltage capacitor	single-turn inductive current sensor	pick-up loop
Hemweg-6 (Chapter 5)	x			x	x
Amer-9 (Chapter 6)				x	x
Hemweg-8 (Chapter 7)				x	x
Roca-3 (Chapter 8)	x	x	x		
Maasvlakte (Chapter 9)	x				x

Table IV *Overview of both measuring techniques used for on-line measurements on generators*

	time-domain measurements	tunable narrow-bandwidth filter
Hemweg-6 (Chapter 5)	x	
Amer-9 (Chapter 6)	x	partly
Hemweg-8 (Chapter 7)	x	x
Roca-3 (Chapter 8)	x	x
Maasvlakte (Chapter 9)	partly	partly

Table V *Overview of unexpected and located PD activity*

Amer-9 (Chapter 6)	Only PD's in phase V. This unexpected result was confirmed by additional measurements.
Hemweg-8 (Chapter 7)	Two additional discharge sources could be located: (i) sparking near the current sensor in phase V, and (ii) sparking inside the step-up transformer.
Maasvlakte (Chapter 9)	Discharge activity in a bus-support-capacitor. Large discharge activity caused by improper installed bleeding-resistor of the generator circuit-breaker.

Chapter 2

PROPAGATION OF PARTIAL DISCHARGE SIGNALS IN A STATOR WINDING

2.1 From abc-model to complex windings

For a correct interpretation of partial discharge measurements, we need to know how the actual electrical activity in a cavity is transferred to the measuring system. A simple engineering model for internal discharges, the *abc*-model, standardized by the IEC [IEC81] is given in Fig. 2.1. A discharge causes a motion of charge q_c within the cavity, capacitor c , resulting in a voltage drop at the terminals of the object. To detect the discharge a coupling capacitor C_c and a measuring impedance Z_m are used. A detailed description of this standard technique can be found in [Kre89]. The measured apparent charge q_{app} is related to the actual charge q_c involved in the discharge according to: $q_{app}/q_c = b/c$. Calibration of the measuring circuit is possible by injection of a known charge into the terminals of the object under test (capacitors a, b, c).

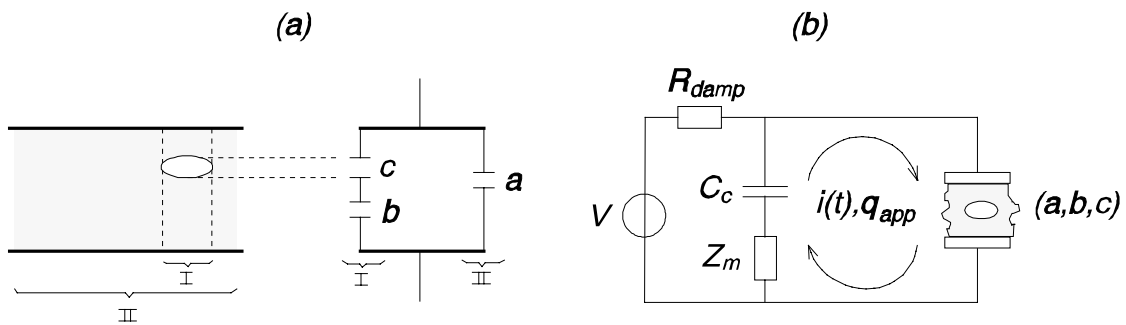


Figure 2.1 (a) *Abc*-model and (b) standard measuring technique for pd's.

For objects that cannot be regarded as lumped capacitors, the *abc*-model is not applicable. Good examples are gas-insulated substations (GIS) and high-voltage cables. A partial discharge excites an electromagnetic wave that propagates along the GIS [Rut97] or the cable. The sound dielectric (capacitance a in Fig. 2.1) can no longer be regarded as just a capacitance, but must be seen as a transmission line. Calibration in pC's can be difficult due to damping and dispersion, caused by for instance semi-conductive layers in cables or spacers in GIS. Reflections of the wave, for instance at the cable-ends, can however be used to locate the discharge [Het95].

Also for complex electrical structures, such as transformer- and stator windings, the *abc*-model is not applicable. During the long path from discharge site to the terminals, where the discharge can be measured, the signal is heavily distorted.

For transformers it is shown in [Tho73], [[Jam86a], [Fuh93] that the partial discharge signal propagates in three modes: (i) the higher frequencies (0.1 to 10 MHz) travel through the capacitive ladder network, formed by the interturn capacitances, (ii) a travelling wave mode (frequencies up to 10 kHz) follows the transmission line formed by the galvanic path of the winding, and (iii) an oscillating component is determined by the internal resonant frequencies of the transformer (10 to 100 kHz). As a consequence, the amplitude and waveform of the response at the terminal strongly depends on the origin of the discharge and on the design of the transformer. Therefore to estimate the apparent charge of the discharge, the origin must be known.

Similar problems arise when measuring partial discharges in stator windings of generators [Pem94]. In this chapter the propagation properties of a stator winding and the resulting consequences for discharge measurements are discussed. In experiments, pulses were injected at various places in the windings of an old 35 MW stator; the responses at the terminals were measured. The experimental setup is described in Section 2.2. The results are given in Section 2.3 and discussed in Section 2.4.

2.2 Experimental setup

To study the propagation of partial discharge signals in a stator winding, we did experiments on the stator of an old 35 MW generator (rotor removed), available in the KEMA laboratory. The stator, shown in Fig. 2.2, has 60 slots, with only one bar per slot. The stator winding has three phases, with 20 bars per phase. The generator data, winding diagram and the numbering method of the bars are given in Appendix A. From now on we will characterize each bar with its phase and number. For instance, bar U_9 is the 9th bar of phase U, or the bar in slot 41 (see Appendix A).

The experimental setup is sketched in Fig. 2.3. A fast pulse (rise-time < 1 ns, duration 50 ns, amplitude 1 V) was injected directly in the winding. A small hole was drilled in the insulation to connect the inner conductor of a coaxial cable directly to the conductor in the bar. The shield of the cable was carefully connected to the stator-iron. To match the pulse generator as correctly as possible, a 50Ω resistor was installed in parallel at the injection point. A similarly attached measuring cable was used to measure the pulse in other parts of the winding. Also the response at the three high-voltage terminals and at the neutral terminal of the generator could be measured. The

injected pulse was measured via a splitter and was used to trigger the digitizer (Tektronix DSA602A). To prevent problems with interference, the digitizer was placed in an EMC-cabinet. Both coaxial cables and connectors had a low transfer impedance (RG223/U with N-type connectors). The coaxial cable braids were correctly grounded at the EMC-cabinet and at the measuring terminals. The data was recorded with a record-length of 5120 points, and with sampling-rates of 100 Msamples/s and 10 Gsamples/s. The higher sampling rate was used for the analysis of the fast mode, described in the following section.

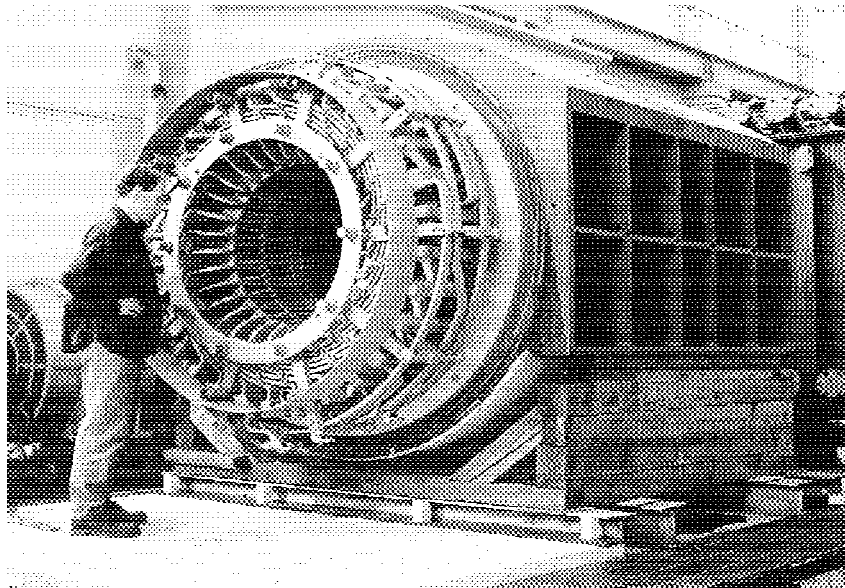


Figure 2.2 A 35 MW stator, available in the KEMA laboratory, used for the propagation study.

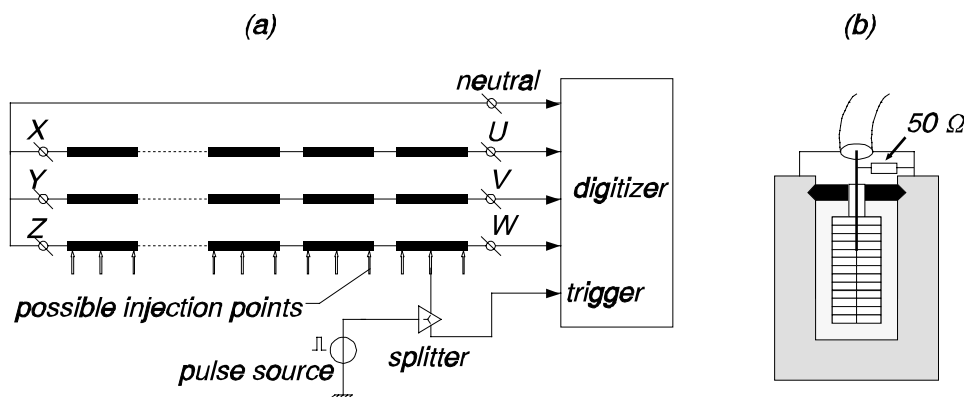


Figure 2.3 (a) Experimental setup, and (b) injection point.

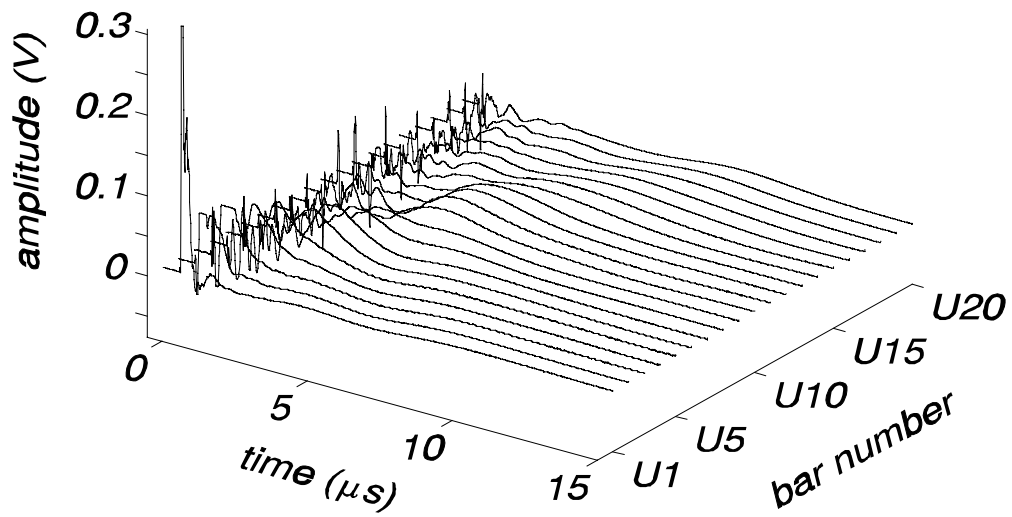


Figure 2.4a Responses at the high-voltage terminal of phase U, when pulses are injected successively in the middle of each bar of this phase.

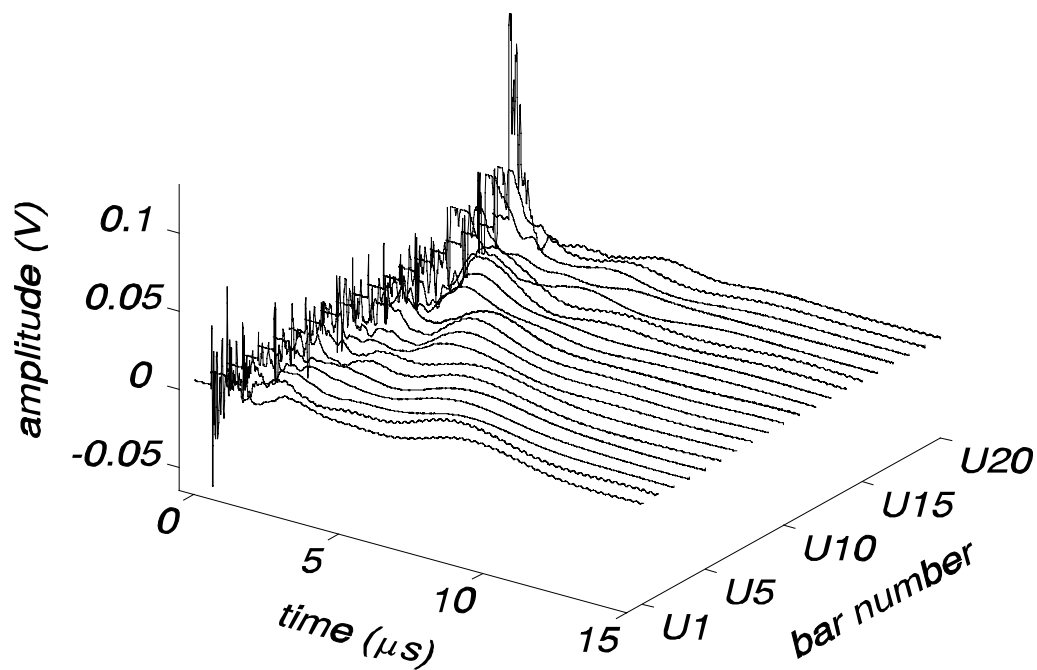


Figure 2.4b Responses at the neutral terminal of phase U, when pulses are injected successively in the middle of each bar of this phase.

2.3 Experimental results

2.3.1 Analysis of the 'fast mode' and the 'slow mode'

Figures 2.4a and 2.4b give the responses at respectively the high-voltage and the neutral terminal of phase U, when pulses are injected successively in the middle of each of the 20 bars of this phase. The bar number is given along one axis. Along the other two axes the signal amplitude and the time are given. We only discuss the results for phase U. The other two phases show similar results, which is plausible since the three phases are similar in geometry and construction.

As can be seen, the responses show two modes. A "fast mode" arrives at the terminals without a significant time delay and contains mainly the higher frequency components. The slow tails in Fig. 2.4a and Fig. 2.4b contain the lower frequency components, which apparently travel through the entire winding. This "slow mode" arrives at the terminals with a delay that depends on the place of injection. Both propagation modes can be separated by means of digital low-pass filtering. To obtain the slow mode, we used a 5th order Butterworth filter with a cut-off frequency of 450 kHz. The fast mode is obtained when the slow mode is subtracted from the original data. An example is given in Fig. 2.5. Figures 2.6a and 2.6b show the slow modes for the responses at respectively the high-voltage and the neutral terminal of phase U. Note that the results are normalized; the maximum value is set to one.

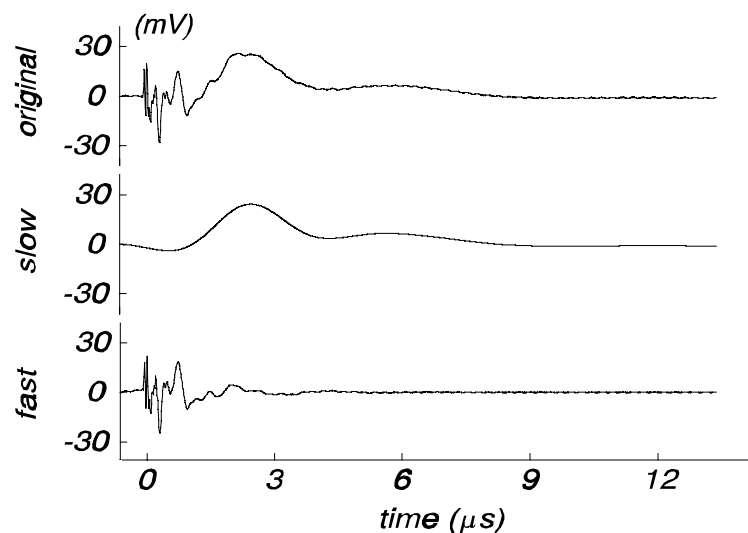


Figure 2.5 Separation of the "slow mode" and the "fast mode". The original data is measured at the high-voltage terminal of phase U, for pulse injection in bar U_8 . The slow mode is derived by low-pass filtering of the original data. The fast mode is obtained after subtraction of the slow mode from the original data.

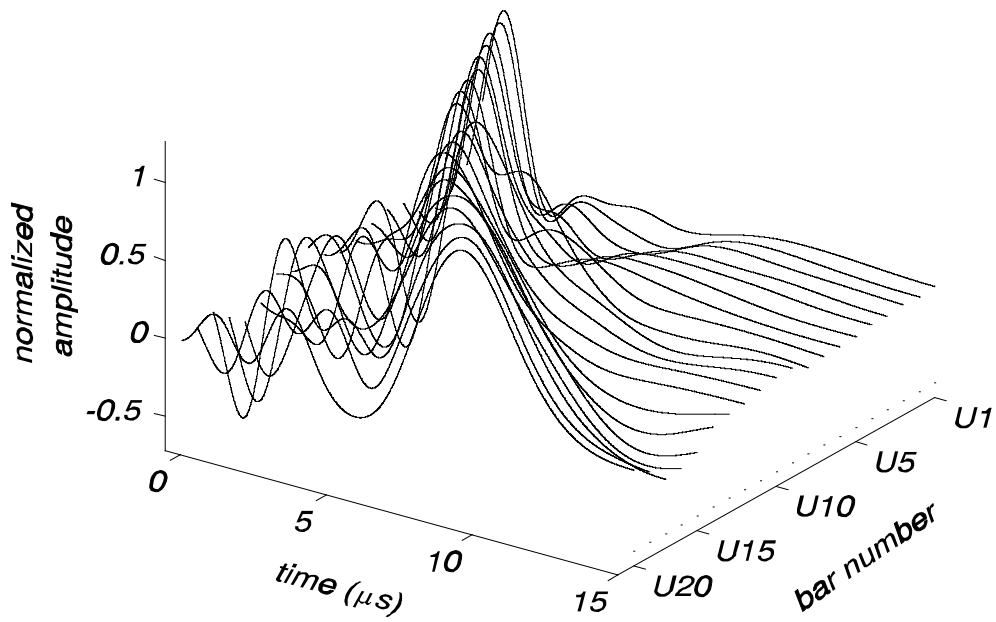


Figure 2.6a Slow modes at the high-voltage terminal of phase U, determined after digital low-pass filtering. Note that the order of the bar numbers is different for the two figures.

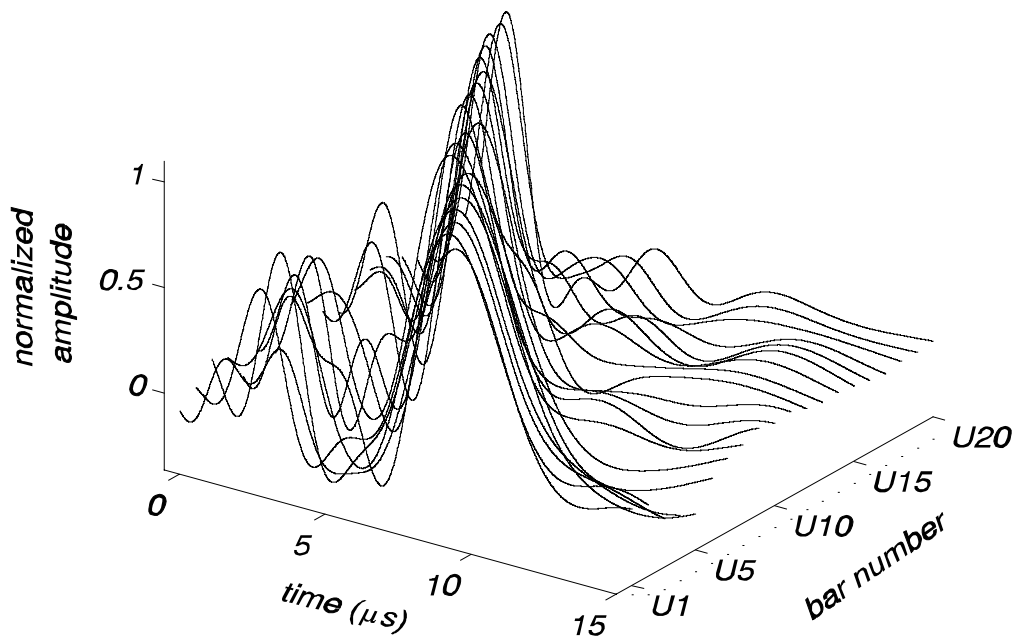


Figure 2.6b Slow modes at the neutral terminal of phase U, determined after digital low-pass filtering.

It is clear from Fig. 2.6 that the **slow mode** travels through the entire winding before it arrives at the terminals of the generator. The time of arrival depends on the place of injection as is shown in Fig. 2.7. Note that Fig. 2.7 gives the results for all 3 phases and all 180 measurements (the stator has 60 bars, measurements are now done for injection at 3 positions in each bar). As time of arrival we took the time of the maximum amplitude. Because the length of the end-windings is different for various parts of the winding, the time of arrival is not fully linear with respect to the bar number. The transit time is $9.8 \mu\text{s}$, for a winding-length of 89 m. Thus the velocity of the slow mode is $9.1 \text{ m}/\mu\text{s}$ or 3 % of the speed of light.

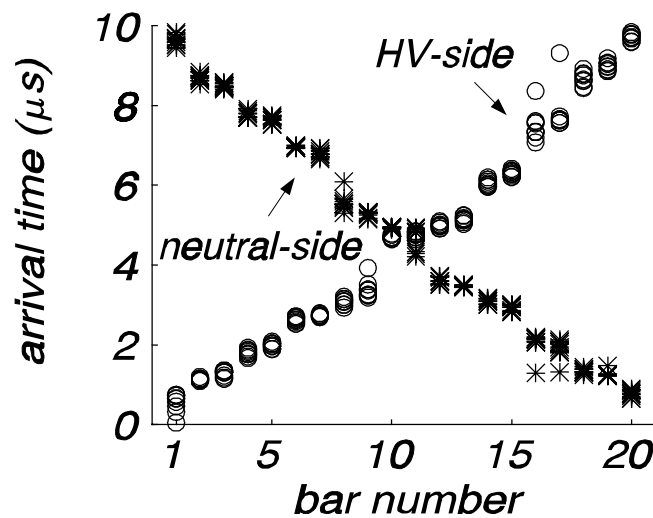


Figure 2.7 Arrival times at the high-voltage and neutral terminals of the slow modes (derived after digital filtering). The figure shows all 180 measurements (the stator has 60 bars, measurements are done for injection at three positions in each bar).

If we look carefully, the **fast mode** arrives at the terminals with a time delay varying from 59 ns to 86 ns, as can be seen in Fig. 2.8. The arrival times depend on the place of injection and are given in Fig. 2.9a for all 180 measurements. The extra transit times Δt_1 and Δt_2 are equal for all measurements and are explained in Fig. 2.9b. This figure shows three bars and their capacitive couplings at the end-windings. Both the neutral terminal and the high-voltage terminal are at the same side of the generator (at the 'beginning'). When pulses are injected at the beginning of a bar, the signal arrives at a terminal with a time delay of 59 ns, partly caused by a delay in the measuring cable (16 ns) and by the transit time of the connection from the winding to

the terminal. It is clear that when a pulse is injected at the end of a bar, it has to travel from 'end' to 'begin' before it can arrive at the terminals. The mean transit time in a bar is 28.2 ns for a bar length of 2.3 m. Thus the velocity of the fast mode is 81.6 m/ μ s or 27 % of the speed of light.

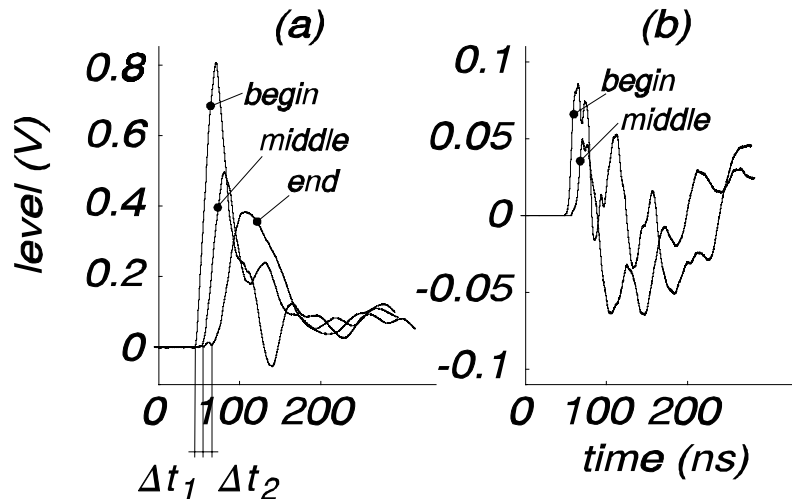


Figure 2.8 Response at the high-voltage terminal of phase U for pulse injection at (a) 3 positions in bar U_p , and (b) 2 positions in bar U_{11} .

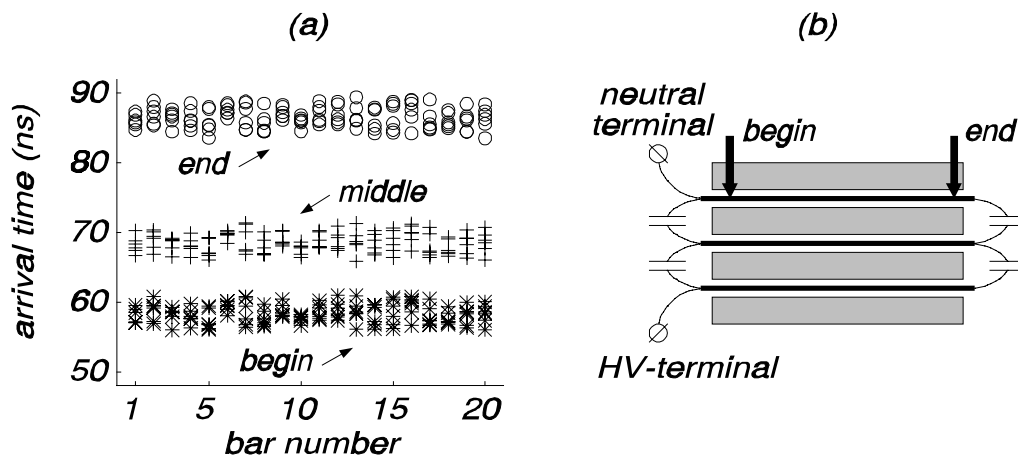


Figure 2.9 (a) Arrival times at the high-voltage and neutral terminals of the fast modes for pulse injection at the beginning, middle and end of all 60 bars, and (b) schematic representation of the propagation of the fast mode.

Figure 2.10 gives the normalized peak values for the fast modes and the slow modes at both terminals of phase U (the peak values are normalized with reference to the largest value). The resulting amplitudes strongly depend on the place of injection and decrease when the pulse is injected further away from the measuring terminal. Especially the higher frequencies (the fast-mode) are heavily damped. At lower frequencies (the slow mode) about 35 % of the winding can be seen with an attenuation less than 50 %. For on-line measurements most partial discharges occur in the high-voltage part of the winding. In that case the rapid attenuation of the higher frequencies is not a serious disadvantage. Moreover we prefer measurements at higher frequencies, since at lower frequencies more interference is present (eg. the rotor excitation system causes interference at frequencies up to 5 MHz, see Chapter 4).

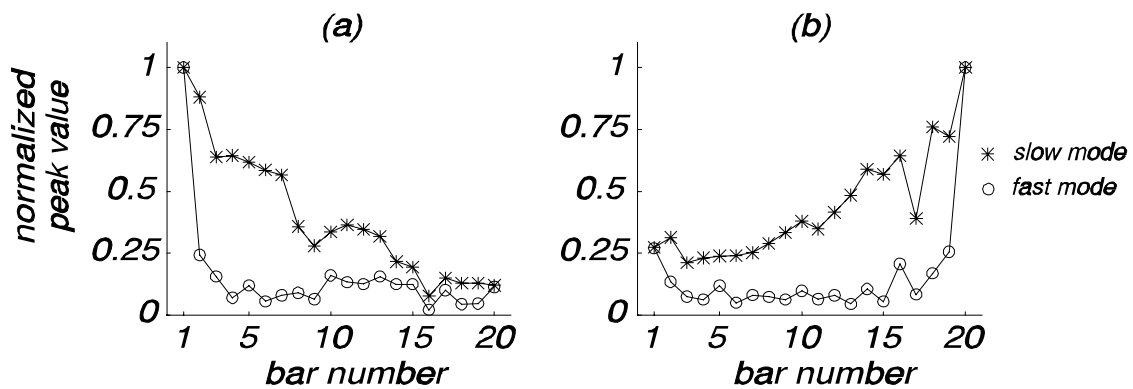


Figure 2.10 Normalized peak values of both the slow-mode and the fast-mode when pulses are injected in each bar of phase U and measured at (a) the high-voltage terminal of phase U, and (b) the neutral terminal.

The data in Fig. 2.10 is measured with an oscilloscope. Similar measurements were done with other instruments: a partial discharge detector according to IEC270 [IEC81] which operates at frequencies up to 500 kHz (Haefely TE571) and a spectrum analyzer tuned to 1 MHz or 15 MHz (Hewlett-Packard HP8495). The combined results for phase V are shown in Fig. 2.11. It is clear that the Haefely detector sees the slow-mode, since it works up to 500 kHz. Both at 1 MHz and 15 MHz, the spectrum analyzer sees the fast-mode.

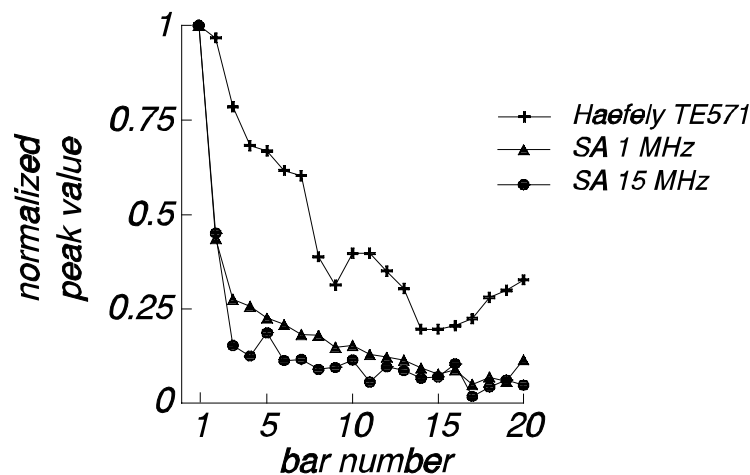


Figure 2.11 Normalized peak values at the high-voltage terminal of phase V, when pulses are injected in each bar of this phase. The amplitudes are measured with the Haefely TE571 partial discharge detector and a HP8494A spectrum analyzer tuned to 1 MHz and to 15 MHz.

2.3.2 The "calibration problem"

In the literature, many authors refer to the "calibration problem" (see e.g. [Kem96] or [Zhu97]). Normally, partial discharge measurements are calibrated by injection of a known charge into the test setup. Since for generators, the response at the terminals (where the discharges are measured) strongly depends on the origin of the discharge, it is often stated that the apparent charge (in pC) of a discharge can only be determined if the place where the discharge occurs is known. This statement is based on measurements of the voltages at the terminals (as in our Fig. 2.10). However, calibration must be done by measuring the charge instead of the voltage at the

terminals. To estimate the charge, the current that is measured at a terminal (the measured voltage divided by 50Ω) is numerically integrated. The charges at all four measuring terminals when pulses are injected in each bar of phase U are given in Fig. 2.12. Due to cross-talk between the phases, charge shows up at all four terminals. This cross-talk will be discussed later in this section.

When the original recorded signals are numerically integrated (during $51.2 \mu\text{s}$, including both the slow-mode and the fast-mode), the total charge at the four terminals depends not very much on the place of injection (Fig. 2.12a). This would suggest that the calibration problem does not exist if the complete response including all frequency components can be measured and integrated. For practical measurements this is however not possible. Standard discharge detectors according to IEC270 [IEC81] only integrate frequencies above 100 to 500 kHz (lower frequencies are rejected to suppress the 50 Hz). Detectors for measurements "in the field" operate at frequencies above 1 MHz to suppress interference. Figure 2.12b gives the charges when only the fast-mode of the response is integrated. Now the charges at the four terminals depend strongly on the place of injection and, compared to Fig. 2.12a, only a fraction of the charges is observed. This shows that lower frequency components contribute most strongly to the apparent charge.

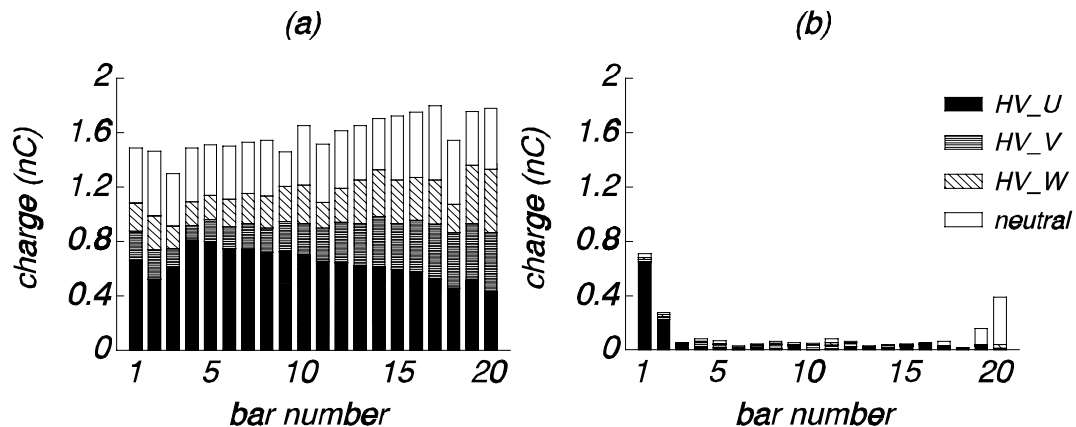


Figure 2.12 Charges at all four terminals when pulses are injected in each bar of phase U. The charges are determined by numerical integration of (a) the complete responses (including both the fast and the slow mode), and (b) only the fast modes.

2.3.3 Cross-talk between the phases

We saw that the response at the terminals consists of two modes. For the slow mode a stator winding acts as a transmission line. So the signals arrive at the generator terminals after a transit time that depends on the origin of the discharge. However due to capacitive and inductive couplings, a second propagation mode (the fast mode) is present at higher frequencies. These couplings not only occur between bars of the same phase, but also cause cross-talk between the phases. This can be seen in Fig. 2.13, which shows the responses at the three high-voltage terminals when a pulse is injected in the 11th bar of phase U. Due to cross-talk, the signal shows up in each phase.

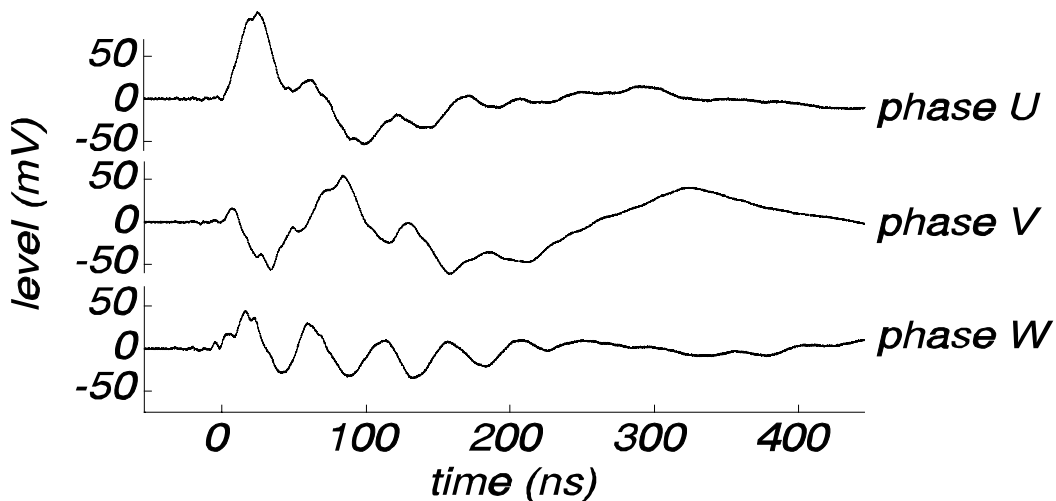


Figure 2.13 *Cross-talk between the phases: pulse injection in the 11th bar of phase U, and the responses at the high-voltage terminals of the three phases U, V and W.*

The cross-talk depends on the place of injection. This is shown in Fig. 2.14, which gives the cross-talk from phase U to the phases V and W, when pulses are injected in each of the 20 bars of phase U. The cross-talk is defined as the ratio of the peak-to-peak values, relative to phase U. For discharges in the first four bars (20 %) of the winding, the largest signal shows up at the terminal of the phase where the discharge occurs. In this case the cross-talk is small and increases nearly linearly with bar number. For discharges deeper into the winding the cross-talk can be >1 , which means that the largest signal does not show up in the phase where the discharge occurs, but in the other phases. In on-line measurements, only discharges from the bars close to the high-voltage terminals occur, thus it is plausible that the largest signal will

show up in the phase where the discharge occurs. This enables a first localization of a discharge; the phase where the discharge occurs can be determined.

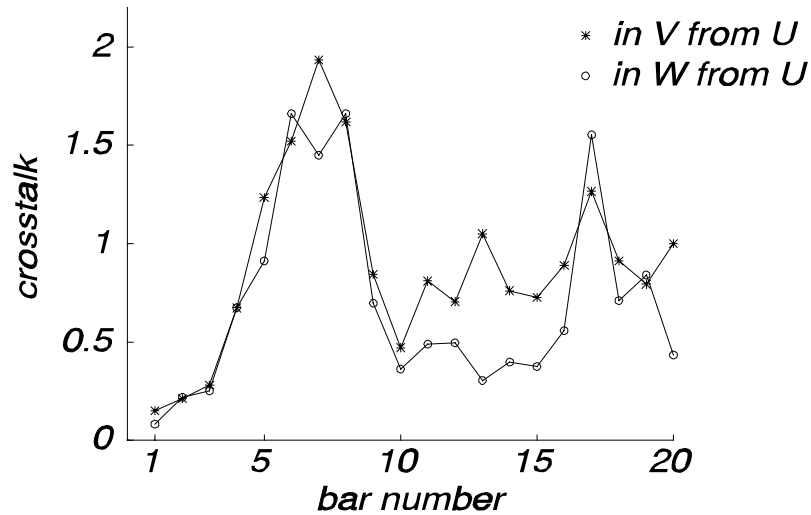


Figure 2.14 *Cross-talk from phase U to the other two phases.*

The capacitive and inductive couplings between the windings play an important role in the propagation of the discharge signal through a stator winding. To determine whether these couplings take place in the slot-section of a winding or in the end-winding region, we removed the end-windings for three adjacent bars. The bars were connected in series by means of a short copper strip, as in Fig. 2.15. A pulse was injected at the beginning of the first bar. The responses were measured at two positions in each bar (points 1 to 6). The results are given in Fig. 2.16. The injected pulse propagates along the three bars in a transmission line mode and without any capacitive or inductive couplings between the three bars. The transit times in a single bar vary between 28 ns and 32 ns and correspond with the results for the fast mode (Fig. 2.9a). Apparently no coupling takes place in the slot-section of the winding, and the earlier described coupling occurs in the end-windings.

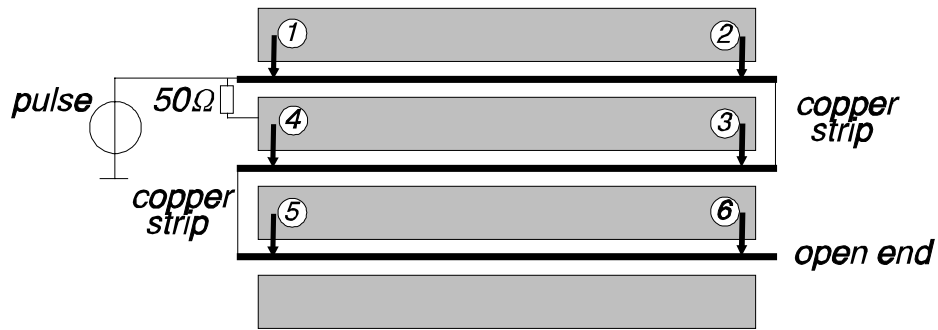


Figure 2.15 Setup for the determination of capacitive or inductive couplings between three adjacent bars (end-windings removed).

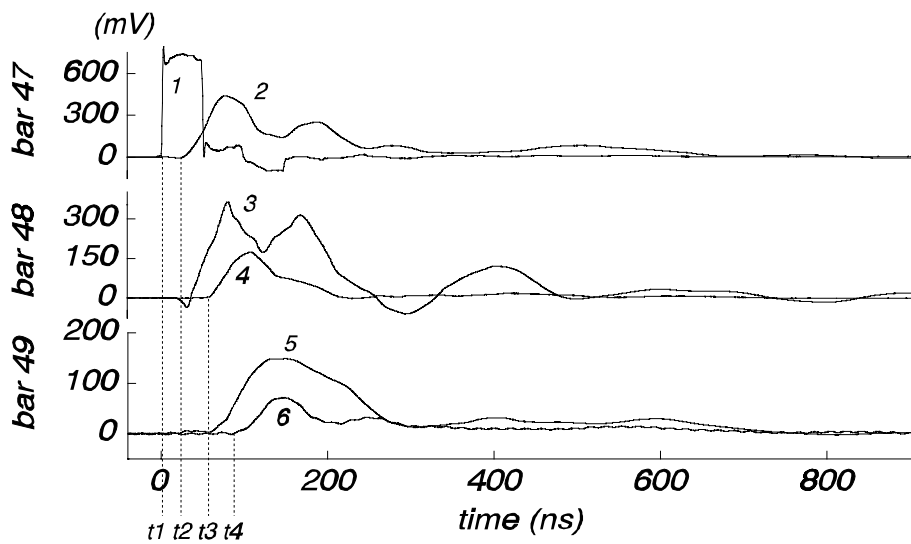


Figure 2.16 Responses at the six measuring points of Fig. 2.15.

2.4 Discussion

The results in the previous section show that a discharge signal follows a complicated path before it arrives at the generator terminals, where it can be measured:

- a stator winding acts as a transmission line. Therefore a discharge signal manifests itself at the generator terminals after a transit time that depends on the origin of the discharge
- due to capacitive and inductive couplings in the end-winding region, a second propagation mode is present for higher frequencies. This 'fast mode' manifests itself at the terminals without appreciable time delay
- the capacitive and inductive couplings also cause cross-talk between the phases
- the amplitudes of both the slow mode (or the transmission line mode) and the fast mode strongly depend on the origin of the discharge and decrease rapidly when the discharge occurs further away from the measuring terminal
- nevertheless the total charge at the terminals (derived by integration of the complete responses over a long enough period, including all frequency components) is only weakly dependent on the origin of the discharge.

These results have been obtained on a relatively small generator (35 MW), with bar lengths of about 3 m (including the end-winding part) and with only one bar in a slot. Generators with larger ratings have bar lengths from 5 to 7 m, while two bars are present in one slot. So we must be careful to generalize the results. Nevertheless, both in England [Wil85] and Australia [Jam86b], [Jam90] similar results were observed for large 500 MW turbine generators. In both papers the velocity of the slow mode is about 7 m/ μ s, which is in good agreement with our value (9.1 m/ μ s). Both authors conclude that the attenuation is much larger for higher than for lower (<1 MHz) frequencies. Not only for turbine generators, but also for hydro generators, similar results were found, and in [Sim95] it is shown that the time delay between the fast mode and the slow mode can be used to locate a discharge.

Pulse propagation through stator windings has been studied by many authors. Especially for the distribution of switching surges in multi-turn motor windings, accurate models have been developed for frequencies up to about 1 MHz [Kee90], [Gue97], [Dic88], [Nar89]. These switching surges have damaged the insulation of many motors, when interturn voltages became too high. The models incorporate a strong coupling between the multi-turn conductors in the same slot, while the coupling in the end-winding region is neglected. For turbine generators, only one or two bars are present in a slot, whereas the end-winding region has much larger dimensions. Thus it

is plausible that coupling between the windings occurs more strongly in the end-winding region and less in the slot-section of the winding, as we also showed in the previous section. Therefore these models, developed for motors, should be adapted for turbine generators.

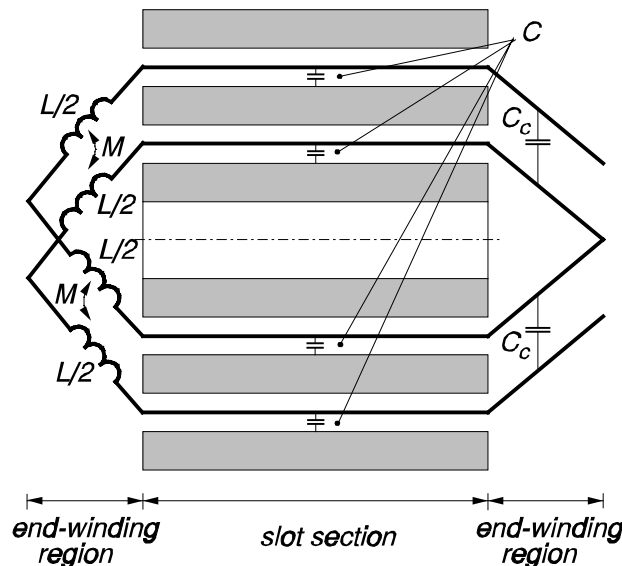


Figure 2.17 Schematic representation of a stator winding.

A simplified representation of a stator winding of a turbine generator is given in Fig. 2.17. The winding is composed of bars in slots that are interconnected in the end-winding region. Each bar in such a winding has the following relevant electrical parameters:

- capacitance C to the stator core (earth), concentrated in the slot-section
- inductance L , mainly determined by the end-winding region (in Fig. 2.17 for simplicity L is only drawn at one side)
- capacitive coupling C_c via the end-windings
- mutual inductance M via the end-windings.

When two bars (sometimes of different phases) are present in one slot, the representation becomes more complex, since capacitive and inductive coupling between the bars in the slot-section must be taken into account. In this discussion, this will be ignored.

Every single bar (including the slot part and the end-windings) can be regarded as a section of a transmission line. For the entire winding, these sections are all connected in series, as in Fig. 2.18. For simplicity, the capacitive and inductive couplings in the end-winding region are not shown in this figure. A partial discharge is

represented by the current-source i_{pd} . The return-path for this current is the stator core. However the stator core is laminated and an important question is how this current can pass the thin insulation layers between the laminations. Another complicated obstruction for the pd current i_{pd} are the cooling channels in the core.

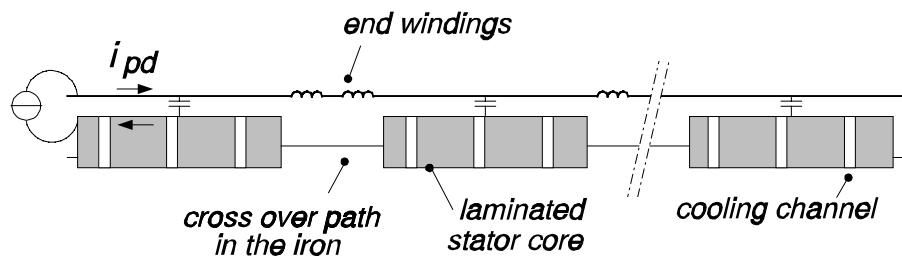


Figure 2.18 Transmission line representation of a stator winding.

Some authors ignore this [Kee90], [Gua97] and assume that the core behaves as solid steel. In this case, the current i_{pd} flows in a thin sheet at the surface of the iron, determined by the skin depth δ [Ram84] (see Fig. 2.19a). To calculate the inductance of this structure, we may regard the iron minus the skin layer as free of magnetic field. So most of the magnetic flux is present in the slot, however the contribution of the magnetic field in the skin layer may not be ignored due to the large relative permeability ($\mu_r > 1000$) of the iron.

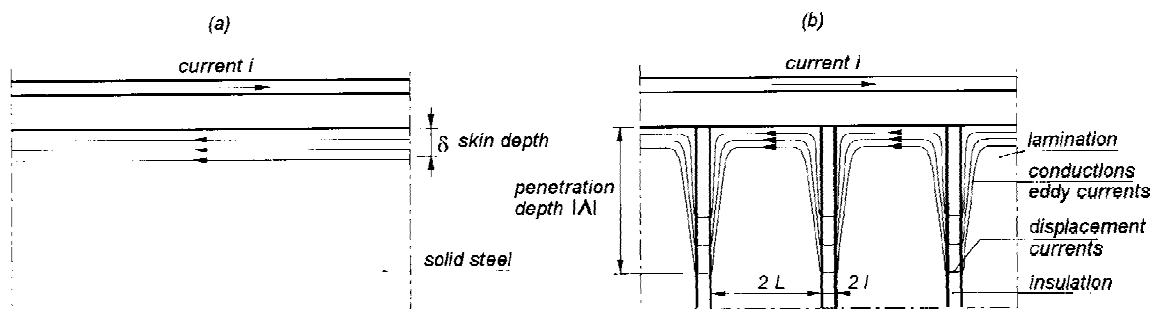


Figure 2.19 Current flow in a stator core; (a) neglecting the presence of laminations by regarding the core as solid steel, and (b) the effect of interlaminar displacement currents for a laminated core.

A more detailed representation for a laminated core is proposed in [Tav88] and is shown in Fig. 2.19b. The iron laminations themselves can carry the current i_{pd} . In the thin layer of insulation between the laminations, the current crosses over as a displacement current. The "penetration depth" Λ , defined in [Tav88] and indicated in Fig. 2.19, is larger than the skin depth δ , however Λ is still small compared to the dimensions of

the stator core, which limits the penetration of flux into the stator core.

Compared to the thin layers of insulation between the iron laminations, a cooling channel is a more complicated obstruction for the pd current i_{pd} . Since a cooling channel forms a relatively small capacitance (between 0.5 and 1 nF for a width between 3 and 10 mm), now only the higher frequencies (> 10 MHz) will cross over as a displacement current. Lower frequencies can only cross over via the tie bars⁴ at the back of the core (see Fig. 2.20). However, normally these tie bars are insulated from the laminations, but due to the appreciable capacitance between a tie bar and the laminations the pd current can flow. Note that DC and very low frequency components, e.g. 50 Hz, can only flow via the single grounding tie bar of the core.

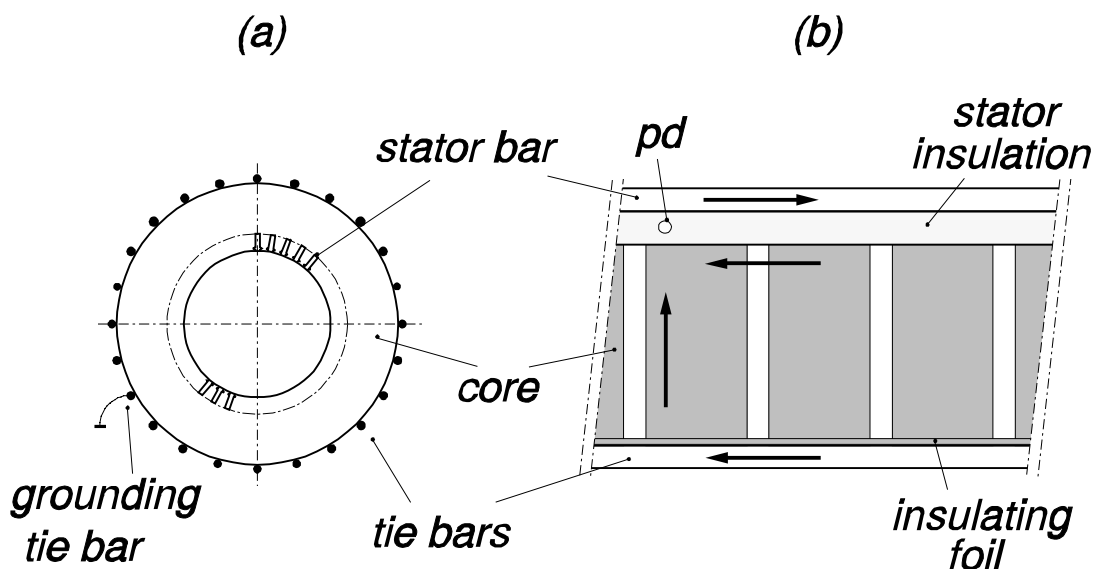


Figure 2.20 The effect of cooling channels on the propagation of pd currents through a stator core. The pd current is indicated with arrows. (A) Cross-section and (b) side view of a stator core.

A possible equivalent circuit for a stator winding (neglecting the effect of laminations and cooling channels in the stator core) is shown in Fig. 2.21. A single bar is represented by a T-section with capacitance C and two inductances $L/2$ (representing the end-windings at both ends of the bar). In contrast to a real transmission line, this T-section has lumped rather than distributed parameters. This series-chain of $L/2$ - C - $L/2$ T-sections has a characteristic impedance $Z_0 = \sqrt{L/C}$ and an overall wave velocity v

⁴a stator core is held together mechanically by many tie bars [Bri91], located at the circumference of the core. Tie bars are also needed to mount the core into a core frame and the generator housing. Normally all these tie bars (except one which grounds the core) are insulated from the stator core by thin foils

$= l / \sqrt{LC}$, where l is the total length of the winding [Gla48], [Dic91]. A partial discharge can be represented by a pulsed current-source, located at the appropriate place in the circuit.

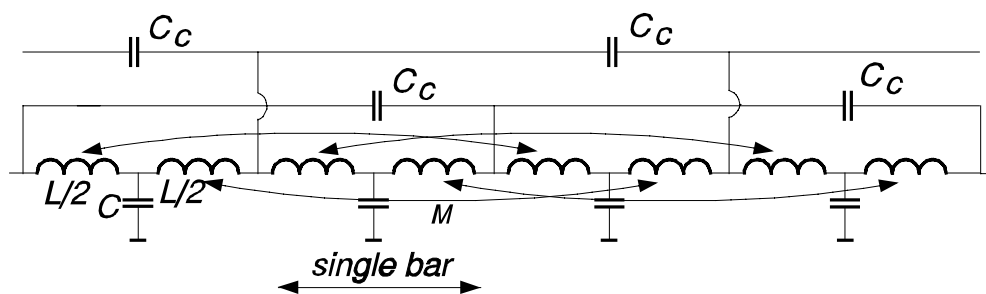


Figure 2.21 Equivalent circuit for a stator winding, neglecting the effect of laminations and cooling channels in the stator core).

Both the values for the overall winding capacitance C_{wind} and the overall inductance L_{wind} have been obtained from measurements at 100 kHz, using a Genrad Precision RLC-meter type GR1689. The measured capacitance for the entire winding C_{wind} is 212 nF and the measured inductance for the entire winding L_{wind} is 0.66 mH. The total length l of the winding is 89 m. Now the calculated wave velocity for the slow mode is 7.52 m/ μ s (for 100 kHz), which is a little less than the measured 9.1 m/ μ s. This is an indication that the inductance L_{wind} drops more for higher frequencies (the slow mode has frequency components up to 400 kHz). The calculated characteristic impedance Z_o is 56 Ω .

2.5 Summary and concluding remarks

To study the propagation of partial discharge pulses in a stator winding, we carried out experiments on an old 35 MW stator. Pulses, simulating discharges, were injected at various places in the winding, and the responses at the terminals were measured. The results show that a discharge signal follows a complicated path before it arrives at the generator terminals, where it can be observed:

- a stator winding acts as a transmission line. Therefore a discharge signal manifests itself at the generator terminals after a transit time that depends on the origin of the discharge
- due to capacitive and inductive couplings in the end-winding region, a second

propagation mode is present for higher frequencies. This 'fast mode' manifests itself at the terminals without appreciable time delay

- the capacitive and inductive couplings also cause cross-talk between the phases
- the amplitudes of both the slow mode (or the transmission line mode) and the fast mode strongly depend on the origin of the discharge and decrease rapidly when the discharge occurs further away from the measuring terminal
- nevertheless the total charge at the terminals (derived by integration of the complete response over a long enough period, including all frequency components) is only weakly dependent on the origin of the discharge.

In the discussion we describe a possible equivalent circuit for a stator winding. The entire winding can be regarded as a transmission line with lumped rather than distributed parameters. In the end-winding region, capacitive and inductive couplings must be taken into account. The described equivalent circuit must be regarded as a first approximation; the formation of a model that fully represents the complex propagation of partial discharge signals through a stator winding is hampered by:

- the 3-dimensional structure of the end-windings makes it very difficult to calculate values for inductances and capacitive couplings
- the thin insulation layers between the laminations of the stator core and the cooling channels in the stator core form complicating factors
- for larger stator windings, two bars (sometimes of different phases) are present in one slot. Now the representation becomes even more complex, since capacitive and inductive couplings between the bars inside the slot-section must be taken into account.

The complicated propagation of discharge signals through a stator winding has the following consequences for partial discharge measurements:

- since at lower frequencies more interference is present (see Chapter 4), we prefer measurements at higher frequencies. Therefore in that case only the 'fast mode' of the discharge signal is measured
- when discharges are measured at the generator terminals, the amplitude of the response depends strongly on the origin of the discharge. Especially the higher frequencies (the fast mode) are heavily damped for discharges that occur deeper into the winding. The consequence is that only discharges close to the measuring terminal can be observed. In practice this is expected not to be a serious disadvantage, since most discharges will take place in the high-voltage part of the winding
- electromagnetic couplings between the windings cause cross-talk between the phases.

This means that a signal measured in one phase does not necessarily originate from a discharge in this phase. To determine the phase where the discharge occurs, simultaneous measurements in all three phases are necessary. In practice, one can assume that the signal with the largest amplitude will show up in the phase where the discharge takes place

- the cross-talk between the phases depends on the origin of the discharge. Observing the cross-talk can therefore provide extra information. A single localized defect causes constant cross-talk. In the normal ageing process many discharge sites will be present in a stator winding, resulting in a large spread for the cross-talk.

Chapter 3

SENSORS FOR PARTIAL DISCHARGE MONITORING

3.1 Introduction

Partial discharges manifest themselves at the terminals of a generator as short current pulses (mA's) and corresponding voltage pulses (mV's). For on-line measurements of these external PD signals, special sensors must be installed at the generator, preferably as close as possible to the discharge source. When abnormal partial discharge levels are observed, extra checks must be possible, for instance by installing more than one sensor in each phase or by using extra sensors of a different type.

After consultation with Dutch utility companies and based upon the first series of measurements, the following requirements for sensors were decided upon:

- sensors should in no way endanger a safe and reliable operation of the generator. Therefore at present no sensors are allowed inside the generator and specifications of the sensors must meet all relevant standards
- installation of the sensors near the generator terminals or in the isolated-phase-bus (IPB) should be simple. For safety reasons, the sensors have to be installed during a generator stop, when the high-voltage system is grounded
- sensitivity must be high enough to measure the small partial discharge signals
- sensors must be more sensitive for the high-frequency PD signals than for the large 50 Hz currents and voltages. This makes differentiating sensors a good choice
- to measure the wave shapes of PD signals, a bandwidth up to 100 MHz is desirable
- good EMC-properties of the sensor are essential to avoid the pick-up of interference, which could lead to false alarms.

Sensors used by other authors do not completely meet these requirements, especially with regard to their EMC-properties (see discussion in Section 1.4). In this chapter we describe the various sensors that are used for the on-line measurements in this thesis [Pem93], [Pem97b]. Special attention is paid to good EMC-properties, therefore the question "precisely which voltage or which current are we measuring?" has to be faced. A capacitive sensor must measure the relevant line integral $\int \mathbf{E} \cdot d\mathbf{l}$ and a properly constructed current sensor should measure the enclosed current only. Also the

way a sensor is installed and connected to a measuring cable is important. The following sensors will be described:

- capacitive sensors: (i) bus-support-capacitors (capacitor inside a support insulator of the IPB) (Section 3.2.3 and Appendix B), (ii) ring capacitors inside the IPB (Section 3.2.4) and (iii) overvoltage capacitors housed inside the coaxial enclosure of a generator circuit-breaker (Section 3.2.5)
- a current sensor which can be installed at a generator terminal (Section 3.3)
- a pick-up loop which can be used as an additional sensor, to locate a discharge source when abnormal signals are observed (Section 3.4).

3.2 Capacitive sensors

3.2.1 Principle

The principle of a capacitive sensor is given in Fig. 3.1. The transfer function for this system is:

$$H(\omega) = \frac{j\omega RC_1}{1 + j\omega R(C_1 + C_2)} \quad (1)$$

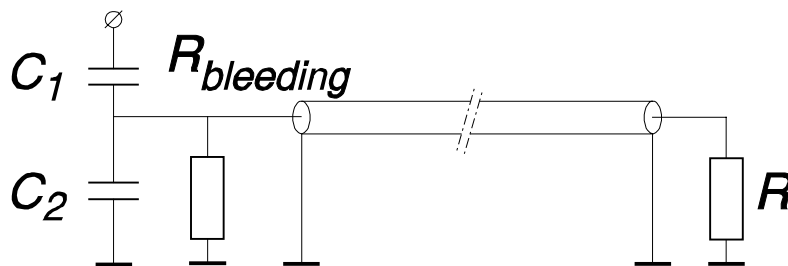


Figure 3.1 Principle of a capacitive sensor.

The sensor has a measuring capacitance C_1 and an unavoidable parasitic capacitance C_2 to ground. In the normal mode of operation, the sensor is connected to a measuring resistor R of 50Ω via a coaxial cable. However, when the coaxial cable is removed, the 50 Hz output voltage can become equal to the high voltage (especially when C_2 is small compared to C_1). This is a dangerous situation and therefore a $10 \text{ k}\Omega$ bleeding resistor is installed as in Fig. 3.1. The output voltage is then limited to a safe

value.

For low frequencies (50 Hz) the transferfunction (1) becomes $H(\omega)_{lf} = j\omega RC_1$ and has a differentiating character. For frequencies $\omega > 1/R(C_1 + C_2)$ the transferfunction becomes $H(\omega)_{hf} = C_1/(C_1 + C_2)$; the sensor then acts as a divider.

3.2.2 EMC-properties of capacitive sensors

The EMC-behavior of a capacitive sensor requires: (i) a compact lay-out so that the relevant line integral $\int \mathbf{E} \cdot d\mathbf{l}$ is correctly measured and (ii) a correct connection of the sensor to a measuring cable, so that common-mode currents are kept away from the sensor. In this section, these two requirements will be discussed more in detail.

It is important to keep the measuring circuit as compact as possible. The capacitive sensor in Fig. 3.2a measures the voltage V_c between the points 1 and 2 according to $V_c = \int \mathbf{E} \cdot d\mathbf{l}$. This measured voltage equals the actual voltage across the IPB. When the capacitor is placed outside the IPB, as in Fig. 3.2b, long leads are needed. Hence the time derivative $d\Phi/dt$ of the magnetic flux in the loop 1-2-3-4-1 is also measured. Mainly outside the IPB interfering magnetic flux can be present.

Common-mode currents [Hou90], [Laa97] on the measuring cable should not cause interference voltages. Thus the shield of the coaxial measuring cable should be correctly connected to the IPB, as in Fig. 3.2c. 'Correctly' means that a good quality plug with a low transfer impedance is used [Hor98] and that 'pig-tails' [Deu93] are avoided. Now a common-mode current I_{cm} , flowing on the cable braid, can continue on the IPB without coupling in interference.

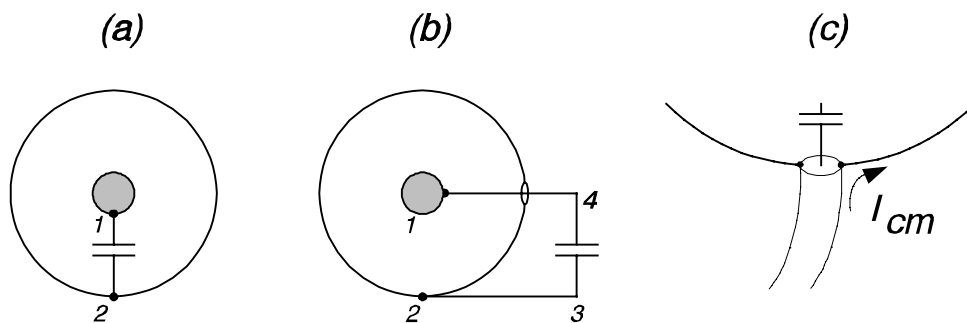


Figure 3.2 Cross-section of an IPB. When a capacitive sensor is correctly installed (a), the voltage across the sensor V_c equals the actual voltage across the IPB. When the sensor is placed outside the IPB (b), the time derivative $d\Phi/dt$ of the flux in loop 1-2-3-4-1 is also measured. When the capacitor is installed inside the IPB, common-mode currents on the measuring cable should not couple in interference (c).

3.2.3 Bus-support-capacitors

We designed a sensor unit that can replace a standard support insulator of the IPB. This sensor, a bus-support-capacitor, is shown in Fig. 3.3 and consists of a mica capacitor (capacitance between 100 and 500 pF) inside an epoxy-resin support insulator. Mica is chosen for its good high-voltage and high-frequency behavior. A bus-support-capacitor has a good sensitivity, bandwidth and EMC-properties. Mechanically and in term of insulation, it has the same specifications as a standard support insulator. A complete description is given in Appendix B.

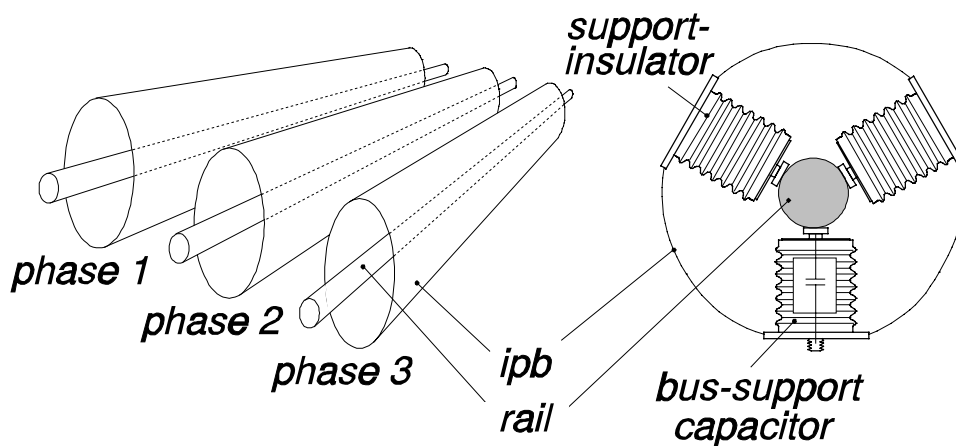


Figure 3.3 A bus-support-capacitor (a mica capacitor housed inside a standard support insulator), installed as a support insulator in the isolated-phase-bus (IPB).

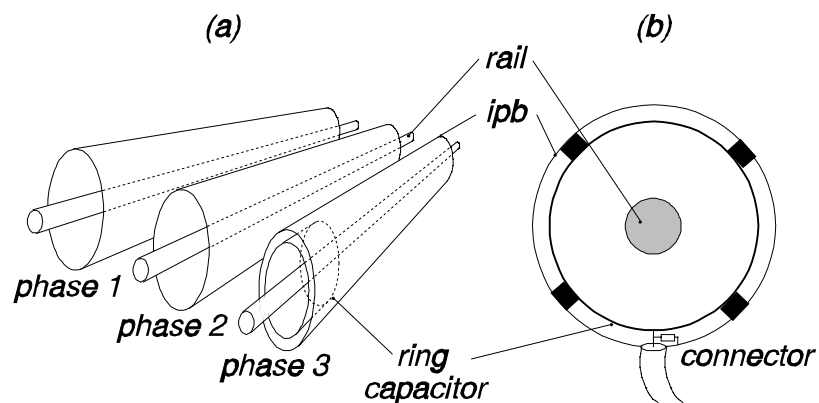
Bus-support-capacitors were built and installed in various power plants, see Table VI. In all cases, the installation could be completed within four hours. For each phase of a generator, two bus-support-capacitors have been installed; one close to the generator and one close to the step-up transformer. With the aid of the transit time between the two capacitors, it can be determined whether a partial discharge comes from the generator or from the step-up transformer.

Table VI Overview of bus-support-capacitors, installed at generators.

power plant	generator line-voltage	rated voltage for bus-support-capacitor	capacitance	commissioning test	installation
Hemweg-6 ⁵	14 kV ± 10 %	17.5 kV	500 pF	March 1993	May 1993
Hunze-4 ¹	14 kV ± 10 %	17.5 kV	500 pF	April 1995	Aug. 1995
Roca-3 gasturbine	15 kV +10 %	17.5 kV	250 pF	Jan. 1996	March 1996
Maasvlakte-1	21 kV +5 %	24 kV	100 pF	July 1996	July 1996 ⁶
Maasvlakte-2	21 kV +5 %	24 kV	100 pF	Feb. 1997	Sep. 1997 ²
Amer-8	21 kV +5 %	24 kV	100 pF	July 1997	April 1998

3.2.4 Ring-capacitors

The ring-capacitors are shown in Fig. 3.4. A metal ring (about 35 cm wide) is installed inside the IPB and connected to an N-connector. At the N-connector, a 10 k Ω bleeding resistor is installed. Ring capacitors were installed at both the gasturbine and the steamturbine generators of the Roca-3 power plant, see Table VII.

**Figure 3.4** Ring capacitors inside the IPB (only shown in phase 3).

⁵ we started with the development of the six bus-support-capacitors for generator Hemweg-6. After this generator was taken out of operation in 1995, the capacitors were re-tested according to the commissioning test program in Appendix B and installed in the Hunze-4 power plant.

⁶ one bus-support-capacitor for the Maasvlakte-1 power plant was slightly damaged during transport from the manufacturer to KEMA. This was only noticed during on-line measurements after installation in the power plant (see Chapter 9). All six capacitors were then removed and when necessary repaired. Again they passed a second commissioning test, after which they were installed in the Maasvlakte-2 power plant.

Table VII *Ring-capacitors and overvoltage capacitors of the Roca-3 power plant.*

generator	ring-capacitors		overvoltage capacitors	
	main capacitance C_1	capacitance to ground C_2	main capacitance C_1	capacitance to ground C_2
gasturbine 169 MW, 15 kV	16 pF	182 pF	132 nF	8 μ F
steamturbine 126 MW, 15 kV	16 pF	182 pF	132 nF	8 μ F

Also the power plants Amer-9 and Hemweg-8 are fitted with ring-capacitors. However, in both power plants they were not used for measurements.

3.2.5 Overvoltage capacitors

Sometimes generators are connected to a generator-circuit-breaker, which is an integral part of the IPB. In the ABB type HEK generator-circuit-breakers [ABB87], overvoltage capacitors are installed inside the coaxial enclosure of the breaker, as shown in Fig. 3.5. The capacitor is designed as a capacitive divider, with a measuring capacitance C_1 is much smaller than the capacitance to ground C_2 (132 nF and 8 μ F respectively). The 50 Hz output voltage is limited (to about 140 V for 15 kV) and no bleeding resistor is required. However a partial discharge measuring instrument must be connected via a high-pass filter (cut-off frequency 100 kHz), since the 50 Hz voltage is too large for its input. These overvoltage capacitors are present in both the gasturbine and the steamturbine generators of the Roca-3 power plant, see Table VII.

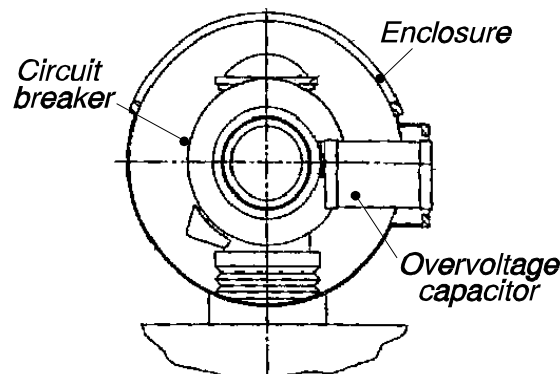


Figure 3.5 *A overvoltage capacitor, housed inside the coaxial enclosure of a generator-circuit-breaker. The generator-circuit-breaker is an integral part of the IPB.*

3.3 Toroidal single-turn inductive current sensor

3.3.1 Introduction

Partial discharges cause fast current pulses that can be measured at the terminals of a generator. A widely used current sensor is the Rogowski-coil [Rog12], [Bel85], with its well known advantages: (i) selectivity (it measures only an enclosed current and its sensitivity for other sources of magnetic fields is zero), (ii) linearity (the coil has an air core, no iron), (iii) the bandwidth can be large, and (iv) it measures the derivative of an enclosed current and is therefore more sensitive for the high frequency discharge signals than for the large 50 Hz currents.

To avoid flashover, the radius of a current sensor around a terminal must be large (at least 230 mm). A Rogowski-coil with a large radius generally has a lower resonance frequency, since the coil has a large parasitic capacitance, especially if additional shielding against interference is used. Several techniques to increase the bandwidth are available for small coils: (i) reducing the number of turns [Hel95], (ii) terminating the coil with its characteristic impedance [Sty82], (iii) using many parallel conductors [Smu86] or (iv) damping internal resonances with resistors between the windings [And71]. However these techniques fail for larger coils.

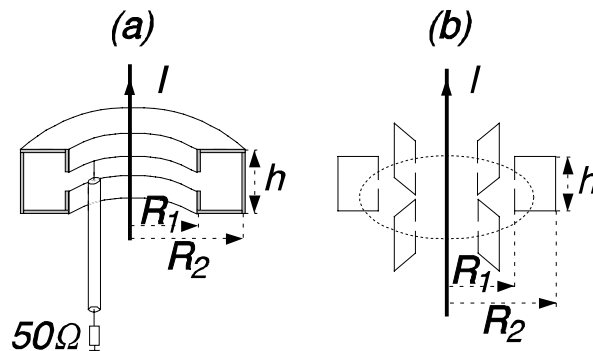


Figure 3.6 (a) The toroidal single-turn inductive current sensor, and (b) its equivalent: a set of single-turn loops positioned at equidistant positions around a conductor.

Since we aim at a resonance frequency of at least 100 MHz, we developed an alternative current sensor (see Fig. 3.6a). This single-turn structure is constructed in two halves, so that it can easily be installed around a generator terminal. The magnetic flux, caused by the enclosed current, induces a voltage over the gap of the structure, which can be measured by means of a $50\ \Omega$ measuring resistor.

This toroidal single-turn current sensor will be described in Section 3.3.3 and it will be shown that this structure behaves nearly similar to the set of single-turn loops

shown in Fig. 3.6b. Due to this similarity we start, in Section 3.3.2, with a discussion of this set of single-turn loops.

3.3.2 Single-turn loops

In Fig. 3.6b, the current I is measured by means of a set of single-turn loops, each having a large bandwidth, positioned at equidistant positions around the conductor. In this Section, the following aspects will be discussed: sensitivity, selectivity, inductance and resonance frequency. In part of this Section, the "single-turn loop" is constructed from a wide metal plate.

Sensitivity⁷; the output voltage V_o of each loop is given by $V_o = j\omega MI$. The mutual inductance M is determined by the dimensions and, for the rectangular loop in Fig. 3.6b, is given by $M = (\mu_o h / 2\pi) \ln(R_1/R_2)$. In practice, M is limited by the available space and the required radius to avoid flash-over. When the voltages of all the loops are added, the total measuring voltage becomes $j\omega nMI$, with n is the number of loops. Thus the sensitivity is increased by a factor n .

Selectivity; preferably a current sensor must only measure an enclosed current and the sensitivity for external magnetic fields must be zero. In other words, a current sensor must correctly measure the contour integral $\oint H \cdot dl$ along the dotted line in Fig. 3.6b. For an enclosed current, this contour integral equals the enclosed current I . For a non-enclosed current, or for any external magnetic field, this contour integral is zero. To approximate this contour integral, the outputs of the loops must be added. It is obvious that the best selectivity is obtained with an infinite number of loops. In the next Section 3.3.3, we however show that an acceptable selectivity is already achieved with four loops at equidistant positions.

The inductance of a loop can be measured as shown in Fig. 3.7. The input impedance Z_{in} is measured by means of a network analyzer [Hew67]. As can be seen, this impedance corresponds at lower frequencies to the $j\omega L_{loop}$ of the loop and shows a peak at the resonance frequency. The inductance depends on the width of a loop (Fig. 3.8). For loops with a width < 0.5 m, the inductance L_{loop} of the rectangular loop can be approximated by $L_{loop} = \mu_o \cdot a \cdot h / \text{width}$ (the line in Fig. 3.8). In this case, the currents through the loop are mainly in the x and y direction and thus the magnetic field inside the loop is in the z direction (see Fig. 3.9a).

⁷for a loop with $R_1=320$ mm, $R_2=400$ mm, $h=120$ mm, the mutual inductance M is 5.4 nH. This gives a total measuring voltage for a set of four loops of 1.4 V/A at 10 MHz.

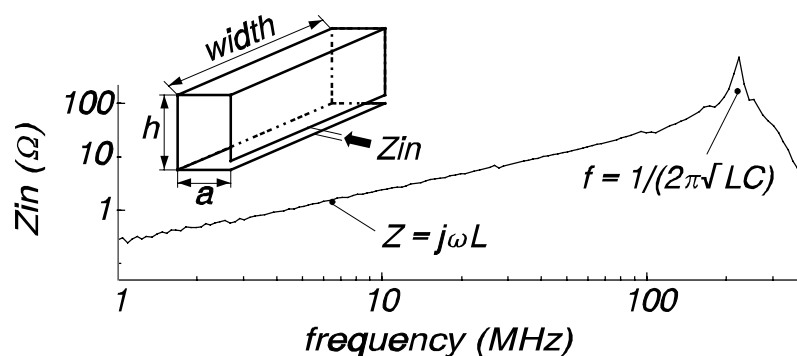


Figure 3.7 Measured input impedance Z_{in} versus frequency for a rectangular single-turn loop with $a=80$ mm, $h=120$ mm and width=0.4 m. The impedance corresponds to an inductance of 40 nH and the resonance frequency is 220 MHz.

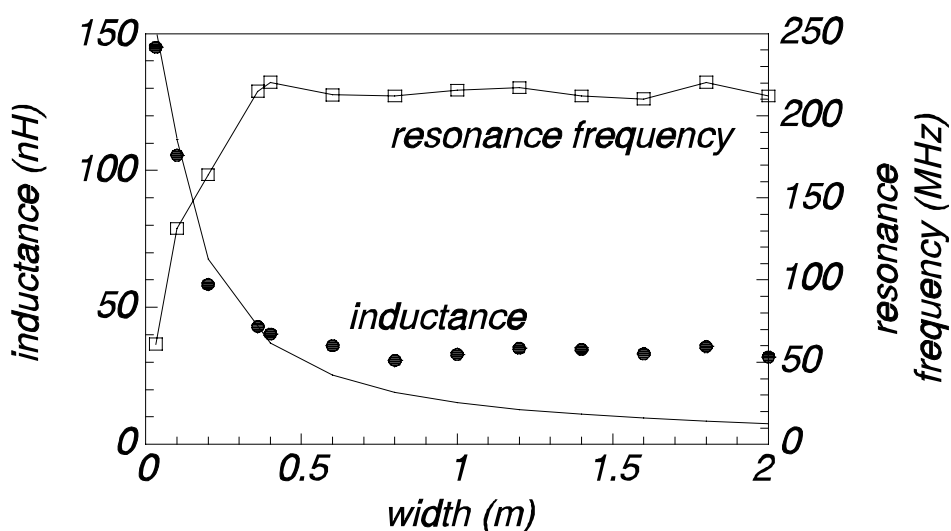


Figure 3.8 Resonance frequency and inductance (dots: measured, line: calculated) versus the width for a single-turn loop with $a = 80$ mm and $h = 120$ mm.

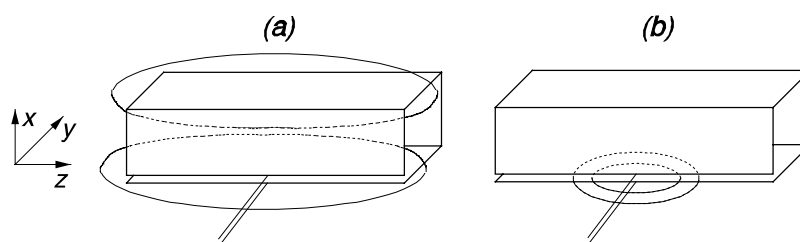


Figure 3.9 (a) Main flux in a single-turn loop, corresponding with currents in the x and y direction. Due to currents in the z -direction near the feedpoint, flux leaks through the gap of the loop (b).

For loops wider than 0.5 m, the measured inductance no longer decreases but has a nearly constant value of about 30 nH. This indicates that, in addition to the main flux as in Fig. 3.9a, an additional flux is present. This flux corresponds with the complicated current distribution near the measuring terminal. Besides currents in the x and y direction, also a strong component is present in the z direction. This z - component is accompanied by a 'leakage flux' through the gap of the loop (Fig. 3.9b). Since this leakage flux is associated with the currents local to the measuring terminal, the inductance no longer depends on the width and remains constant.

The resonance frequency is associated with the total inductance and by the parasitic capacitance across the gap of the loop. As expected, for loops with a width <0.5 m, the resonance frequency increases with increasing width. However for wider loops, the resonance frequency remains nearly constant at about 230 MHz.

3.3.3 The toroidal single-turn current sensor

In the previous Section 3.3.2 it was shown how a current I can be measured by means of a set of single-turn loops, positioned at equidistant positions around the conductor. A high resonance frequency can be obtained by using wide loops; for a width >0.5 m the resonance frequency was found to be about 230 MHz.

The practical realization of this principle is shown in Fig. 3.10a [Bau78], [Tin93]. Instead of a set of wide single-turn loops, a toroidal single-turn structure which completely encloses the conductor is used. Now the mechanical rigidity is better and installation of the sensor is much simpler than for a set of individual loops. The magnetic flux, caused by the enclosed current, induces a voltage over the gap of the structure. This voltage is measured by connecting coaxial cables at several equidistant points, and all measured voltages are added. In this Section, the following aspects will be discussed: sensitivity, selectivity, the addition of the voltages of the several measuring points, flux leakage and resonance frequency.

Sensitivity; the output voltage V_o at each measuring point is given by $V_o = j\omega MI$. The mutual inductance M for a current which is positioned in the center of the sensor (current I_l at $[a, \beta] = [0, 0^\circ]$, see Fig. 3.10b) is given by $M = (\mu_o h / 2\pi) \cdot \ln(R_1 / R_2)$. In practice, M is limited by the available space and the required radius R_1 to avoid flash-over to the generator terminal. When the voltages of all the measuring points are added, the total measuring voltage becomes $j\omega nMI$, with n is the number of measuring points. Thus the sensitivity is increased by a factor n [Sch94b].

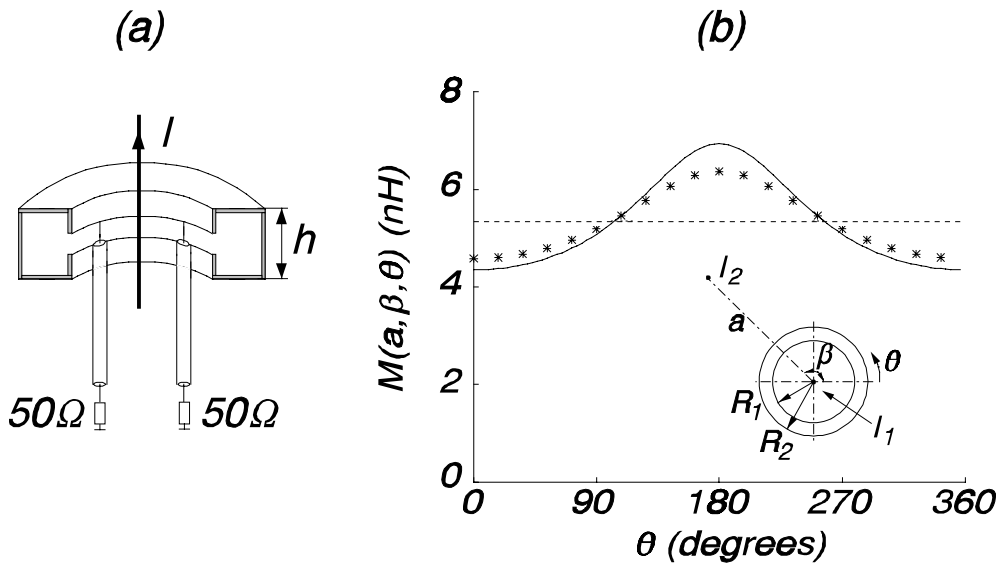


Figure 3.10 (a) The toroidal single-turn inductive current sensor, and (b) its mutual inductance $M(a, \beta, \theta)$ when only one measuring cable is connected at position θ . The mutual inductance for the case that only I_1 is present is given by the dotted line. When also the return conductor is present at location I_2 , the total mutual inductance is given by the solid line (calculated) and the asterisks (measured). ($R_1=0.32$ m, $R_2=0.4$ m, $h=0.12$ m, I_1 positioned at $[a, \beta]=[0, 0^\circ]$, I_2 positioned at $[a, \beta]=[1.57$ m, $180^\circ]$).

Selectivity; besides the flux caused by the enclosed current I_1 , also flux from a non-enclosed current I_2 can couple in and will cause a voltage at the measuring points. This 'flux-leakage' will be discussed in detail at the end of this Section. Due to this flux leakage, the voltage at a measuring point turns out to be nearly the same as the output voltage of a single-turn loop at the same position.

This is illustrated in Fig. 3.10b. The sensor, with one measuring point, encloses a current I_1 in the center (position $[a, \beta] = [0, 0^\circ]$). Outside the sensor, at position $[a, \beta] = [1.57$ m, $180^\circ]$, the return conductor carrying current $I_2 = -I_1$ is present. If only current I_1 would be measured, the mutual inductance $M(a, \beta, \theta)$ does not depend on the position of the measuring point and is equal to 5.4 nH (dotted line). However, as can be seen, also the flux belonging to the return current I_2 couples in, resulting in an $M(a, \beta, \theta)$ which depends on the position of the measuring point.

The mutual inductance $M(a, \beta, \theta)$ for a non-enclosed current at position $[a, \beta]$ can be approximated by equation (2), which is valid for a rectangular single-turn loop at position $[R_1, R_2, \theta]$. As can be seen from Fig. 3.10b, the calculated $M(a, \beta, \theta)$ (solid

line) is not exactly equal to the measured values. This shows that the toroidal single-turn current sensor slightly suppresses the flux from a non-enclosed current, which is of course an advantage. It can be seen from equation (2) that there are some positions at which the sensitivity $M(a, \beta, \theta)$ for a non-enclosed current I_2 is zero. This is the case when $a \cdot \cos(\beta - \theta) = \frac{1}{2} \cdot (R_1 + R_2)$.

$$M(a, \beta, \theta) = \frac{\mu_o h}{4 \pi} \ln \frac{R_2^2 + a^2 - 2 a R_2 \cos(\beta - \theta)}{R_1^2 + a^2 - 2 a R_1 \cos(\beta - \theta)} \quad (2)$$

$$R_1 < R_2 < a$$

The above analysis is valid for only one measuring point. To increase the selectivity, more than one measuring point must be used and the voltages of all these points must be added. It is obvious that the best selectivity is obtained with an infinite number of measuring points.

To determine how many measuring points are needed to obtain an acceptable selectivity, a selectivity ratio will be used. This is the ratio of the sensitivity for a non-enclosed current $M(a, \beta, \theta)$ and the sensitivity for a current through the center of the sensor $M(0, 0, \theta)$. The selectivity ratio will be calculated for n measuring points at equidistant positions θ_i and is defined as:

$$\text{Selectivity Ratio} = \sum_{i=1}^n \left| \frac{M(a, \beta, \theta_i)}{M(0, 0, \theta_i)} \right| \quad (3)$$

$$\text{with } \theta_i = \frac{2 \pi (i - 1)}{n}, \quad i = 1, 2, \dots, n$$

Figure 3.11 shows the selectivity ratio for 2 up to 9 measuring points. The magnitude of the selectivity ratio is represented by four shadings: white, light gray, dark gray and black. The darker the area, the larger the selectivity ratio, or the higher the sensitivity for non-enclosed currents. As can be seen, the sensitivity for non-enclosed currents decreases rapidly with increasing number of measuring points.

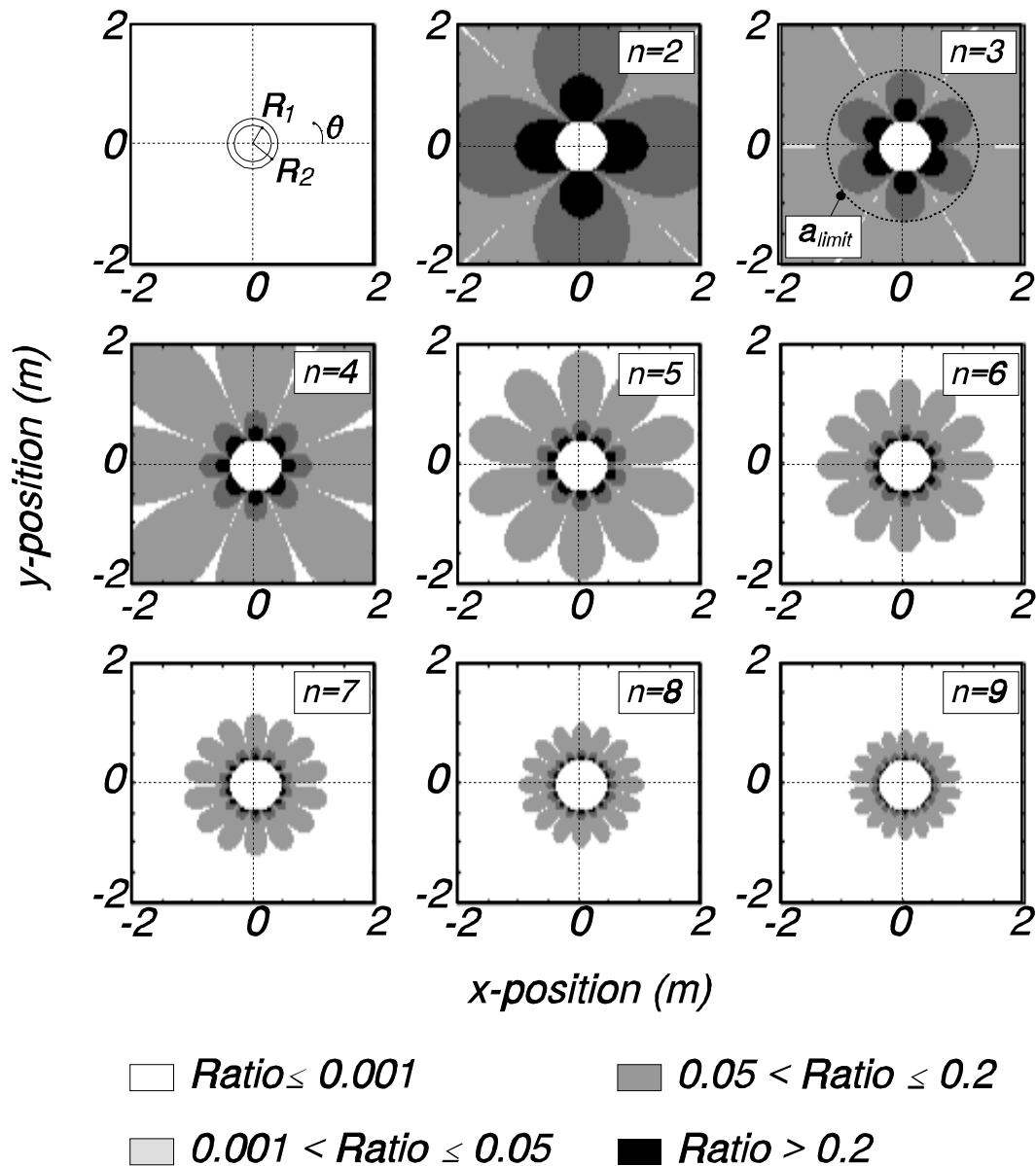


Figure 3.11 The selectivity ratio calculated for various number of measuring points $n = 2$ to 9 , for a sensor with $R_1 = 0.32$ m, $R_2 = 0.4$ m, and varying a and β ($a > R_2$). The measuring points are positioned according to equation (3).

As a limit, we accept a selectivity ratio of maximum 0.05. This means that when the enclosed and the non-enclosed current have equal magnitudes, 5 % of the non-enclosed current will be seen by the sensor. So all positions in Fig. 3.11 with a white or a light gray color are acceptable. If we look at the figure for $n = 3$, all

positions at a distance $a > 1.2$ m from the center of the sensor are acceptable. This distance a_{limit} is indicated with the dotted circle. Figure 3.12 gives this distance a_{limit} as a function of the number of measuring points. For a large number of measuring points, a_{limit} reaches the outer radius of the sensor R_2 .

For measurements on generators, sensors will be installed around the three high-voltage terminals of the generator. The distance between the terminals is at least 1.2 m [Pee98]. This means that with four measuring points an acceptable selectivity is achieved (for $n = 4$, $a_{limit} = 0.9$ m). Also the summation of the voltages is much easier for four measuring points than for five measuring points, as will be shown later in this Section.

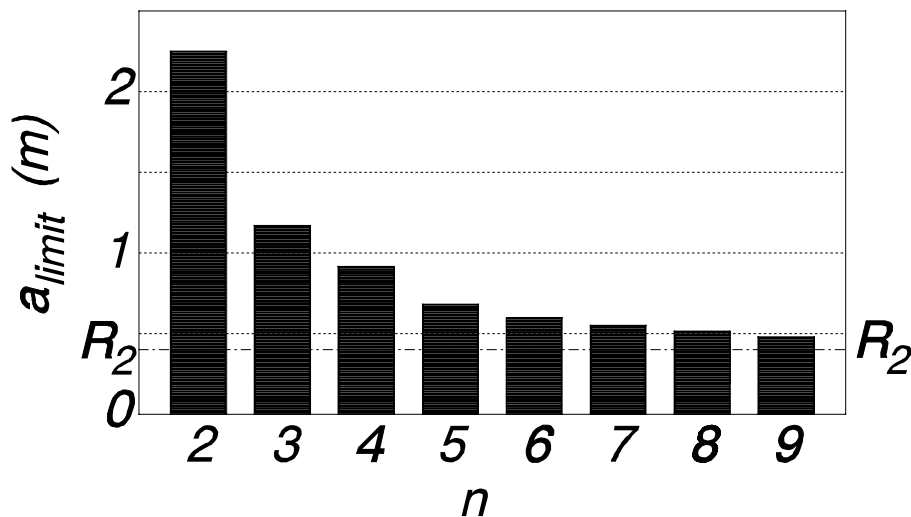


Figure 3.12 The calculated distance a_{limit} versus the number of measuring points. The toroidal single-turn inductive current sensor is nearly insensitive for a non-enclosed current if the distance to the center of the sensor is $> a_{limit}$ ($R_2 = 0.4$ m).

Figure 3.13 shows experimental results of using more than one measuring point. We used the same configuration as for Fig. 3.10b, now however with 2, 3 or 4 equidistant measuring positions. The sensor encloses a current I_1 , which is positioned in the center of the sensor. The bars give the sum of the voltages at the various measuring points. It can be seen that the total measured voltage increases when more measuring points are used.

Figure 3.13 also gives the results when a second conductor, carrying $I_2 = -I_1$ is positioned outside the sensor at $[a, \beta] = [1.57 \text{ m}, 180^\circ]$. The measurements were done for three different positions of the first measuring point, indicated in the Figure as an

offset θ_o . For $n = 2$, a small amount of flux from conductor I_2 is measured, resulting in a deviation of the total voltage compared to the situation where only I_1 is enclosed of 9.5 %. When three measuring points are used, this deviation is less than 5 %, and when four measuring points are used, the deviation is less than 2.5 %.

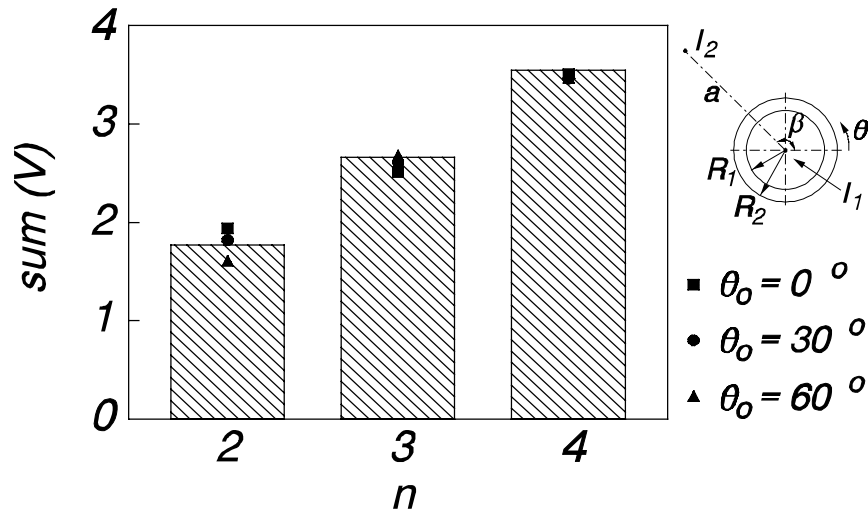


Figure 3.13 The hatched bars give the sum of the output voltages for 2, 3 or 4 equidistant measuring points, for an enclosed current I_1 positioned in the center of the sensor. The points give the sum of the output voltages when also a second conductor, carrying a current $I_2 = -I_1$, is present outside the sensor at $[a, \beta] = [1.57 \text{ m}, 180^\circ]$, and for three different offsets θ_o of the first measuring point.

At each measuring point, the induced voltage is measured by means of a resistor R of 50Ω at the end of a long measuring cable. A balun transformer (see Fig. 3.14) makes it possible to connect these resistors in series. The balun transformer must be used, otherwise the sensor is short-circuited. A description of the balun transformer is given in Appendix C. As described there, the output voltage is equal to $j\omega nMI$. So the system measures the derivative of the enclosed current I , and the output voltage is increased by a factor n . This can also be seen in Fig. 3.15, which shows the measured transfer function in the frequency range from 0.1 to 100 MHz.

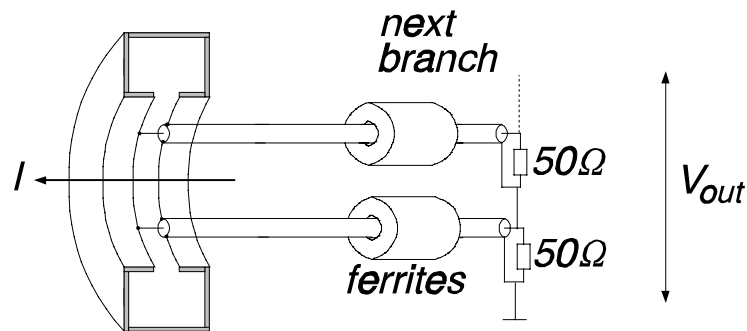


Figure 3.14 Toroidal single-turn inductive current sensor and the balun transformer.

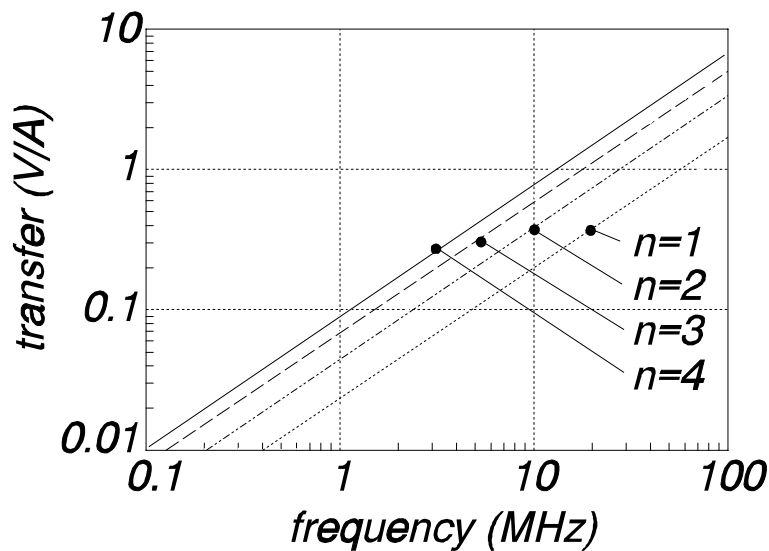


Figure 3.15 Measured transfer function of a toroidal single-turn inductive current sensor and balun transformer for $n = 1$ to 4. The transfer function is equal to $j\omega n M$.

As for the single-turn loop (Section 3.3.2), the behavior of the toroidal single-turn current sensor is strongly influenced by the magnetic flux which leaks in or out through the gap of the sensor. This flux leakage will be illustrated for the situation where a current is injected into the sensor. The main part of this current is in the z and r direction, and the corresponding flux remains inside the sensor, as in Fig. 3.16a. This flux corresponds to an inductance $L_{main} = (\mu_o h / 2\pi) \ln(R_1/R_2)$. However, due to the θ -currents near the injection point, a strong additional flux leaks in and out of the gap, as shown in Fig. 3.16b.

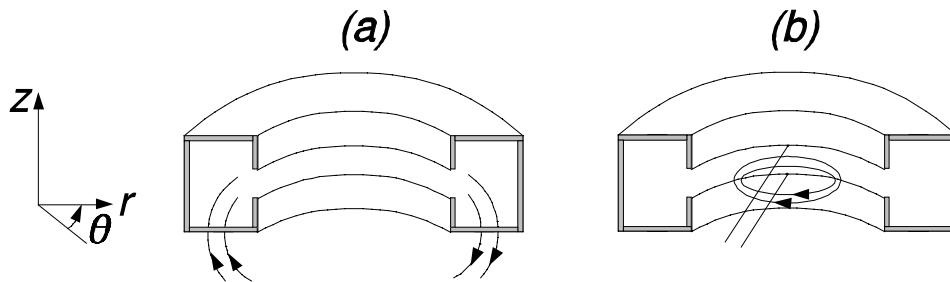


Figure 3.16 (a) Main flux in a toroidal single-turn inductive current sensor, corresponding to a current in the z and r direction. Due to currents in the θ direction, flux leaks in and out of the gap of the sensor (b).

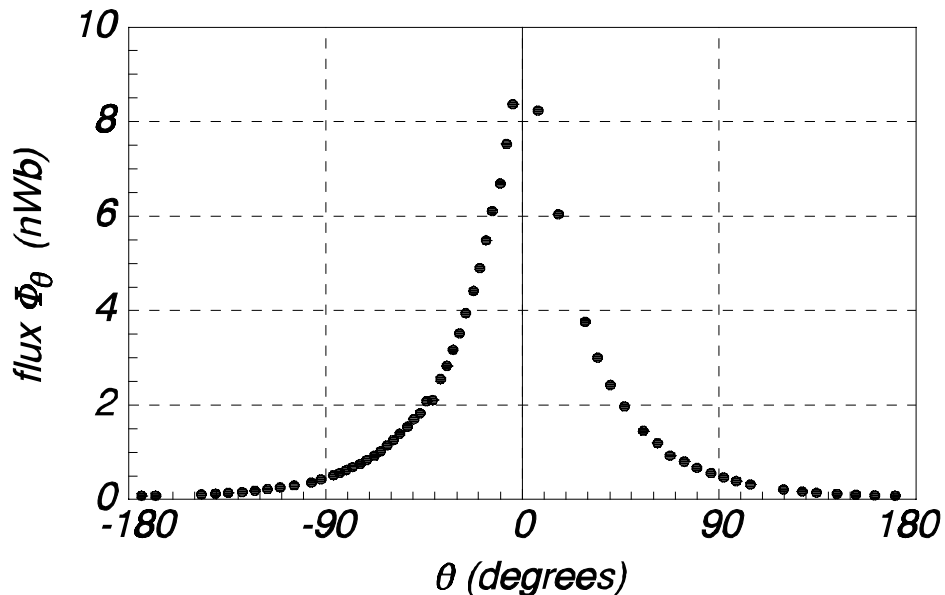


Figure 3.17 Local magnetic flux Φ_θ along the gap of the toroidal single-turn inductive current sensor, when a current of $0.4 A_{\text{rms}} / 1 \text{ MHz}$ is injected at $\theta = 0^\circ$.

A measurement of the flux leakage is given in Fig. 3.17. A current of $0.4 A_{\text{rms}}$ at a frequency of 1 MHz was injected into the sensor at $\theta = 0^\circ$ and the voltage along the gap was measured as a function of θ . From this measured voltage, the flux Φ_θ through the (z,r) cross section at the measuring point can be determined from $V_{\text{meas}} = j\omega\Phi_\theta$. When no flux leakage would occur, this flux would be constant at every position. However, as can be seen, the local flux strongly depends on the measuring position which is only possible when flux leaks to the outside through the gap.

The resonance frequency f_o of the toroidal single-turn inductive current sensor is mainly determined by the total inductance and by the parasitic capacitance across the gap. The resonance frequency can be derived from a measurement as in Fig. 3.18 [Hew, 1967]. By means of a network analyzer, the input impedance Z_{in} is measured. At lower frequencies, this impedance corresponds to the total inductance of the sensor, in this case 38 nH. The peak corresponds to a resonance frequency of 235 MHz.

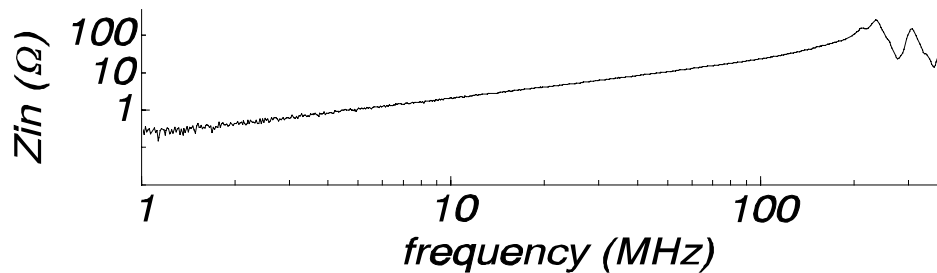


Figure 3.18 Measured input impedance Z_{in} of a toroidal single-turn inductive current sensor. At lower frequencies the impedance corresponds to an inductance of 38 nH and the resonance frequency is 235 MHz.

Toroidal single-turn inductive current sensors were built and installed in various power plants. An overview is given in Table VIII.

Table VIII Overview of toroidal single-turn inductive current sensors, installed at generators.

power plant	Number of sensors	R_1 (m)	R_2 (m)	h (m)	M (nH)	L (nH)	f_o (MHz)	installation
for testing in TUE lab	1	0.32	0.40	0.12	5.4	38	222	-
Hemweg-6, HV terminals	3	0.45	0.52	0.20	5.4	-	-	Oct. '91
Hemweg-6, LV terminals	3	0.26	0.34	0.06	3.2	-	-	Oct. '91
Amer-9	3	0.23	0.35	0.18	14.3	59	129	Feb. '94
Hemweg-8	3	0.23	0.45	0.065	8.5	49	152	Oct. '94

3.4 Pick-up loops

When abnormal partial discharge patterns are recorded, one has to verify that: (i) the recorded signals are indeed caused by discharges and not by interference, and (ii) whether the discharges come from the generator or from other high-voltage components (e.g. the step-up transformer, measuring transformers or support-insulators in the IPB). Valuable information can be derived when two or more high-frequency sensors are used in each phase. Now, if we measure the transit-times between the sensors, the signal-source can often be localized.

A simple, but effective additional sensor that can be used for this purpose is a pick-up loop as in Fig. 3.19. Such a pick-up loop can be positioned near a current-carrying conductor to measure the derivative of the enclosed magnetic flux (therefore it is more sensitive to high-frequency partial discharges than to large 50 Hz currents). In most cases, pick-up loops are positioned outside the region of reduced flux in the isolated-phase-bus (IPB, see Appendix D); therefore close to the terminals of the generator, or close to the step-up transformer or auxiliary transformers (or other possible signal sources). Examples are given in Chapters 6, 7 and 9. However, in some cases it is possible to place the pick-up loops between the grounded sheaths of the IPB, as is shown in the Hemweg-6 power plant (Chapter 5).

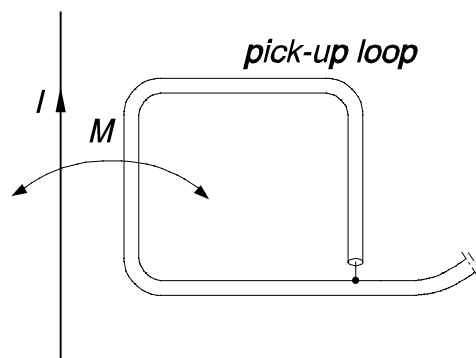


Figure 3.19 A simple pick-up loop that can be used as an additional sensor to locate a discharge source

Pick-up loops were used for measurements at 4 generators. An overview is given in Table IX. The loops used for these measurements were constructed by connecting the inner-conductor of a coaxial cable (RG224) to the outer conductor as in Fig. 3.19. The pick-up loops have a resonance frequency of 25 MHz. The sensitivity depends on the position of the loop relative to the current carrying conductor.

Table IX *Overview of measurements with pick-up loops.*

generator	position of the pick-up loops	discussion of results
Hemweg-6	between grounded sheaths of the IPB	Chapter 5, Section 5.4
Maasvlakte-1	near the terminals of the generator, the step-up transformer and auxiliary transformers	Chapter 9, Section 9.2
Amer-9	near the generator terminals and near sparking shaft-grounding and excitation brushes	Chapter 6, Section 6.3.3
Hemweg-8	near the terminals of the generator and the step-up transformer	Chapter 7, Section 7.4.2

Chapter 4

MEASURING TECHNIQUES AND SIGNAL HANDLING

4.1 Introduction

Measurements on partial discharges in generators, during regular operation of the generator, can be hampered by the intense interference present in a power plant. Although state-of-the-art EMC techniques reject interference to a large extent, disturbances can still couple into the stator winding and show up at the sensors, even when the measuring system itself is fully protected against interference. This remaining interference has to be rejected by a proper refinement of the measuring process.

A method to reject this remaining interference is to take advantage of the fact that both PD signals and interference have different signal characteristics, such as: position on the 50 Hz waveform, resonance frequencies, rise-time and pulse duration, repetition rate, pulse polarity and magnitude, and finally magnitude distribution. To separate interference from partial discharges, characteristics have to be found which are unique for PD signals. As an example, Table X gives a comparison of signal characteristics for PD-signals and interference caused by a radio transmitter.

Table X *Overview of different characteristics for a PD signal and interference caused by a radio-transmitter.*

signal characteristic	PD signal	interference from radio transmitter
position on 50 Hz voltage	grouped in 1 th and 3 th quadrant	continuous
frequency spectrum	broad and/or many resonance peaks	narrow
resonance frequencies	many	one central frequency
pulse polarity	different for both half-cycles of the 50 Hz	-
magnitude distribution	broad	peaked

For the practical realization of this principle, we developed two alternatives. In the first alternative PD pulses are measured in the time-domain on a pulse-by-pulse basis. By means of signal processing, remaining interference pulses are rejected. This technique is described in Section 4.2 and illustrated by measurements on the 125 MW

generator Hemweg-6. For the second alternative, a tunable narrow-bandwidth filter is used. The filter is tuned to a frequency where PD's are strong and interference is weak. This technique is described in Section 4.3 and is illustrated by measurements on the 650 MW generator Hemweg-8. The full results of the measurements on these generators are discussed in Chapter 5 (Hemweg-6) and Chapter 7 (Hemweg-8).

4.2 Time domain measurements

4.2.1 Measuring system and procedure

The first method to distinguish between PD's and interference is to measure pulses in the time-domain on a pulse-by-pulse basis [Pem95]. By means of signal processing each pulse is judged individually, and thereby classified as either a true partial discharge or as interference or cross-talk from the other phases.

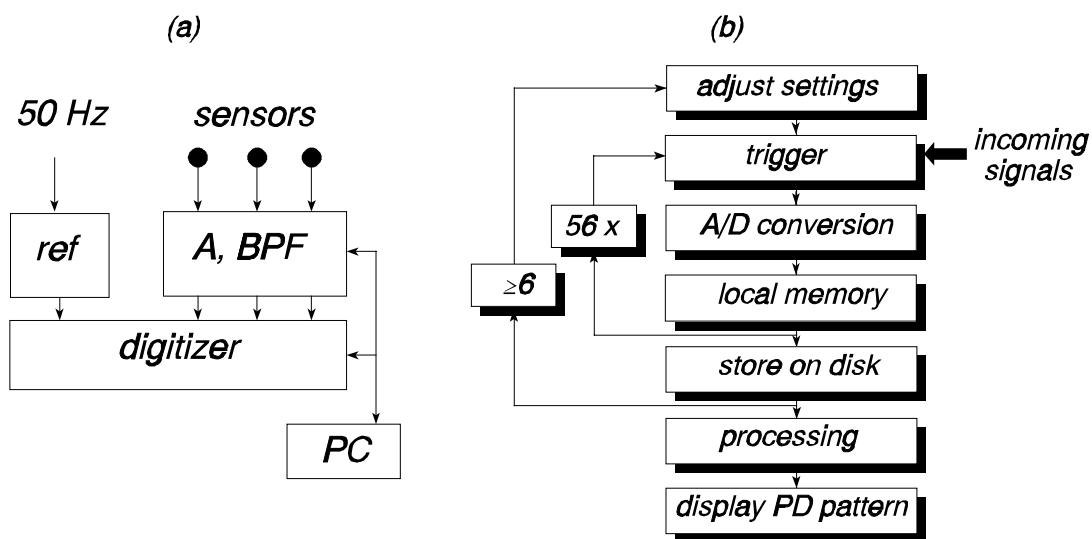


Figure 4.1 (a) *Measuring system and (b) procedure for time domain measurements.*

Figure 4.1a shows the measuring system for the time domain measurements. The system can work with three sensors; one in each phase. All sensor outputs are recorded simultaneously by a digitizer with 500 MSamples/s and a record length of 5120 samples (Tektronix DSA602A). For signal conditioning, an amplifier A (amplification between 1 and 50) and a band-pass-filter BPF (lf cut-off at 1 kHz, hf cut-off adjustable between 20 and 100 MHz) is used in each channel. To determine the

position of a signal on the 50 Hz voltage waveform, a reference signal is recorded on a 4th channel. All settings and measurements are controlled by a portable computer.

Partial discharges are recorded on a pulse-by-pulse basis. The measuring procedure is given in Fig. 4.1b. When a signal triggers the digitizer, the four input channels are recorded simultaneously and stored in the local memory of the digitizer. Now the digitizer is ready for the next event. After one sequence of 56 events (one sequence produces $56 \times 4 = 224$ files), the local memory is full and the data is saved to the hard-disk of the computer. Now the system is ready for a next sequence of 56 events, possibly with different trigger-settings.

During a measuring session, several sequences are recorded with varying trigger-settings (note that during each sequence, the trigger-settings are constant). Usually at least six sequences are recorded, with six different trigger-settings. In this case each phase acts as trigger-source during at least two sequences, each sequence having a low trigger-level (10 % of the maximum signal amplitude) and a high trigger-level (60 % of the maximum signal amplitude). Now during a measuring session $6 \times 56 = 336$ events are recorded. With a sample-rate of 2 ns/sample and a record-length of 5120 points, the total measuring time is $336 \times 2 \cdot 10^{-9} \times 5120 = 3.44$ ms.

During measurements in various power plants, it was found that the rotor excitation system causes relatively low frequency interference signals which appear at six fixed positions on the 50 Hz voltage. An example is given in Fig. 4.2. With the 'smart-trigger' options of the digitizer, these signals could be rejected. In this case, for all the time-domain measurements the oscilloscope was only triggered by signals with a rise-time $t_{rise} < 5$ ns.

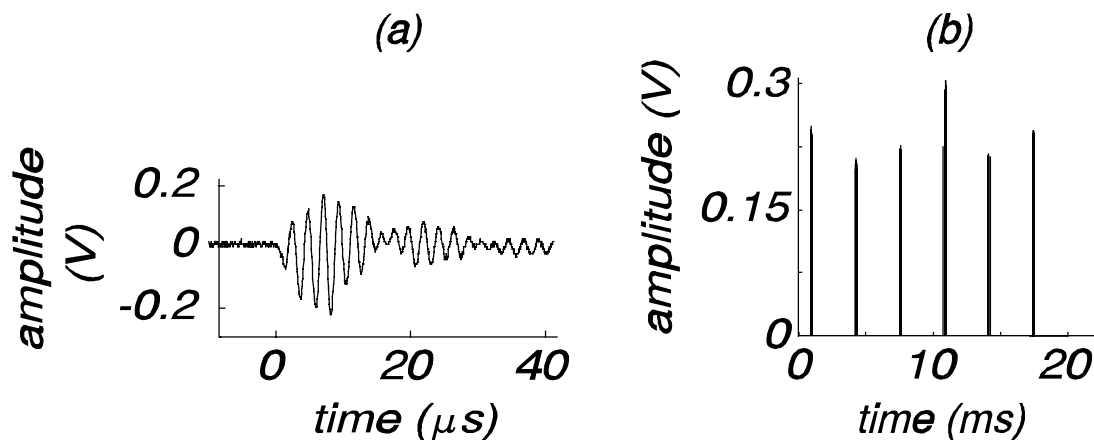


Figure 4.2 (a) Typical interference signal caused by the excitation system, since (b) the signals appear at six fixed positions on the 50 Hz voltage. These signals can be rejected by 'smart triggering'.

4.2.2 Measurements on generator Hemweg-6

When a measuring session is finished and all the data is stored on the hard-disk of the computer, the true partial discharges must be separated from interference by means of signal processing. To illustrate this process, we discuss on-line measurements on the 125 MW turbine generator Hemweg-6 (see also Chapter 5). In each phase of this generator, four sensors have been installed: single-turn Rogowski-coils around the high-voltage and neutral terminals and two bus-support-capacitors in the IPB; one close to the generator and one close to the step-up transformer.

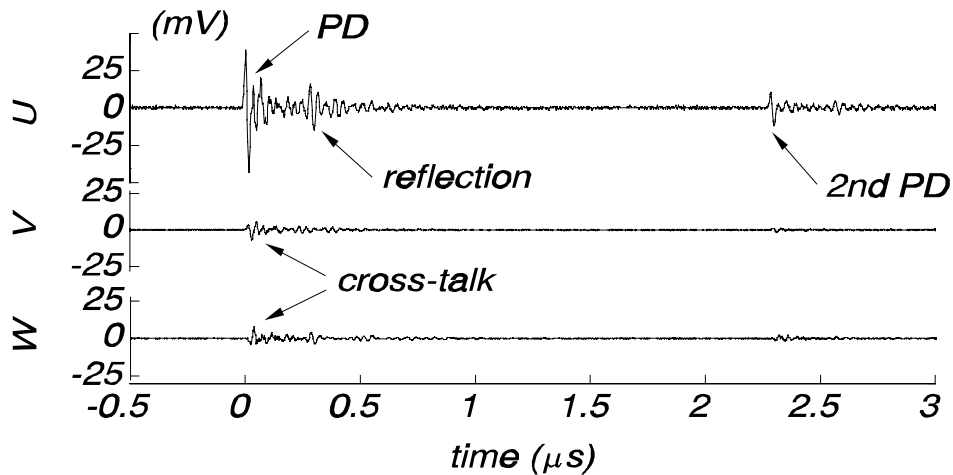


Figure 4.3 Two partial discharges in phase U, occurring within $2.5 \mu\text{s}$. The signals in the other two phases are caused by cross-talk.

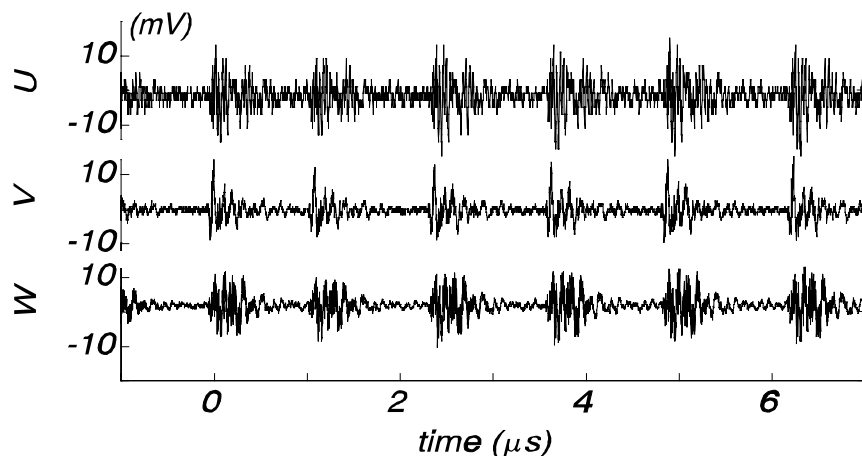


Figure 4.4 Example of a 'burst' type interference signal.

The recorded signals can be grouped in three categories: (i) signals caused by partial discharges, (ii) signals caused by cross-talk between the phases, and (iii) interference signals. A typical record of a true partial discharge, recorded with the Rogowski-coils at the HV-terminals, is shown in Fig. 4.3. Due to cross-talk between the phases, a signal shows up in all three phases. It is concluded that the discharge occurs in phase U because: (i) phase U has the largest amplitude, (ii) the signal starts with a bipolar pulse, since the Rogowski-coils measures the derivative of the enclosed PD-current, and (iii) the pulse shows a small reflection at the step-up transformer (indicated with an arrow). The length of the IPB between generator and transformer is 42 m. Since the pulse travels with the speed of light (3.3 ns/m), the corresponding reflection time is $2 \cdot 42 \cdot 3.3 = 277$ ns. Note that within $2.5 \mu\text{s}$ a second discharge occurs in phase U.

A typical example of an interference signal is shown in Fig. 4.4. This 'burst' type of signal is apparently caused by a local controller. Every half hour this controller gives, during about 30 s, a train of pulses with a repetition frequency varying between 200 kHz and 1 MHz.

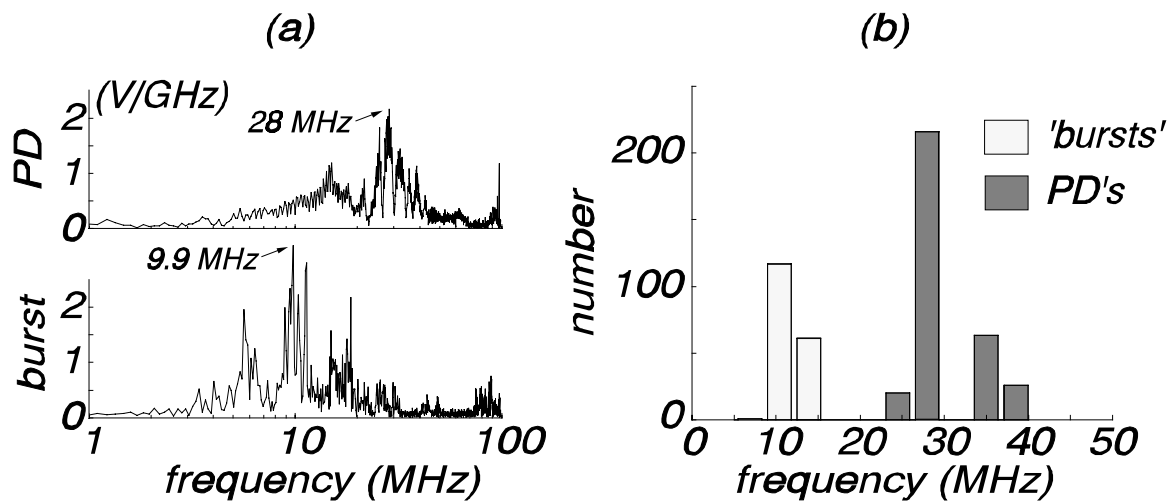


Figure 4.5 (a) Calculated frequency spectra of a PD-signal and the 'burst' type interference signal. The arrows indicate the 'dominant frequency'. (b) Histogram of the dominant frequency.

A trained human observer can easily classify this 'burst' as interference, however discrimination by a computer is more easily done in the frequency domain than in the time domain. This is illustrated in Fig. 4.5a, which shows the FFT of the PD signal in phase U as in Fig. 4.3 and a 'burst' signal. It is clear that the highest amplitude frequency components for the PD pulse are concentrated between 20 and 40 MHz, while the largest amplitudes in the 'burst' signal are at frequencies between 8

and 15 MHz. We can therefore discriminate between PD's and interference by means of the 'dominant frequency'; the frequency where the frequency spectrum has the largest amplitude. In Fig. 4.5a the dominant frequencies are indicated with arrows.

Figure 4.5b gives a histogram of the dominant frequencies of 504 measurements. All signals with a dominant frequency between 20 and 40 MHz are classified as partial discharges. When the dominant frequency is less than 15 MHz, a signal is classified as interference.

As a final check of the correctness of the classification criteria, the amplitudes of both signal categories are plotted versus their position on the 50 Hz voltage. Figure 4.6a gives the result for all signals classified as partial discharges. The obtained pattern is typical for partial discharges: the discharges are concentrated in the first and third quarter-cycle of the 50 Hz voltage. In addition, the discharges have different polarities for both half-cycles of the 50 Hz voltage (not shown in Fig. 4.6a; the figure gives the absolute values). The pattern for the 'burst' type signals is shown in Fig. 4.6b. The bursts are distributed over the whole 50 Hz waveform, which confirms that these signals are not caused by partial discharges.

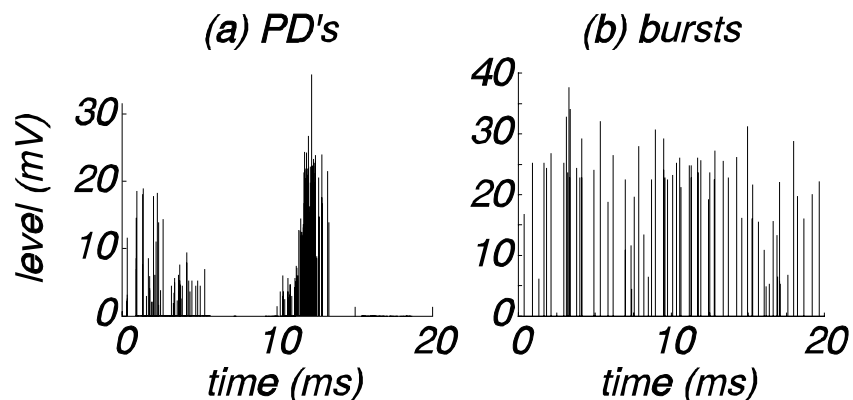


Figure 4.6 Amplitudes versus their position on the 50 Hz voltage waveform for (a) all signals classified as PD's in phase U, and (b) all signals classified as 'bursts'.

4.2.3 Procedure for the signal processing

The advantage of time-domain measurements is that each individual pulse can be judged, so that cross-talk and interference are optimally rejected. However, the signal characteristics needed for the automatic discrimination are different for each generator. In addition, they can also vary for various measurements on the same generator, for instance when new interfering equipment is installed in the power plant.

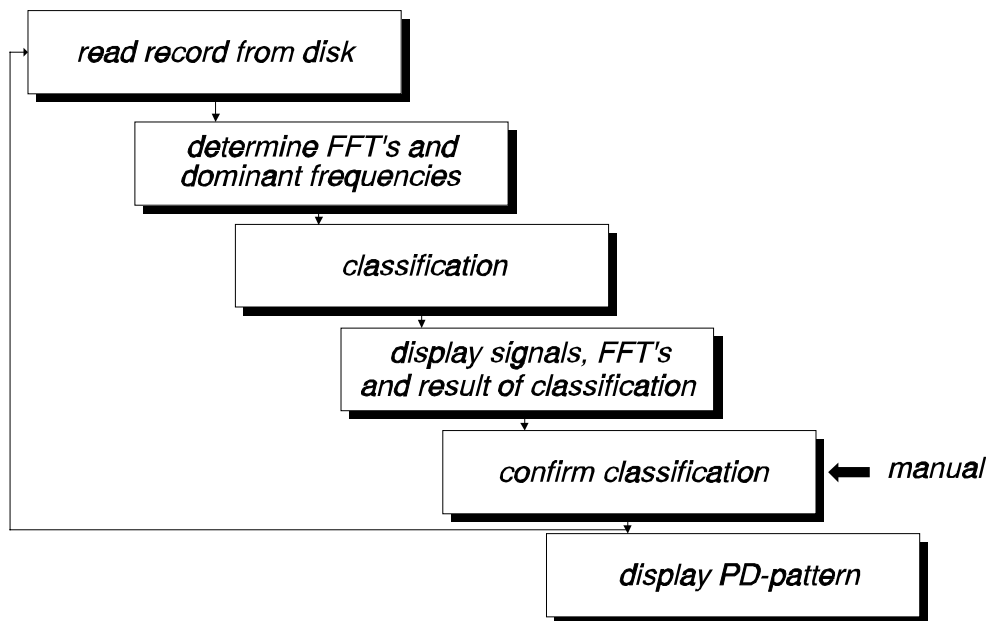


Figure 4.7 Procedure for the signal processing.

As a consequence, a reliable and fully automated signal processing is difficult. Therefore we opt for a partially automated procedure, which requires confirmation of each classification by an expert. This procedure is shown in Fig. 4.7. The computer calculates the frequency spectra for each recorded event⁸ by means of an FFT-transformation, and determines the dominant frequency f_d . For the measurements on generator Hemweg-6 (see Section 4.2.2) classification is done according to the following criteria:

- if $(20 \text{ MHz} < f_d < 40 \text{ MHz})$ then classify as partial discharge
- if $(f_d < 15 \text{ MHz})$ then classify as interference.

This automatic classification by the computer must be confirmed by an expert. For this purpose all three sensor-signals of the event, their calculated frequency spectra, the dominant frequencies and the result of the classification are shown on the computer screen. An example is given in Fig. 4.8. The computer screen consists of two windows. The large window shows the three waveforms with their frequency spectra in which the dominant frequencies are indicated. The second window gives the result of the classification and contains five selection-fields. An expert can confirm or correct the classification by means of a mouse-click on the relevant selection-field.

⁸each event consists of four files; three sensor outputs and a 50 Hz reference signal

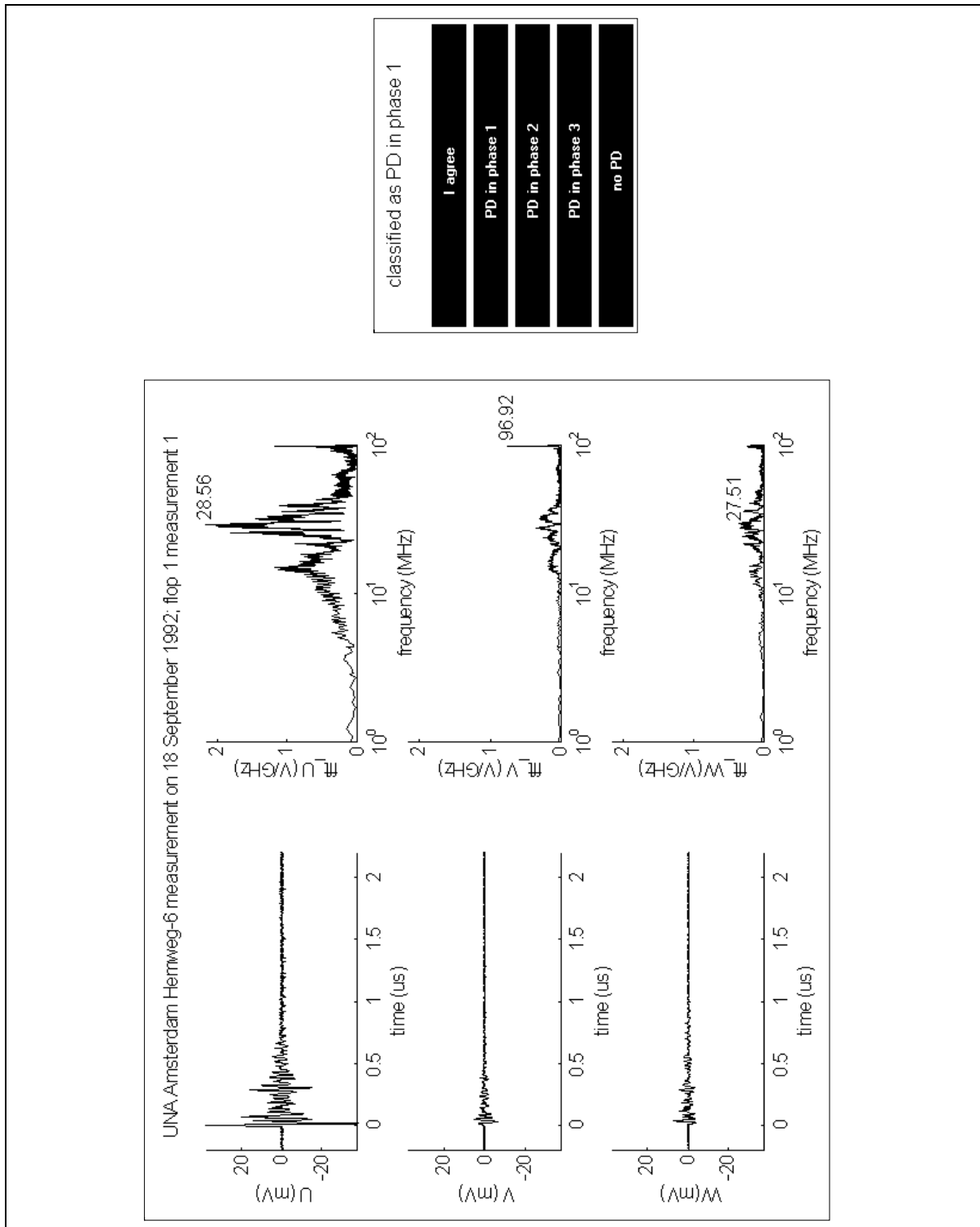


Figure 4.8 Example of the computer-screen used for final classification by an expert.

4.3 A tunable narrow-bandwidth detector

4.3.1 General

For the second measuring method, a tunable narrow-bandwidth detector is used. The detector is tuned to a frequency where partial discharges are strong and no interference is present. The rejection of cross-talk is more complex, but can also be achieved by a good selection of the tuning frequency [Pem96]. As a tunable-narrow-bandwidth detector we use a spectrum analyzer (HP 8594A). The analyzer is used in the 'zero-span mode' [Hef91], where it is tuned to a fixed frequency. The amplitude at this frequency is monitored during several cycles of the 50 Hz voltage. The bandwidth of the filter is determined by the 'resolution-bandwidth' [Hef91] of the spectrum analyzer and is set to 300 kHz around the tuning frequency.

4.3.2 Measurements on generator Hemweg-8

To illustrate the use of a spectrum analyzer as a tunable narrow-bandwidth detector, we discuss on-line measurements on the 650 MW generator Hemweg-8 (see also Chapter 7), which is fitted with current sensors around the high-voltage terminals.

Figure 4.9 gives the frequency spectrum as recorded in phase V. This spectrum shows several peaks, which are a result of resonances in the stator winding or reflections in the IPB. Preferably, for PD measurements the detector is tuned to one of these peaks, and an important question is to which peak. The peak at 40 MHz is caused by a local transmitter and the activity above 80 MHz is caused by FM-radio stations. This shows that, although our measuring system itself does not pick up interference, interference couples into the stator windings and causes 'legitimate' signals at the sensors.

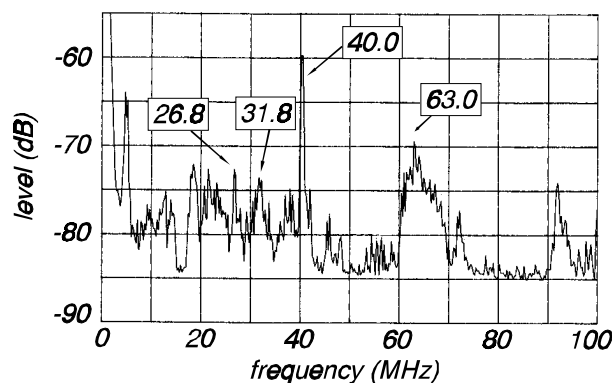


Figure 4.9 *Measured frequency spectrum for phase V of generator Hemweg-8.*

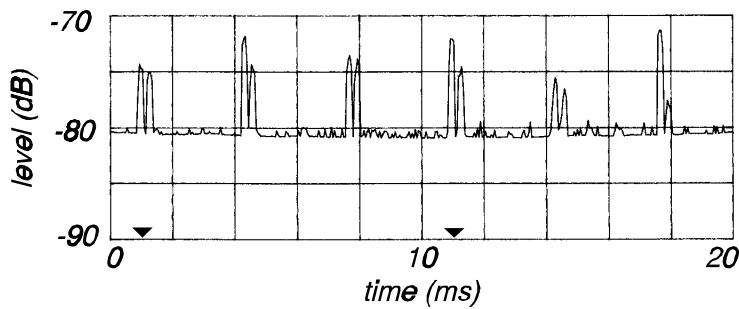


Figure 4.10⁹ Unsuitable tuning (to 2 MHz); only interference from the rotor excitation pulses is measured, at a repetition frequency of 300 Hz.

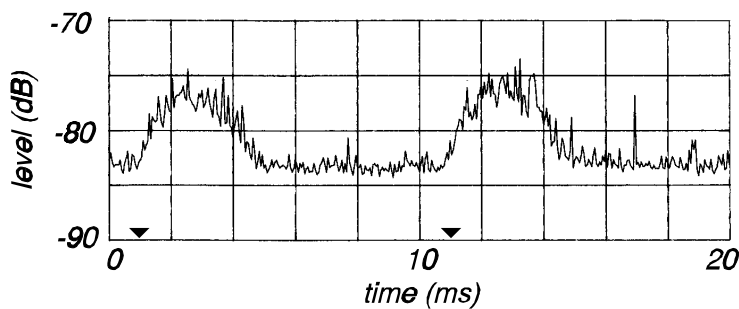


Figure 4.11² Favorable tuning (to 26.8 MHz); only partial discharges from phase V are measured.

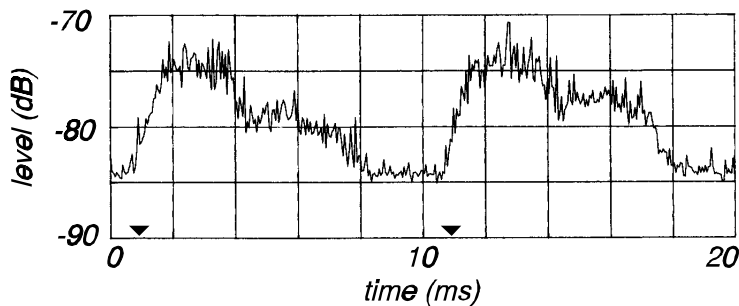


Figure 4.12² Tuning to 31.8 MHz. The result shows discharges in phase V and cross-talk from phase W.

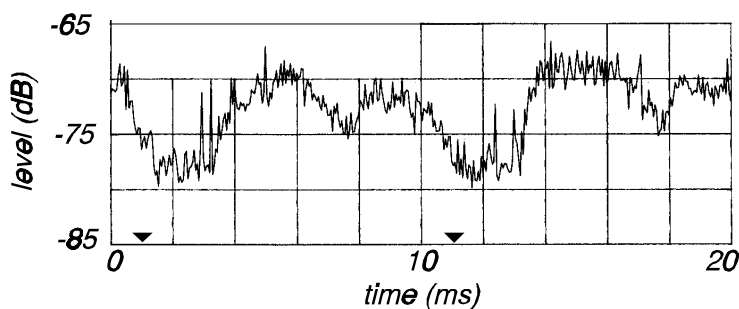


Figure 4.13² Tuning to 63 MHz. The result is dominated by cross-talk from the phases U and W.

⁹the actual zero-crossings of the 50 Hz voltage in phase V are indicated with markers

Figure 4.10 gives the result when the spectrum analyzer is tuned to a relatively low frequency of 2 MHz. As can be seen, at this unsuitable frequency only interference from the rotor excitation system is measured. When the spectrum analyzer is tuned to the peak at 26.8 MHz, a correct partial discharge pattern for phase V is measured (Fig. 4.11). As expected, the discharges are concentrated in the first and third quadrant of the 50 Hz voltage.

Tuning to the peak at 31.8 MHz gives the sum of a similar discharge pattern, and an additional discharge pattern that is shifted -120° in phase. This pattern is apparently caused by discharges in phase W. Due to cross-talk between the phases, these discharges also show up in phase V. When we tune the analyzer to 63 MHz, a completely different pattern is recorded (Fig. 4.13). It looks as if here the cross-talk from the other phases dominates the result and no discharges of phase V are recorded.

The figures 4.10 to 4.13 show clearly that the tuning frequency has a great influence on the results of the measurements. Especially the cross-talk between the phases plays an important role. In Chapter 2 we found that this cross-talk strongly depends on the location of a discharge. From the figures 4.10 to 4.13 it can be concluded that the cross-talk also depends on the measurement frequency.

To find the best tuning frequency, for each phase a series of zero-span measurements is done at 30 different tuning frequencies (from 10 to 70 MHz, with an interval of 2 MHz). At each tuning frequency, the discharge activity is recorded during 3000 cycles of the 50 Hz voltage, with the analyzer in the 'hold max' mode. Thus the total measuring time at each tuning frequency is 60 s. The duration of a complete scan per phase is $30 \cdot 60 = 1800$ s. The measuring procedure is controlled by a laptop computer and is shown schematically in Fig. 4.14.

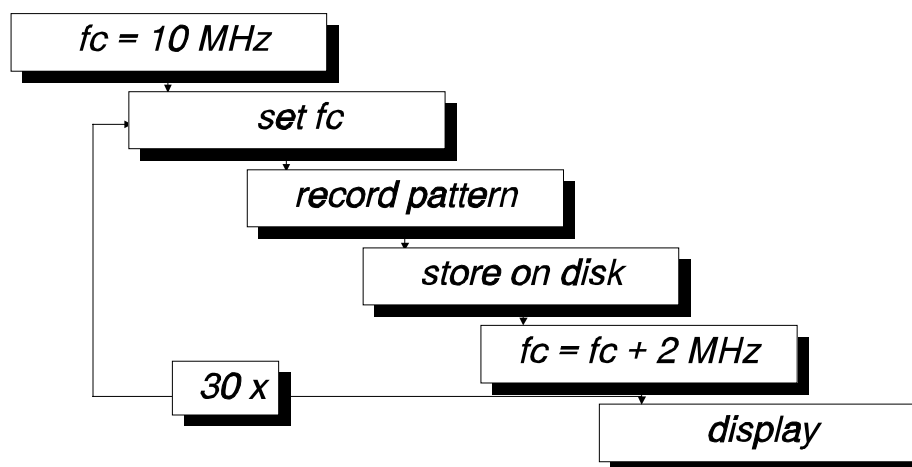


Figure 4.14 Procedure for the recording of a series of zero-span measurements at various tuning frequencies f_c .

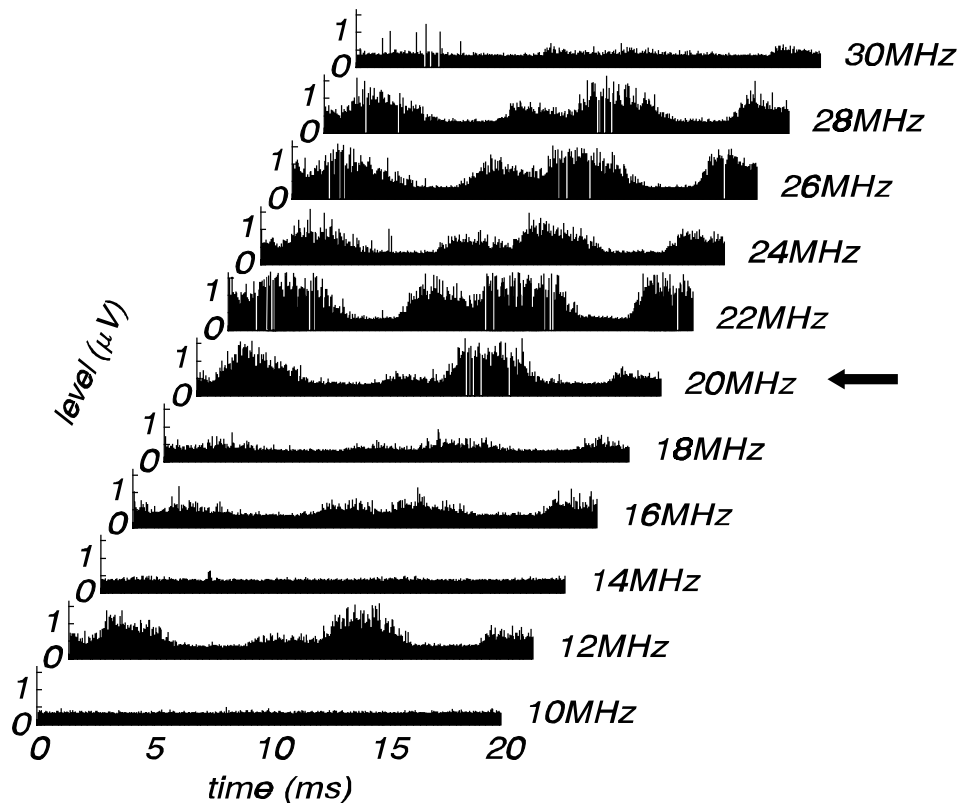


Figure 4.15 Results of zero-span measurements for phase V of generator Hemweg-8, measured at various tuning frequencies.

Figure 4.15 shows the results for phase V of generator Hemweg-8. Only the results for tuning frequencies from 10 to 30 MHz are shown. In this case the best choice is 20 MHz, since at this frequency: (i) the largest signal is recorded, thus the sensitivity is maximum, (ii) little cross-talk takes place (in contrast to e.g. 22 MHz), and (iii) no interference can be recognized. At some frequencies, e.g. at 10 or 14 MHz, hardly any activity is recorded.

In Fig. 4.15 the 'best' tuning frequency turns out to be 20 MHz. However, one must realize that this might not be the case for follow-up measurements. For instance when discharges come from a different location in the winding, their response at the generator terminals can be different (see Chapter 2). Also the installation of new interfering equipment can cause problems. Hence at each new measuring session, the whole set of patterns at the 30 different tuning frequencies must be recorded.

4.4 Concluding remarks

It is obvious that the two described measuring methods each have their own advantages and disadvantages, as shown in Table XI.

Table XI *Advantages and disadvantages for time-domain measurements and the tunable-narrow bandwidth detector*

time-domain measurements	tunable narrow-bandwidth detector
requires the presence of an expert, especially for the selection of trigger-conditions	simple and in most cases effective. Can be carried out by a non-specialist
the complete waveforms of incoming pulses are recorded	only amplitude information and no phase information of an incoming pulse is obtained, at the tuning frequency only
each recorded pulse can be judged individually, thus enabling optimal rejection of interference and cross-talk	cross-talk and interference must be rejected by a good, generator-specific choice of the tuning frequency
signal processing is difficult, generator-specific and time-consuming	no post-processing of data is needed
signal processing can only be partially automated. An expert is necessary to confirm of correct the decisions made by the computer	fully automatic; requires however an extra half hour to select the best tuning frequency
wide bandwidth	limited bandwidth
as an extra check on the nature of the discharges, the signal polarity can be determined	signal polarity can not be determined
the effective measuring time is limited by the amount of recorded data and the time needed for signal processing. Normally 6 sequences of 56 events are recorded, with a sample-rate of 2 ns/Sample and a record-length of 5120 points. Thus the total measuring time is 3.44 ms	at each tuning frequency, the measuring time is 60 s
the results form only a single PD-pattern for each phase	for each phase, 30 PD-patterns are recorded and must be used for evaluation of the result
necessary measuring method if abnormal signals have to be identified	most suitable method for continuous and periodic on-line measurements

A direct comparison between both techniques is made at two generators. For generator Hemweg-8 in Amsterdam, both techniques were used in combination with toroidal single-turn inductive current sensors. The results are discussed in Chapter 7. In the Roca-3 power plant in Rotterdam, both techniques were used in combination with capacitive sensors (bus-support-capacitors). The results are given in Chapter 8.

In general, the tunable narrow-bandwidth detector is most suitable for continuous and periodic on-line measurements on a generator. In special cases, when abnormal partial discharge patterns are recorded, the time-domain measurements give more information. For practical partial discharge monitoring to assess the condition of generators, we suggest the following strategy [Pem98]:

- continuous monitoring of the partial discharge level by means of a tunable narrow-bandwidth detector, tuned to the 'best' tuning frequency
- recording at regular intervals of the partial discharge patterns by means of a tunable narrow-bandwidth detector and, to verify the choice of the best tuning frequency, at 30 different tuning frequencies
- in case of abnormal patterns, the results must be verified by means of time-domain measurements. These measurements require the presence of experienced personnel. Extra information about the discharge source can then be obtained by means of transit-time measurements between two sensors.

Chapter 5

MEASUREMENTS ON TURBINE GENERATOR HEMWEG-6

5.1 Introduction

Turbine generator Hemweg-6 was a 125 MW generator of the UNA-Hemweg power plant in Amsterdam. The generator has been in operation from 1968 until December 1994 and had a nominal output voltage of 14 kV. The main generator data are given in Appendix A.

For measurements on this generator, we used capacitive sensors, inductive sensors and pick-up loops. Six single-turn inductive current sensors were installed around the three neutral and the three high-voltage terminals. In each phase, two bus-support-capacitors have been installed in the isolated-phase-bus; one close to the generator and one closer to the step-up transformer. Pick-up loops were placed between the grounded sheaths of the IPB. Figure 5.1 gives an overview of the sensor positions.

All measurements were done by means of the time-domain measurement technique as described in Chapter 4. An analysis of the recorded signals for Hemweg-6 is already given in Section 4.2.2. Here we found that the recorded signals can be grouped in three categories: (i) signals caused by partial discharges, (ii) signals caused by cross-talk between the phases, and (iii) interference signals. Discrimination between partial discharges and interference is possible by means of the 'dominant frequency' f_d . Typical values for Hemweg-6 are: for interference f_d is less than 15 MHz, while for partial discharges f_d is between 20 and 40 MHz.

In this Chapter we will concentrate on the following aspects:

- the external propagation of PD-signals; since generator Hemweg-6 is fitted with sensors at both the high-voltage side and the neutral-side, the propagation of PD-signals through the isolated-phase-bus and in the generator-neutral can be studied. The results are given in Section 5.2
- comparison of inductive and capacitive sensors; the comparison will be made by means of the recorded PD-patterns and is given in Section 5.3
- a discussion of the recorded PD-patterns is given in Section 5.4
- measurements with pick-up loops will be discussed in Section 5.5.

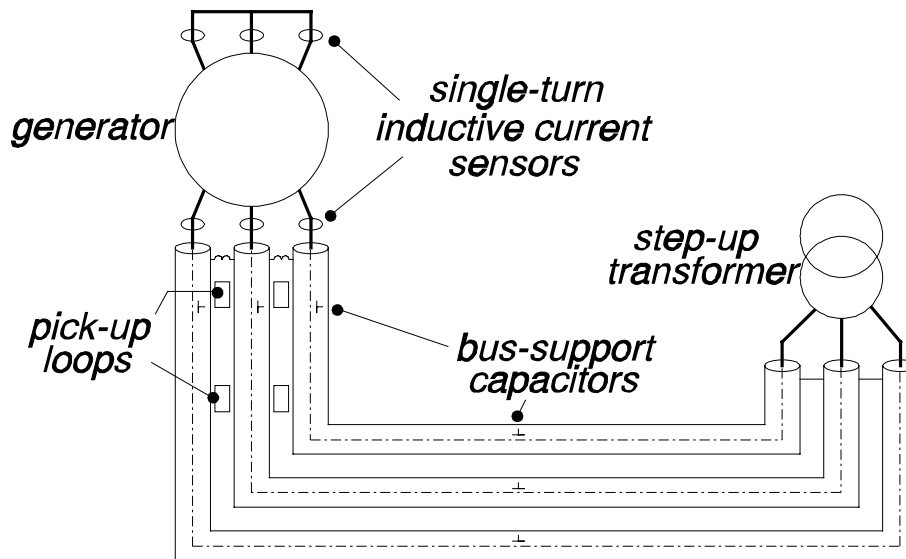


Figure 5.1 Overview of sensors installed at generator Hemweg-6. Single-turn inductive current sensors are installed at the six generator terminals, six bus-support-capacitors are installed in the IPB and two pick-up loops are placed between the grounded sheaths of the IPB.

5.2 External propagation of PD-signals

Partial discharges cause travelling waves in the stator windings. In Chapter 2 we found that the propagation of these waves inside the generator is strongly influenced by the capacitive and inductive coupling between the windings. Due to this coupling, the signals propagate in two modes and in addition cross-talk to other phases occurs. A heavily distorted fraction of the PD signal manifests itself at the generator terminals, as an "external PD current", where it can be measured.

Not only the interior of the generator, but also the exterior influences the PD signal. This is shown schematically in Fig. 5.2. On the high-voltage side, the external PD signal propagates along the IPB, which forms a good quality transmission line. At the step-up transformer the signal reflects back towards the generator. The circuit is closed via the large parasitic capacitance between the IPB and the generator. Due to cross-talk inside the generator, signals will also show up in the other two phases, where they propagate in a similar manner.

Part of the PD signal manifests itself at the neutral side, mainly via capacitive and inductive coupling inside the generator. Now the external circuit is closed via the

other two phases. Consequently, there is not only cross-talk inside the generator but also outside it. The sum of the three neutral currents tends to be zero and therefore the current through the neutral grounding connection is nearly zero. Nevertheless the neutral grounding connection is a popular place for installing current sensors for on-line PD measurements [Tim92]. However one may question the value of these measurements since the neutral connection hardly carries any high-frequency PD current.

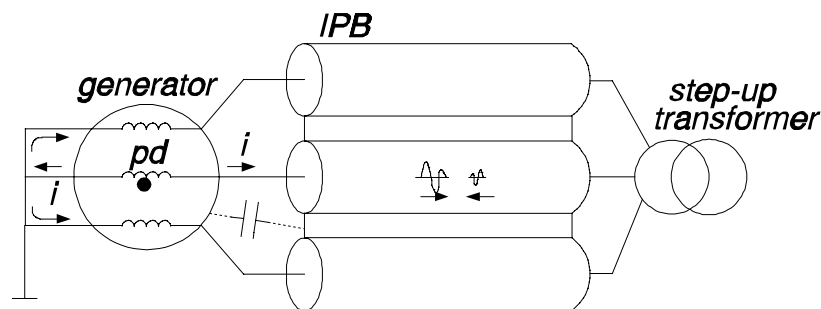


Figure 5.2 Propagation of external partial discharge signals.

The external propagation of PD signals will be illustrated by measurements carried out on generator Hemweg-6. A first measurement is shown in Fig. 5.3. Instead of a discharge, a pulse with a pulse-width of 10 ns and an amplitude of 1.5 V (Fig. 5.3a) is injected at the capacitive sensor at the transformer side of phase U and is measured by means of the three capacitive sensors at the generator side (Fig. 5.3b), the inductive sensors at the three high-voltage terminals (Fig. 5.3c) and the inductive sensors at the three neutral terminals (Fig. 5.3d). Note: the different transit times of the signals are caused by the transit times along the IPB and by different lengths of measuring cables. Since the latter are unfortunately unknown, it is not possible to analyze the transit times.

At the high-voltage side the injected signal shows up at both the capacitive sensor and the inductive sensor of phase U. Due to the differentiating character of both sensors, bipolar pulses are measured. No significant signal is present in the other two phases, which shows that no cross-talk takes place in the IPB or near the generator terminals. The sum of the currents as measured by the inductive sensors (Fig. 5.3c) is not zero, thus the circuit must be closed via a parasitic capacitance between the IPB and the generator.

A small fraction of the injected signal shows up at the three neutral terminals of the generator (Fig. 5.3d). Since the signals show no clear pulse and arrive simultaneously at the three neutral terminals, we assume that they are caused by capacitive and inductive coupling inside the generator. The calculated sum of the three currents is

zero (Fig. 5.3e), which confirms that the neutral grounding connection carries no PD current.

The external propagation of a true partial discharge signal, measured during regular operation of the generator, is shown in Fig. 5.4. We assume that this discharge occurs close to the high-voltage terminals of phase U, because the cross-talk to the phases V and W is small (Fig. 5.4c). Nevertheless, a small fraction of the signal shows up at the neutral side (Fig. 5.4a). The signals at the neutral side are probably caused by capacitive and inductive couplings between the windings, since no clear pulse can be recognized and the signals show up without significant transit time. Because the sum of the three external neutral currents is zero, the "external circuit" must be closed via the other two phases. As a consequence, a signal measured at the neutral terminal of one phase does not necessarily belong to a PD in that phase.

At the high-voltage side, the partial discharge manifests itself at the generator terminals and propagates with the speed of light along the IPB. The sum of the currents as measured with the three current sensors at the high-voltage terminals is not zero. Thus the external circuit must close via a parasitic capacitance between the generator and the IPB, as indicated in Fig. 5.2.

The transit-time Δt_1 is 7 ns for all three phases and corresponds with the distance (≈ 2 m) between the inductive sensors at the generator terminals and the capacitive sensors at the generator side. The transit-time Δt_2 is 70 ns for phase U, 56 ns for phase V and 66 ns for phase W, and again corresponds with the distance (≈ 20 m) between the capacitive sensors at the generator and at the step-up transformer side. At the step-up transformer, the signal reflects back towards the generator. The reflected signals are indicated with arrows. The reflection time as measured with the inductive sensors is 252 ns and corresponds with twice the transit-time along the IPB (≈ 76 m). The reflection time as indicated for the capacitive sensor at the generator side is 238 ns and corresponds with twice the transit-time between the sensor and the step-up transformer (≈ 72 m). The transit-times between various sensors and reflections of the PD signals can be used to verify whether partial discharge activity takes place inside the generator or for instance near the step-up transformer. In the case of Hemweg-6, all recorded partial discharge signals originated from the generator. No discharges from other sources could be detected.

Due to cross-talk inside the generator, at the high-voltage side the partial discharge in phase U shows up in all three phases. In the case of Fig. 5.4 this cross-talk is small, which is an indication that the discharge occurs close to the high-voltage terminal of phase U. The signals caused by the cross-talk propagate in a similar manner as the PD signal in phase U.

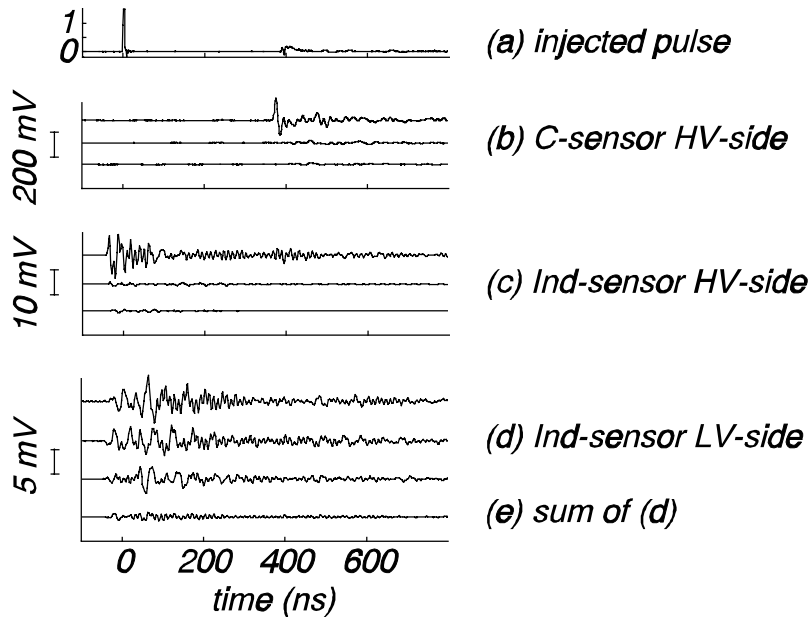


Figure 5.3 Propagation of a pulse injected at the capacitive sensor at the transformer side of phase U (a) and measured by the capacitive sensors at the generator side (b), the inductive sensors at the high-voltage terminals (c) and the inductive sensors at the neutral terminals (d). Note that the transit times are not corrected for the different lengths of measuring cables.

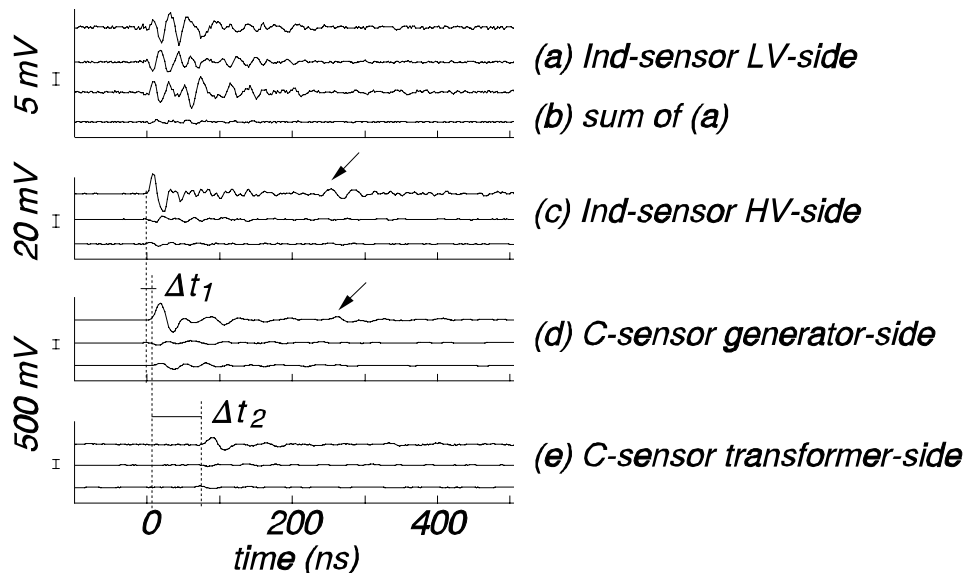


Figure 5.4 Partial discharge in phase U, measured by the inductive sensors at the neutral side (a), the inductive sensors at the high-voltage side (c), the capacitive sensors at the generator side (d) and the capacitive sensors at the transformer side (e).

5.3 Comparison of inductive and capacitive sensors

Looking at the waveshapes of Fig. 5.4, it is clear that the output voltages of the bus-support-capacitors are a factor 22 larger than the outputs of the single-turn inductive current sensors. In other words: the sensitivity of the bus-support-capacitors is much larger than of the current sensors. However, a good comparison between two sensor types can only be made by comparing the recorded partial discharge patterns.

The PD patterns for all three phases are given in Fig. 5.5. The levels recorded with the inductive sensor (Fig. 5.5a) are much smaller than the levels measured with the bus-support-capacitors (Fig. 5.5b). However, the patterns measured by both sensor types show great similarity. So both sensor types give good results; the best sensitivity however is obtained with bus-support-capacitors.

5.4 Partial discharge patterns

The PD patterns recorded during on-line measurements are given in Fig. 5.5. The PD pattern for phase U differs greatly from the patterns of the other two phases. This was also the case during off-line measurements carried out later during stand-still of the generator (Fig. 5.7). Compared to the other two phases, the magnitudes of the partial discharges in phase U are much larger, especially during the negative cycle of the 50 Hz voltage. Such an asymmetric pattern is generally associated with partial discharges at an interface between the insulation and a conductor [Gul91], [Sto97]. In this case, the large PD's during the negative cycle are an indication for discharges between the stator bars and the stator core, the so called slot discharges [McD90], [Sto95], [Wil90].

In Chapter 2 we showed that the cross-talk of PD signals between the phases might give information about the location of the discharges. It was shown there that, at least for the stator bars close to the high-voltage terminals, the largest signal will show up in the phase where the discharge occurs. The signals in the two neighboring phases are caused by cross-talk, which we define as the ratio of the peak-to-peak values of the signals in the neighboring phases relative to the peak-to-peak value of the PD signal. Figure 5.6 shows the cross-talk as function of the PD-level for each of the three phases of generator Hemweg-6. Note that the PD levels are normalized; the maximum PD value is set to 100 %. Again phase U shows a different behavior compared to the other two phases. Most of the discharges in phase U give only a small cross-talk to the other two phases. This is an indication that most discharges in this phase occur close to the

high-voltage terminal. The cross-talk for partial discharges in the other two phases has a large spread, which is an indication that those discharges occur at locations distributed along the stator winding.

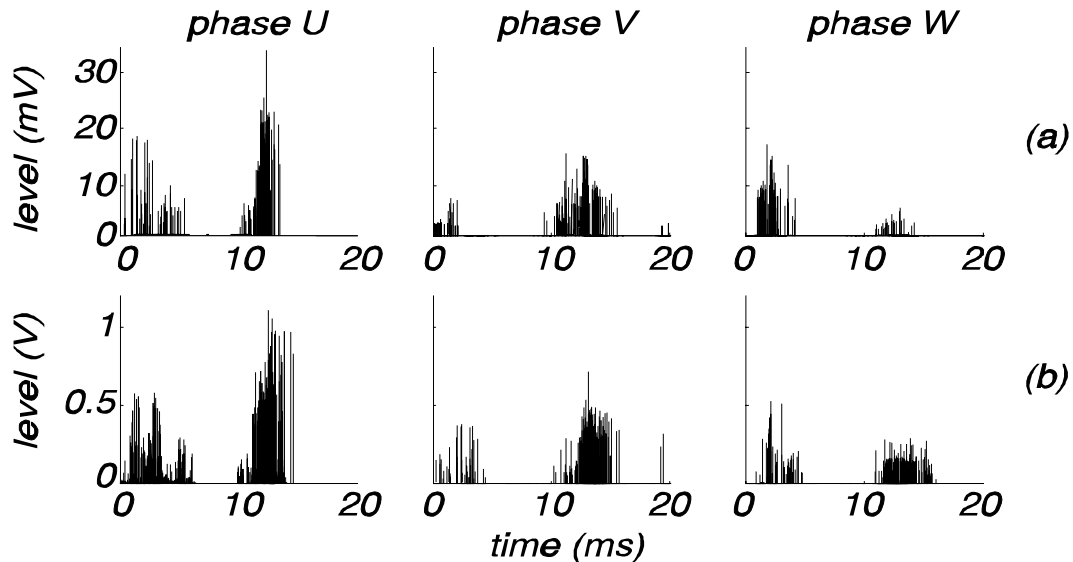


Figure 5.5 Partial discharge patterns for the three phases of generator Hemweg-6, as recorded by means of (a) single-turn inductive current sensors and (b) bus-support capacitors.

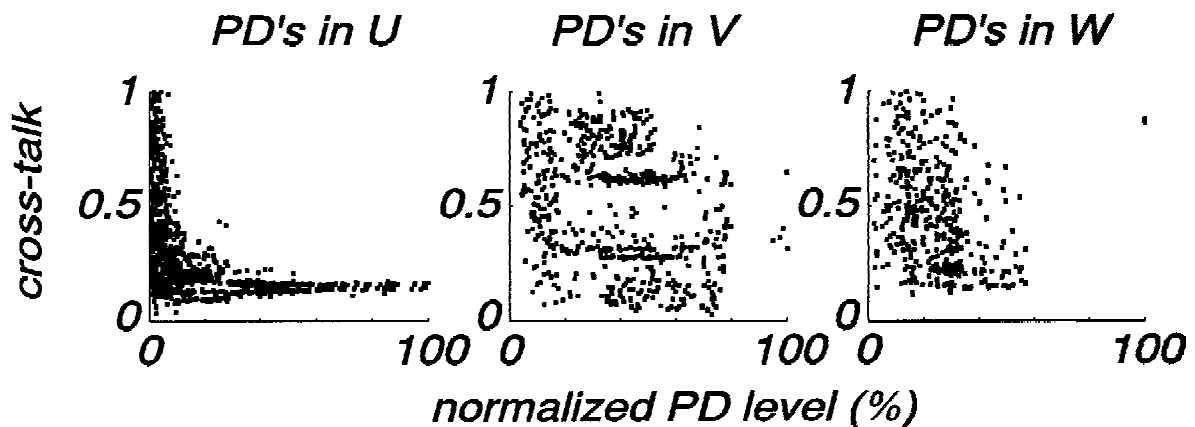


Figure 5.6 Cross-talk versus the normalized PD levels for PD's in each of the three phases of generator Hemweg-6. The cross-talk is defined as the ratio of the peak-to-peak values of the signals in the neighboring phases relative to the peak-to-peak value of the PD signal.

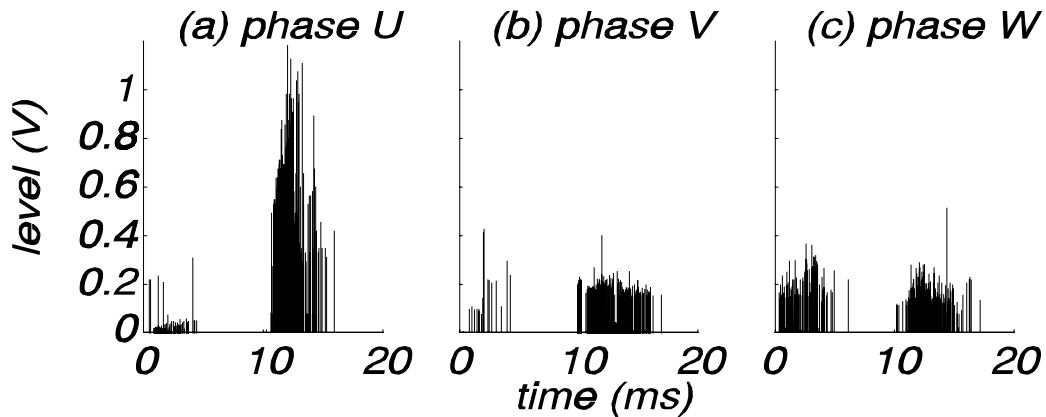


Figure 5.7 Off-line recorded partial discharge patterns for the three phases of generator Hemweg-6, measured at 8.4 kV by means of the three bus-support-capacitors at the generator side.

A further inspection of the generator was welcome to find and locate the source of the large discharges in phase U, for example a visual inspection or a localization by scanning the winding with an electro-magnetic probe [Sed89]. Unfortunately this was not possible since shortly after the final shut-down of the Hemweg-6 power plant in December 1994, the generator was dismantled. We only had the opportunity, shortly before dismantling, to carry out additional off-line PD measurements on a stand-still generator.

The off-line measurements were carried out for each phase separately, while the other two phases were grounded. The winding was energized by means of a mobile-test transformer and all measurements were carried out at voltages ranging from 0 to the line-voltage of 14.5 kV. Now also the low-voltage part of the stator winding is stressed with the applied voltage. During normal operation the voltage increases linearly with the length of the winding and the maximum voltage to ground equals $14.5/\sqrt{3} = 8.4$ kV. Therefore the PD patterns at 8.4 kV were used for the comparison with the patterns as recorded during regular operation.

These off-line PD patterns are given in Fig. 5.7. The results show great similarity with the patterns recorded during regular operation (Fig. 5.5). Again phase U has much larger PD levels compared to the other two phases.

5.5 Measurements with pick-up loops

Field measurements with pick-up loops (see Section 3.4) have been carried out in the Hemweg-6 power plant. The loops were placed between the grounded sheaths of the IPB (see Fig. 5.8). Now the loops measure the derivative of the local magnetic flux. The magnetic fields between the sheaths are determined by the construction of the IPB, as is shown in [Sen83]. A detailed discussion of magnetic fields in an IPB is given in Appendix D.

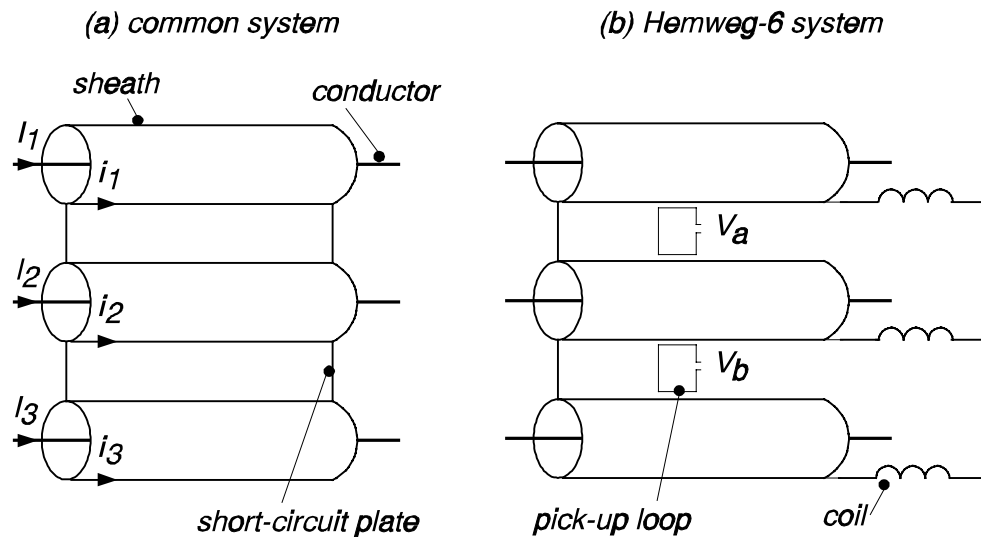


Figure 5.8 (a) A commonly used IPB system and (b) the IPB of the Hemweg-6 power plant. For Hemweg-6, pick-up loops are placed between the grounded sheaths of the IPB (the coils are positioned at the generator side).

A commonly used IPB system is shown schematically in Fig. 5.8a. At both ends, the sheaths are short-circuited with wide short-circuiting plates. This allows the flow of large 50 Hz currents in the sheaths (i_1 , i_2 and i_3 in Fig. 5.8a). These sheath currents tend to be equal and opposite to the conductor currents and largely cancel the magnetic field between the sheaths (typically the remaining field is only 4 % of what it would be without IPB [Sen83]). Consequently, the well-known advantages of this system are, that even under short-circuit conditions: (i) the residual magnetic fields outside and between the sheaths are small, (ii) the electromagnetic forces between the conductors are strongly reduced, and (iii) eddy-current losses in nearby steel-constructions remain small.

For some types of IPB's the sheath currents are kept at a lower value by

interconnecting the sheaths via coils, as was done in the Hemweg-6 power plant in Amsterdam (Fig. 5.8b). To determine the remaining field in this case, measurements were carried out in this power plant. The results are discussed in detail in Appendix D. It turns out that the remaining magnetic field is 60 % for 50 Hz, which means that a considerable magnetic field is present between the sheaths. At the higher frequencies of the partial discharge pulses, one may question how effective the iron cores of the coils are. However already the relatively thin copper bars, connecting the sheaths via the coils, introduce inductance. Therefore we expect also high frequency flux to be present between the sheaths.

This can be seen in Fig. 5.9a, which shows a partial discharge, measured with two loops between the sheaths of phase U and phase W. One loop is close to the generator. The second loop is placed at 2.1 m distance from the first loop. The time difference between the first peaks in V_a and V_b is 33 ns. The distance between the loops of 2.1 m gives a difference of 7 ns. The resulting 26 ns is caused by the difference in cable lengths of 5.2 m. At the step-up transformer end of the IPB, the signal is reflected back to the generator. The reflection times of 210 ns and 196 ns are equal to twice the transit time from the loops to the transformer. Obviously the PD signal in Fig. 5.9a comes from the generator.

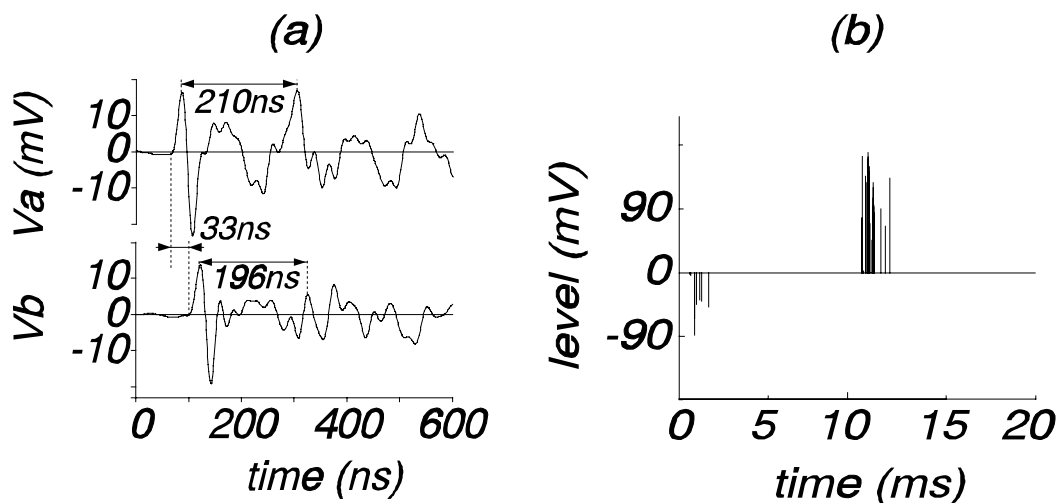


Figure 5.9 Partial discharge signals in generator Hemweg-6, measured with pick-up loops between the phases U and W. (a) Loop V_a is close to the generator, loop V_b at 2.1 m distance from loop V_a . The transit time of 33 ns and the reflections at 210 ns and 196 ns show that this signal comes from the generator. (b) Partial discharge pattern, relative to the 50 Hz voltage in phase U.

We did 40 measurements as in Fig. 5.9a and all signals turned out to come from the generator. Figure 5.9b gives the amplitudes of the signals measured with the loop close to the generator versus their timing with respect to the 50 Hz voltage. The pattern is typical for partial discharges; the discharges are concentrated in the first and third quadrant of the 50 Hz voltage and the pulses have different polarities for both cycles. The plotted 50 Hz voltage is synchronous with the voltage in phase U, thus it is plausible that the discharges in Fig. 5.9b are from this phase. However this cannot be determined precisely, since the loops measure activity from both phases U and W.

5.6 Conclusions

The propagation of a partial discharge signal is not only influenced by the interior of the generator but also by its external connections. We found that:

- a partial discharge inside the generator manifests itself at both the three high-voltage and the three neutral terminals. The largest signal will be present in the phase where the discharge occurs
- at the high-voltage side, the PD signal propagates along the IPB and reflects at the step-up transformer. The signal-path is closed via the parasitic capacitance between the IPB and the generator. The signals in the neighboring phases, caused by the cross-talk inside the generator, propagate in a similar manner
- the transit-time between various sensors and reflections of the PD signal can be used to verify whether discharge activity takes place in the generator or for instance near the step-up transformer
- at the neutral side, the PD signal-path is closed via the other two phases. As a consequence, a signal measured at one of the neutral terminals does not necessarily belong to a PD in that phase.

Measurements on generator Hemweg-6 were carried out by means of both single-turn inductive current sensors and bus-support-capacitors:

- both sensor types give good results: the PD patterns measured by both sensors are similar
- the best sensitivity is obtained with bus-support-capacitors.

An analysis of the PD patterns for the three phases of generator Hemweg-6 leads to the following conclusions:

- compared to the other two phases, the PD levels in phase U are much larger,

especially in the negative cycle. The observed asymmetric pattern for phase U is generally associated with slot-discharges. Additional investigations to confirm the presence of slot-discharges were unfortunately not possible

- most discharges in phase U give only a small cross-talk to the other two phases. Therefore it is assumed that most discharges in phase U occur close to the high-voltage terminal
- the cross-talk for the phases V and W has a large spread, which is an indication that the PD's in these phases occur more distributed along the stator windings
- off-line measured PD-patterns are similar to the patterns as recorded during regular operation of the generator.

Partial discharges could also be detected and located by means of pick-up loops between the grounded sheaths of the IPB.

Chapter 6

MEASUREMENTS ON TURBINE GENERATOR AMER-9

6.1 Introduction

Since 1994 several measuring sessions have been carried out on the 650 MW turbine generator Amer-9 of EPZ at Geertruidenberg. This generator has been in operation since 1992 and has a nominal output voltage of 21 kV. The main generator data are given in Appendix A. The measurements have been done by means of single-turn inductive current sensors, permanently installed around the three high-voltage terminals of the generator. During the 1.5 year period from February 1994 to July 1995 five measuring sessions were carried out. A sixth session took place in February 1997.

In Section 6.2 we give the results of the six sessions. The measurements have been done with a digital oscilloscope, according to the procedure described in Section 4.2. The outputs of the three sensors were recorded simultaneously on a pulse-by-pulse base. On a fourth channel a reference signal was recorded to determine the phase position on the 50 Hz voltage. Special attention is paid to: (i) the analysis of the measured waveshapes, and (ii) a comparison between the various sessions.

During all six sessions, only discharges from phase V were observed. This was a surprising result and we therefore carried out a series of additional measurements. The results of these additional measurements are given in Section 6.3.

6.2 Time domain measurements

6.2.1 Measured waveshapes

A typical record of a true partial discharge is shown in Fig. 6.1. In all three phases a signal is present, clearly indicating cross-talk between the phases. It is concluded that the discharge occurs in phase V because: (i) phase V has the largest amplitude, (ii) the signal starts with a nice bipolar pulse, as is expected because the current sensors measure the derivative of an enclosed current, and (iii) the initial pulse is reflected in the IPB at a connection to an excitation transformer (at 7.5 m from the generator), which forms a discontinuity of the transmission line structure of the IPB.

Since the pulse travels with the speed of light (3.3 ns/m), the corresponding reflection time is $2 \cdot 7.5 \cdot 3.3 = 50$ ns, which can be recognized in the signal in the V-phase.

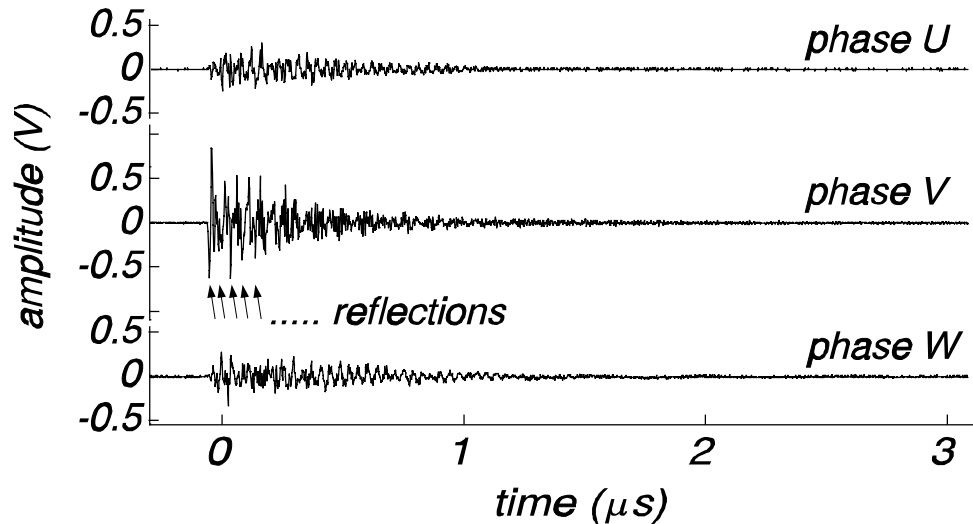


Figure 6.1 A partial discharge in phase V, measured simultaneously in all three phases. Due to cross-talk between the phases, the signal also shows up in the phases U and W.

To obtain the actual partial discharge current, the measured signal in the V-phase is numerically integrated. The result, given in Fig. 6.2, shows a fast initial pulse, followed by several other pulses caused by the reflections in the IPB.

The reflection can also be recognized in the frequency spectrum of a PD signal (derived by FFT-transformation), as can be seen in Fig. 6.3b. This frequency spectrum is dominated by a large peak at 20 MHz, which corresponds with a period of 50 ns. Besides this peak, significant activity is present at frequencies between 35 and 60 MHz. The 20 MHz component caused by the reflections is also present in the cross-talk (Fig. 6.3a,c), but at lower amplitude. In addition, the cross-talk signals show a second peak at 26..27 MHz. This helps in the discrimination between the actual PD signal and the signals due to cross-talk:

- the signal with the largest amplitude shows up in the phase where the discharge occurs, and the corresponding frequency spectrum of the PD signal is dominated by a peak at 20 MHz
- in the other two phases, signals show up due to cross-talk. These signals have a smaller amplitude and their frequency spectra show a reduced peak at 20 MHz and a larger peak at 26..27 MHz.

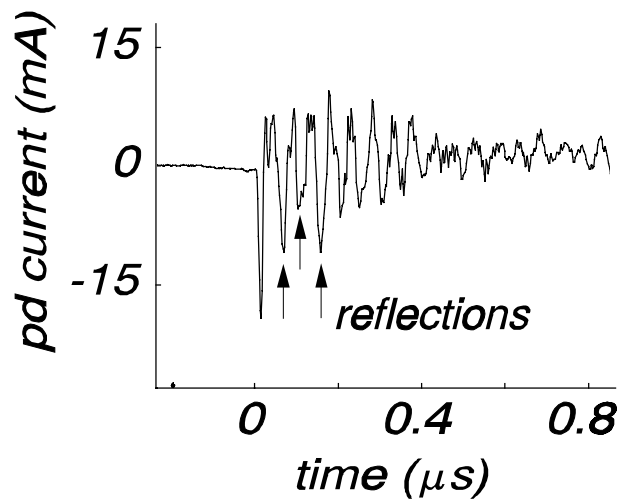


Figure 6.2 Partial discharge current in phase V, derived after integration of the measured PD signal in Fig. 6.1.

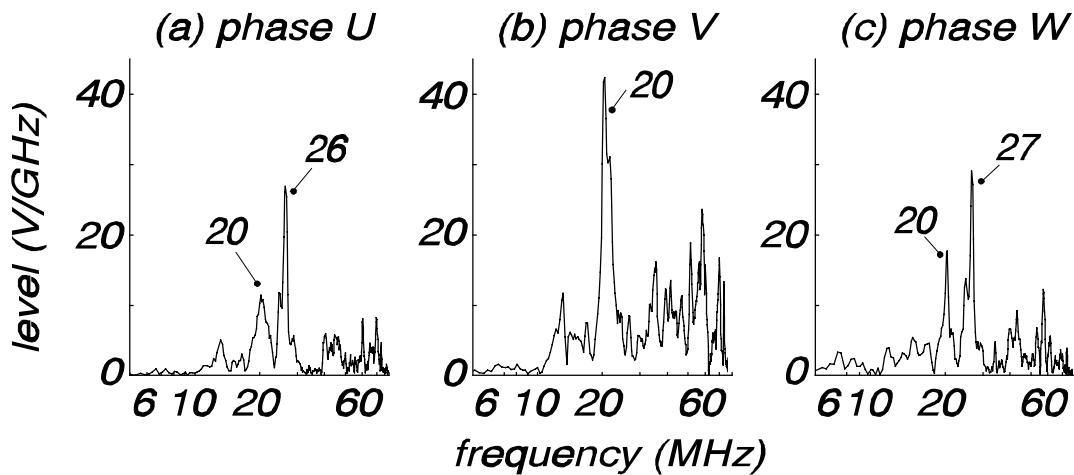


Figure 6.3 Frequency spectra of the PD signals in Fig. 6.1.

In addition to the partial discharge signals as in Fig. 6.1, other signal types are present. Two examples are given in Fig. 6.4. For both signals, no transient character or reflections can be recognized. Therefore they are regarded as interference; the source is unknown. The dominant frequencies¹⁰ are 2.7 MHz for Fig. 6.4a and 78 MHz for Fig. 6.4b.

¹⁰for an explanation of the 'dominant frequency', see Section 4.2

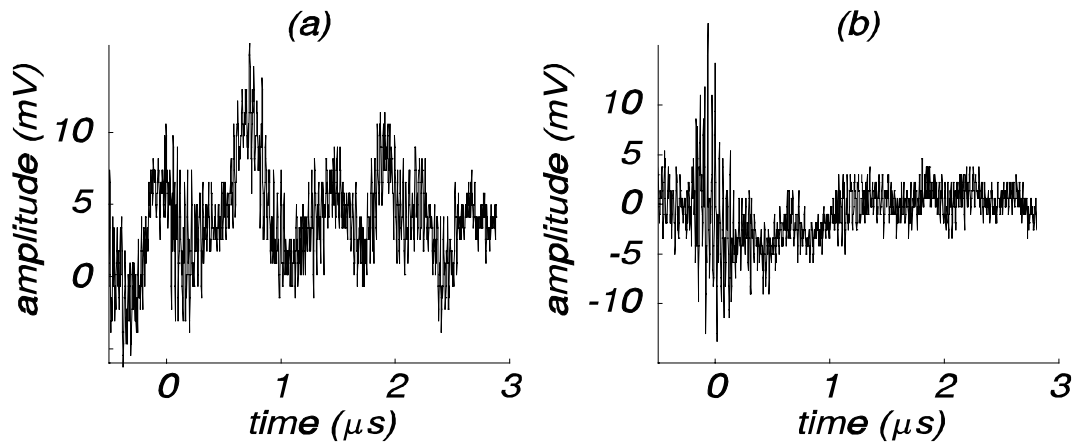


Figure 6.4 Two signals that are regarded as interference; (a) has a dominant frequency of 2.7 MHz and (b) has a dominant frequency of 78 MHz.

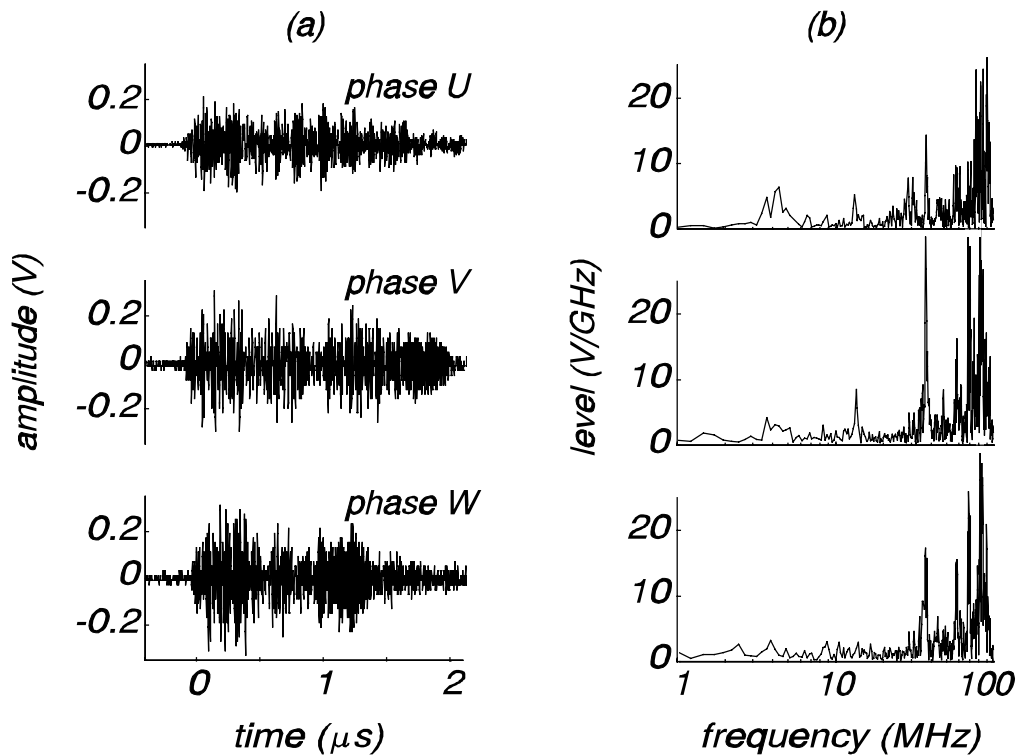


Figure 6.5 (a) Example of three signals (recorded simultaneously) that are regarded as interference and are rejected for further analysis. (b) The calculated frequency spectra show dominant frequencies at 32 MHz and 80 MHz.

An example of an other class of signals, which have a transient character, is given in Figure 6.5. The signals are dominated by very high frequencies (dominant frequencies are 32 MHz and 80 MHz), thus it is likely that they are caused by partial discharges. However, the amplitude of the signals is nearly similar for all three phases, and again no structure can be recognized in the signal. These signals form a 'grey' category. It was decided to reject this category for further analysis. This decision was motivated by the fact that: (i) all signals in this category occur at a fixed position with reference to the 50 Hz voltage (see Fig. 6.7c), and (ii) for all measuring sessions, only 6 % of the recorded signals belong to this category.

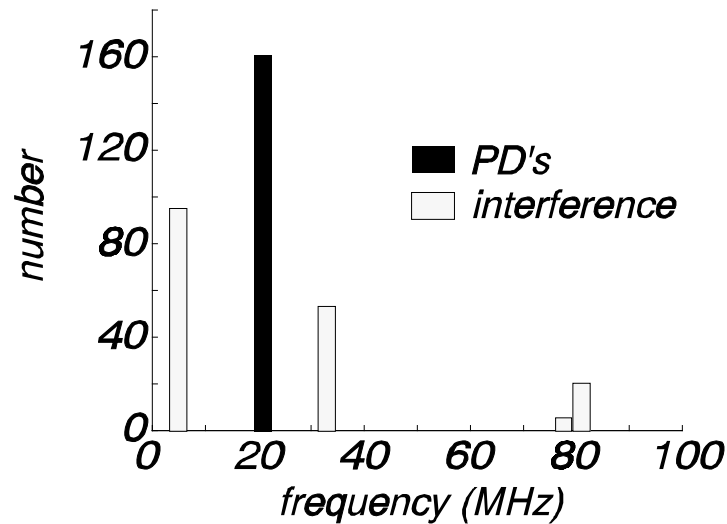


Figure 6.6 Histogram of the dominant frequencies for 336 events.

Figure 6.6 shows a histogram of the dominant frequencies for 336 events, recorded at 18 July 1995. All signals with a dominant frequency near 20 MHz are identified as partial discharges in phase V. The signals with dominant frequencies near 3 MHz, 32 MHz or 80 MHz are regarded as interference. For most sessions, only a few interference signals were recorded. However, for unknown reasons during the sessions at 24 February 1995 and 18 July 1995 the majority of the signals were caused by interference. An overview is given in Table XII. The interference signals are not used for any further analysis.

Table XII Results of the analysis for all six measuring sessions. The Table gives the percentage of signals that are identified as interference.

session	28/2/94	9/6/94	19/10/94	24/2/95	18/7/95	25/2/97
% interference signals	0 %	40 %	13 %	70 %	52 %	0 %

6.2.2 Partial discharge patterns

Partial discharges are characterized by a typical PD 'pattern'; observed when we plot the amplitudes of the discharges versus their position on the 50 Hz voltage. Normally, PD's in voids in the insulation are grouped in the first and third quadrant of the 50 Hz cycle and have opposing polarities for both half-cycles of the voltage.

During the measuring session at 24 February 1995, about 70 % of the recorded events were classified as interference (see Table I). The result of the classification for this session were:

- 101 events are classified as PD's in phase V and correspond with the waveshapes as in Fig. 6.1
- 217 events are classified as interference and have waveshapes as in Fig. 6.4
- 18 events belong to the 'grey' category as in Fig. 6.5 and are regarded as interference.

To verify whether the classification criteria (based on the dominant frequencies) are correct, the PD patterns are plotted for each category. The pattern for the signals identified as PD's in phase V is given in Fig. 6.7a. The pattern is typical for partial discharges: the PD's are grouped in the first and third quadrant of the 50 Hz cycle. The pattern for the interference-signals (Fig. 6.7b) shows no phase-related structure; the signals are randomly distributed over the 50 Hz voltage. In addition, the interference signals have a small amplitude, compared to the PD signals. Finally, the signals in the 'grey' category occur at a fixed position with reference to the 50 Hz voltage (Fig. 6.7c). These results suggest that we used the correct classification criteria.

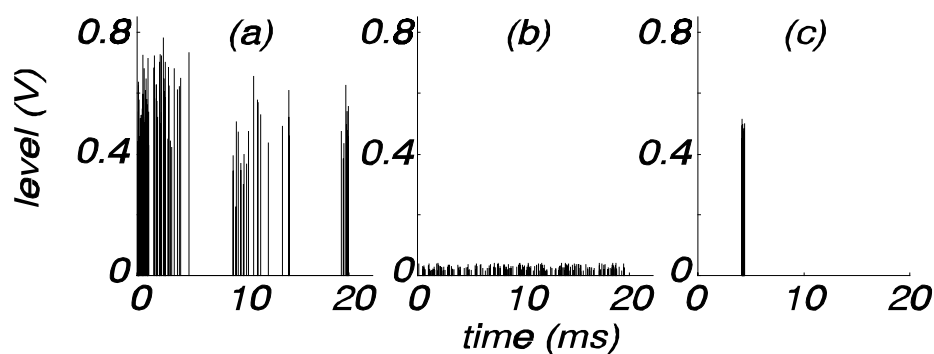


Figure 6.7 *Partial discharge patterns for the measuring session at 24 February 1995. The patterns are plotted only for signals recorded in phase V and classified as: (a) PD's in phase V (absolute values), (b) interference (peak-peak values), and (c) the 'grey' category (peak-peak values). The time axes are synchronous with the high-voltage in phase V.*

Figure 6.8a shows the partial discharge patterns for the session at 28 February 1994 for all measured signals (for each phase 336 signals were recorded). The time axis corresponds with the voltage in phase W. For this session, all signals were classified as partial discharges (see Table I). As can be seen, for each phase the signals are present at similar positions with reference to the 50 Hz voltage. This is an indication that all signals originate from discharges in one phase; evidently phase V since for this phase the largest signals are present. When discharges would be present in all three phases, several patterns should be visible, shifted over 120° in phase (or 6.7 ms in time).

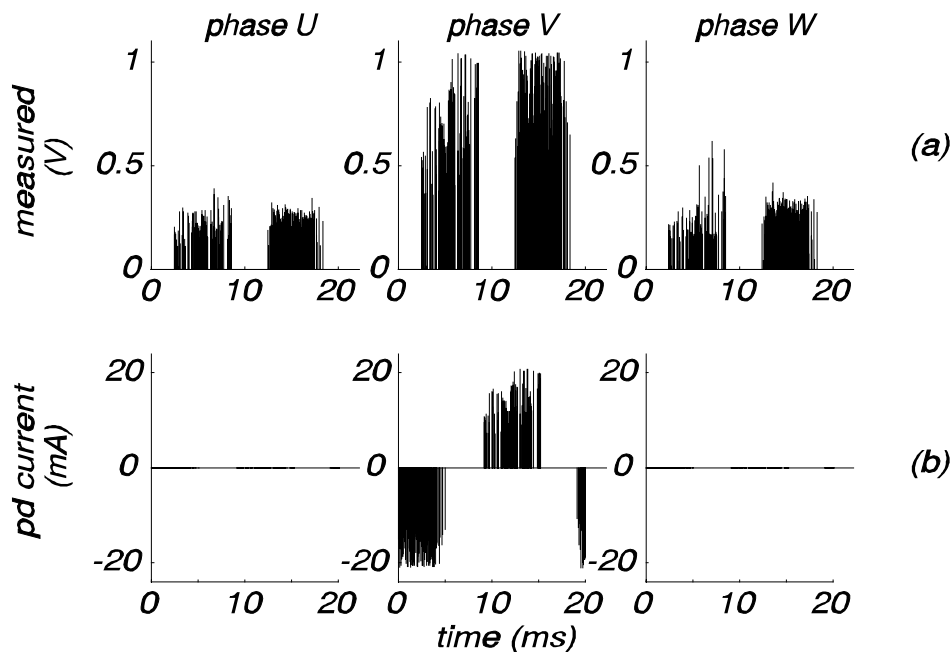


Figure 6.8 PD patterns for the measurements of 28 February 1994, (a) before and (b) after classification of the signals. (a) Gives the absolute values of the amplitudes of each signal versus their position on the 50 Hz voltage. The time axis is synchronous with the voltage in phase W. (b) Gives the amplitudes of the PD currents (after integration of the measured PD signals) versus their position on the 50 Hz voltage. The time axes are now synchronous with the actual high-voltage in each phase.

After analyzing all signals as described in the previous section, the amplitudes of all PD-currents (derived after numerical integration of the measured PD signal) are plotted versus their position on the actual 50 Hz voltage in their phase. The results are shown in Fig. 6.8b. Surprisingly only discharges are present in phase V. The pattern is typical for partial discharges: (i) the discharges are concentrated in the first and third quarter-cycle of the 50 Hz voltage of phase V, and (ii) the discharges have different polarities for both half-cycles of the 50 Hz voltage.

Six measuring sessions have been carried out. During all sessions the 650 MW generator was operating at full load under similar conditions. For five sessions, the results are almost identical, as can be seen in Fig. 6.9 (to obtain a more compact presentation than in Fig. 6.7b absolute values of all amplitudes are plotted). Remarkably, during the second session a different pattern was recorded, although the generator was running at conditions similar to the other sessions. The amplitudes are about a factor 10 less; this inconsistency cannot be explained.

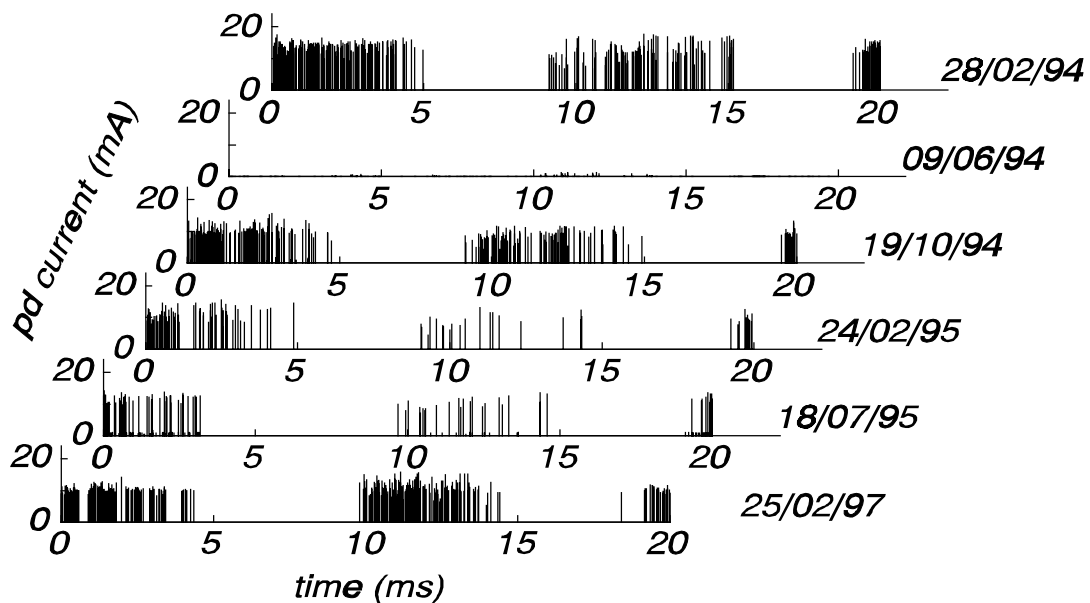


Figure 6.9 Partial discharge pattern for phase V for all six measurement sessions.

We were surprised by the fact that for all measurements only discharges in phase V showed up. For a generator in good condition (and we assume that Amer-9 is in a good condition since it is a relatively new and well maintained generator) we expect similar discharge behavior for all three phases. Therefore we did several additional measurements (see next Section) to verify whether the results of our measurements were correct.

6.3 Additional measurements

To verify the results as discussed in the previous Section, several additional measurements were done:

- simultaneous measurements at each of the four measuring terminals of the current sensor in phase V. The measurements are done with an oscilloscope
- zero-span measurements with a spectrum analyzer, to see whether similar results are obtained with this different measuring technique
- with pick-up loops near possible signal sources, to determine whether the measured signals come from the generator or from other sources. The signals from the pick-up loops are recorded by both a spectrum analyzer and an oscilloscope.

6.3.1 Simultaneous measurements at each of the four sensor terminals

Figure 6.10 gives a result of simultaneous measurements at each of the four measuring terminals of the current sensor in phase V. At each terminal, a similar signal is measured. This can only be the case when the signals are a result of a current through an enclosed conductor (in this case a PD current through the terminal of phase V). Other sources, for instance a current through a neighboring conductor, would give signals with different amplitudes. A special situation occurs when sparking occurs close to the sensor. This happened during some of the measurements on generator Hemweg-8, where sparking at a sensor occurred which caused a large signal at the terminal close to the spark, whereas no signals were seen at the other three terminals. This case is discussed in Chapter 7.

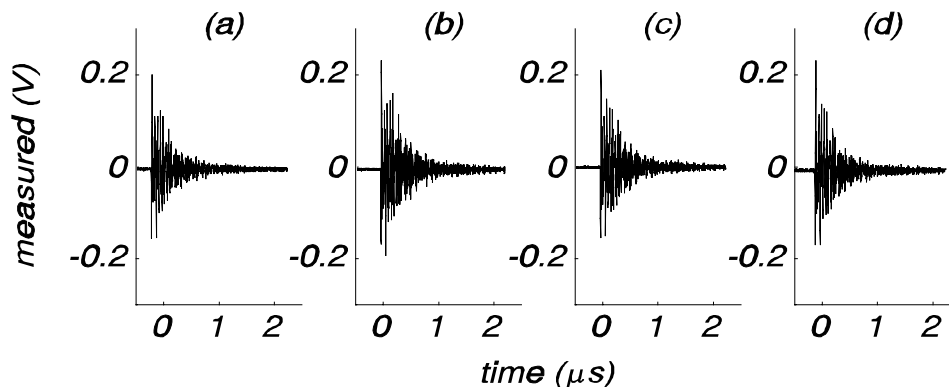


Figure 6.10 *Simultaneous measurements at each of the four measuring terminals of the inductive current sensor in phase V.*

6.3.2 Zero-span measurements with a spectrum analyzer

Figure 6.11 gives the results of zero-span measurements with a spectrum analyzer. These measurements were done to verify whether similar results are obtained with a different measuring technique. Compared to time-domain measurements, no trigger-settings are needed and a longer measuring time is possible. For each phase, the tuning frequency was 20 MHz and 999 sweeps of 40 ms were recorded (thus the total measuring time is 40 s). The time axis is synchronous with the high-voltage in phase W. The results are similar to the results obtained in the previous Section (see Fig. 6.8a); the discharges occur in phase V, the signals in the other two phases occur at the same position on the 50 Hz voltage and are a result of cross-talk.

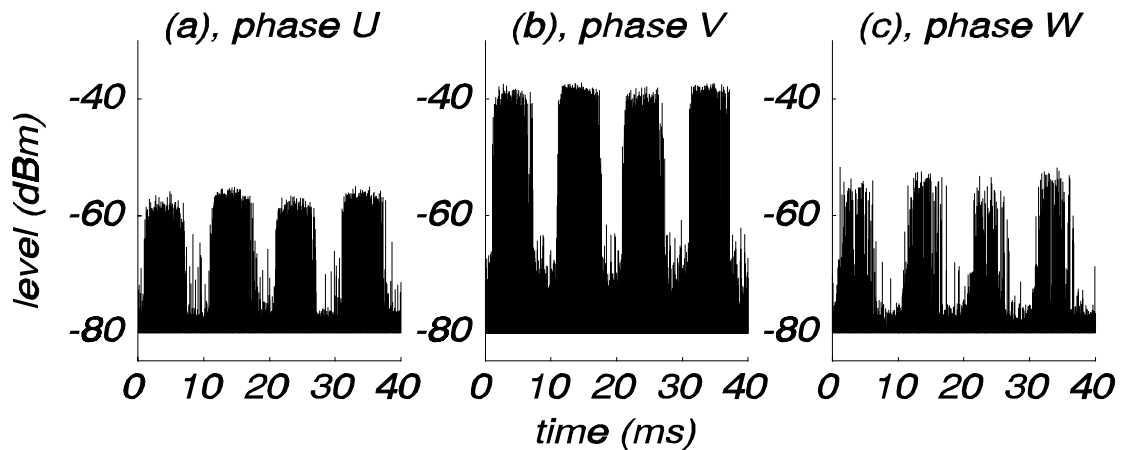


Figure 6.11 *Zero-span measurements with a spectrum analyzer. The analyzer is tuned to 20 MHz and for each phase 999 sweeps of 40 ms were recorded. The time axis is synchronous with the high-voltage in phase W.*

6.3.3 Measurements with pick-up loops

We also did measurements with pick-up loops near possible signal sources: (i) close to the high-voltage terminal of phase V, where we expect the PD signal, (ii) between the sheaths of the ipb, (iii) near the excitation brushes and the slip-rings of the generator rotor and (iv) near the shaft-grounding brushes of the turbine shaft. Signals are recorded with a spectrum analyzer (one channel only) or with a digital oscilloscope.

Figure 6.12 shows the results of zero-span measurements with a spectrum analyzer (tuning frequency 20 MHz, 50 sweeps of 20 ms). When the pick-up loop is placed near the high-voltage terminal of phase V, the PD pattern is measured (Fig. 6.12a). Also with a pick-up loop between the sheaths of the ipb we see the discharge pattern, however the signals are very small (Fig. 6.12b). On any other location, no signals were detected (Fig. 6.12c,d).

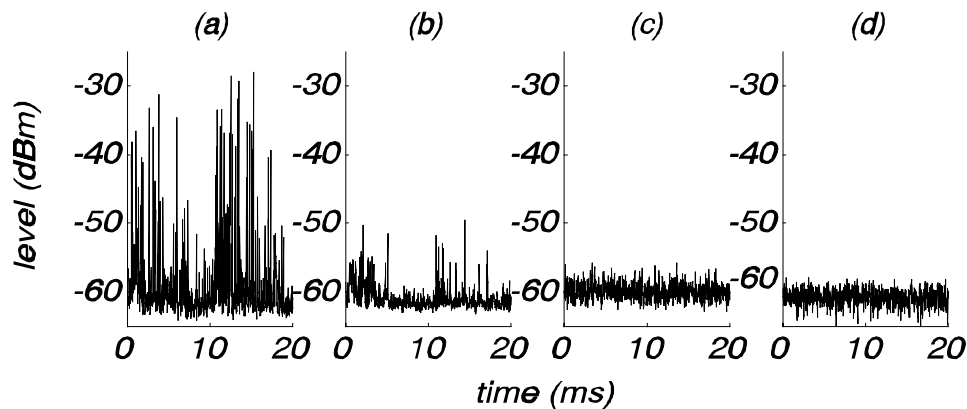


Figure 6.12 Zero-span measurements with a spectrum analyzer tuned to 20 MHz and with a pick-up loop at various positions; (a) near the high-voltage terminal of phase V, (b) between the sheaths of the ipb (between phases U and V), (c) near the brushes and sliprings of the rotor excitation system and (d) near the shaft-grounding brushes of the turbine-shaft.

With the oscilloscope more than 2000 measurements were made with pick-up loops at various positions, and since the oscilloscope has four channels, several combinations of sensors could be recorded simultaneously. An example of a time domain measurement with the oscilloscope is given in Fig. 6.13. The figure shows a simultaneous measurement with the inductive current sensor of phase V (Fig. 6.13a) and three pick-up loops, positioned: between the sheaths of the IPB (Fig. 6.13b), near the brushes and sliprings of the rotor excitation system (Fig. 6.13c) and near the shaft-grounding brushes (Fig. 6.13d). Only with the single-turn current sensor for phase V appreciable signals were seen. At any other position only weak, insignificant signals were recorded.

Only for one measurement a signal was seen at an other position. For this record the outputs of the three inductive current sensors were recorded simultaneously with the signal of a pick-up loop near the brushes and slip-rings of the rotor excitation

system. The record is shown in Fig. 6.14 and shows a peak near the sliprings, probably due to local sparking of the brushes. The signal is not seen by the current-sensors at the generator terminals.

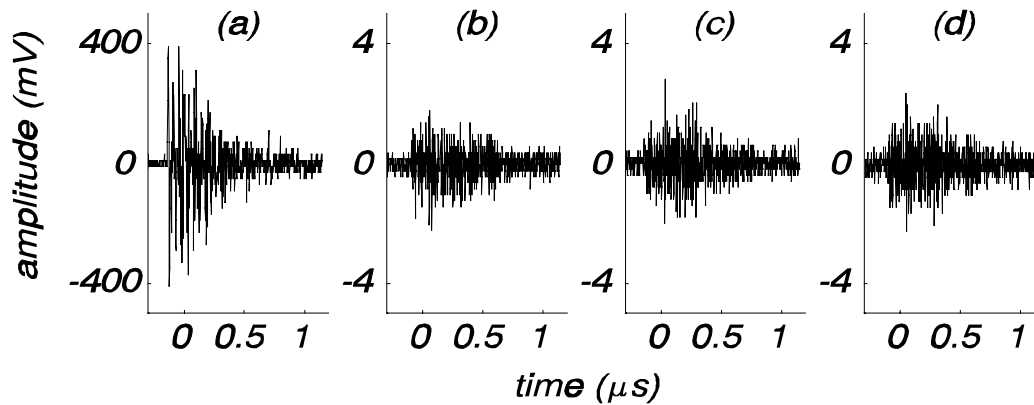


Figure 6.13 Simultaneous measurements in the time-domain (all triggered by (a)) with (a) the inductive current sensor of phase V, (b) a pick-up loop between the sheaths of the ipb (between phases U and V), (c) a pick-up loop near the brushes and sliprings of the rotor excitation system, and (d) a pick-up loop near the shaft-grounding brushes. Note that the vertical scale is different for the four figures.

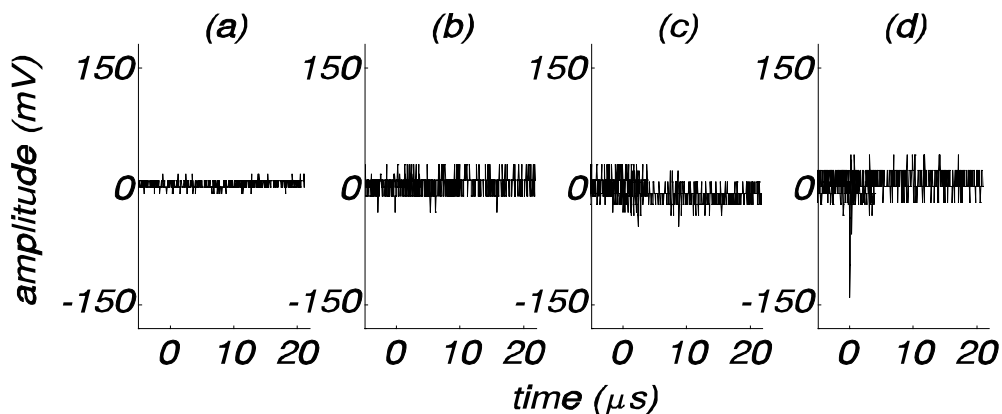


Figure 6.14 Simultaneous measurements with the inductive current sensors (triggered by spark) in (a) phase U, (b) phase V, (c) phase W, and (d) a pick-up loop near the brushes and sliprings of the rotor excitation system.

6.4 Conclusions

From the time-domain measurements on generator Amer-9 it was found that a partial discharge inside the generator causes a signal in each of the three phases. The signal with the largest amplitude shows up in the phase where the discharge occurs. Due to cross-talk, in the other two phases signals are present with a smaller amplitude. In addition to the PD signals, interference was recorded. Discrimination between signals due to partial discharges, cross-talk between the phases and interference is possible by determining the dominant frequency-component in the frequency spectrum:

- partial discharges show a large peak in their frequency spectrum at 20 MHz, which is caused by reflections of the PD-pulses at a discontinuity in the IPB. The reflection time is 50 ns (or $1/50 \text{ ns} = 20 \text{ MHz}$)
- a weaker 20 MHz peak can also be seen in the signals resulting from cross-talk, however for the cross-talk a larger peak is present at 26 or 27 MHz
- interference signals are characterized by dominant frequencies of 3 MHz, 32 MHz or 80 MHz.

The classification criteria were confirmed by the PD-patterns: the patterns for signals classified as PD's are typical for partial discharges, while the patterns for signals classified as interference show no phase-related structure.

During the six measuring sessions, the recorded partial discharge patterns were nearly similar. In all sessions, only discharges coming from phase V were recorded. This unexpected result was confirmed by additional measurements:

- simultaneous measurements at each of the four measuring terminals of the current sensor in phase V show that an honest enclosed current is measured
- zero-span measurements with a spectrum analyzer give results similar to the time-domain measurements
- measurements with pick-up loops at various positions show that all measured signals come from the generator. Only near the high-voltage terminal of phase V, and at no other position, significant signals have been detected.

We must conclude that partial discharges are only observed in phase V. No explanation for this result can be given.

Chapter 7

MEASUREMENTS ON TURBINE GENERATOR HEMWEG-8

7.1 Introduction

Turbine generator Hemweg-8 is a 650 MW generator of the UNA-Hemweg power plant in Amsterdam. The generator has been in operation since 1993 and has a nominal output voltage of 21 kV. The main generator data are given in Appendix A. All measurements on this generator have been done by means of single-turn inductive current sensors, permanently installed around the three high-voltage terminals of the generator. Since November 1994 the following measuring sessions have been carried out:

- between November 1994 and December 1995, four sessions of time-domain measurements, according to the procedure of Section 4.2. The results are shown in Section 7.2
- in 1996 four sessions with a spectrum analyzer in the zero-span mode, according to the procedure of Section 4.3. The results are given in Section 7.3
- during 1996 and 1997 additional measurements were taken to locate two discharge sources: (i) sparking near the current sensor of phase U, and (ii) sparking inside the step-up transformer. This is described in Section 7.4.

7.2 Time domain measurements

7.2.1 Measured waveshapes

A typical record of a true partial discharge is shown in Fig. 7.1. Due to cross-talk between the phases, a signal shows up in all three phases. It is concluded that the discharge occurs in phase W because: (i) phase W has the largest amplitude, (ii) the signal starts with a bipolar pulse, since the current sensors measure the derivative of an enclosed current, and (iii) the pulse reflects in the IPB at a connection to a voltage transformer (the reflections are difficult to recognize in Fig. 7.1 and will be discussed later in this Section).

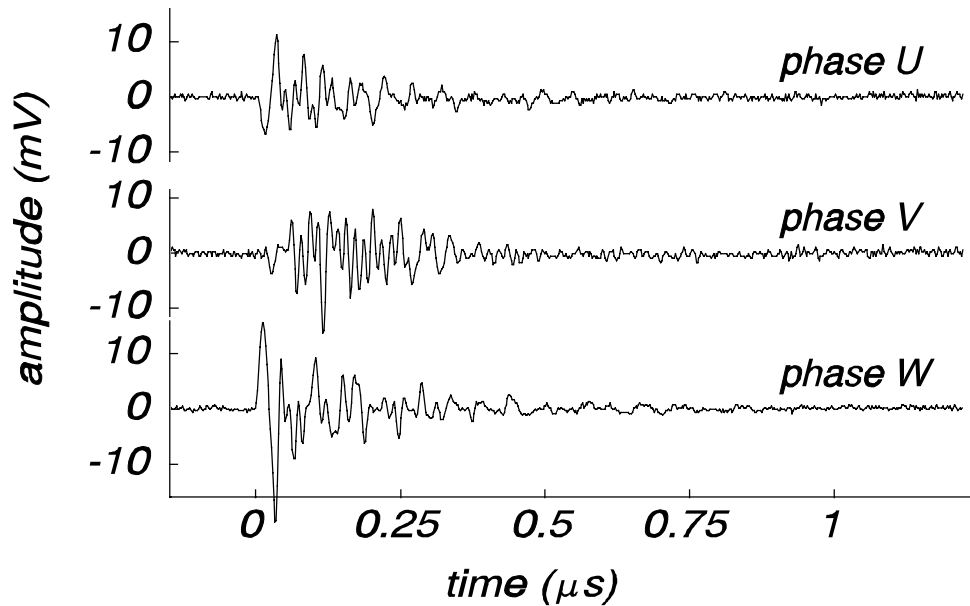


Figure 7.1 A partial discharge in phase W, observed simultaneously in all three phases. Due to cross-talk between the phases, signals also shows up in the other two phases.

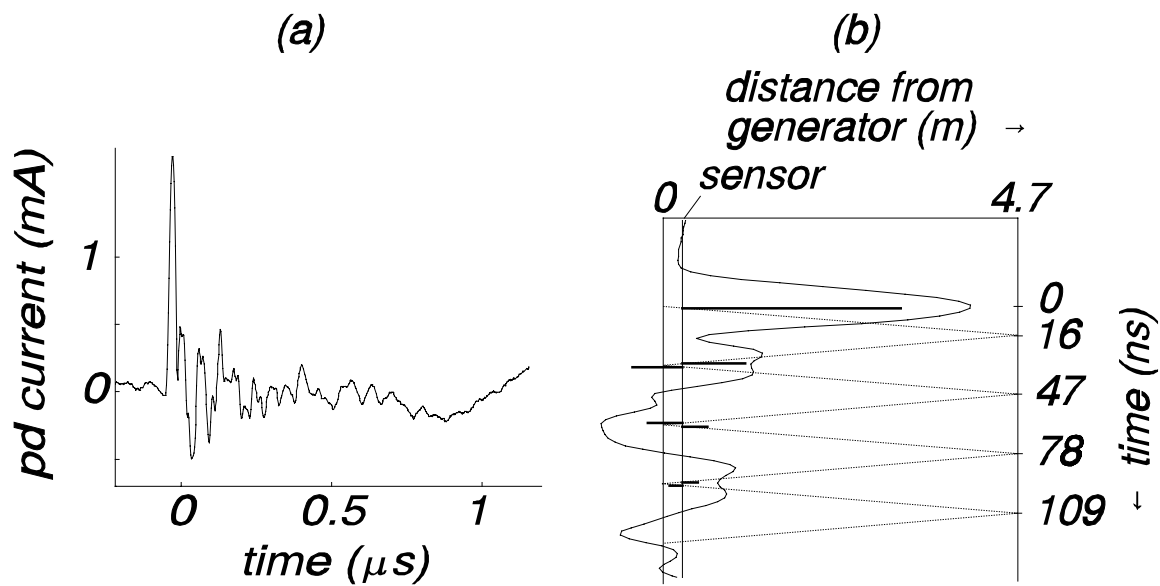


Figure 7.2 (a) The partial discharge current, derived after integration of the measured partial discharge signal from Fig. 7.1, and (b) the corresponding reflection diagram for this current pulse. The x-axis gives the distance along the IPB, the y-axis gives the propagation time. The heavy lines schematically indicate the reflected signals, where the reflection coefficients at the right and the left were assumed to be positive and negative.

To obtain the actual partial discharge current, the measured PD-signal is numerically integrated. An example is shown in Fig. 7.2a. The PD-current starts with a fast pulse, followed by several other pulses partly due to reflections in the IPB. These reflections are caused by a connection to a voltage transformer (at 4.7 m from the generator), which forms a discontinuity of the transmission line structure of the IPB. Since the pulse travels with the speed of light (3.3 ns/m), the corresponding reflection time is $2 \cdot 4.7 \cdot 3.3 = 31$ ns. A more detailed analysis of the reflections is given in the reflection diagram in Fig. 7.2b. It can be seen that after 15.5 ns the signal is reflected back towards the generator, with a positive reflection coefficient. At the generator, the signal is reflected with a negative reflection coefficient.

The calculated frequency spectra of the recorded signals are shown in Fig. 7.3. The spectra show several peaks, probably caused by resonances and reflections inside the generator. When determining the dominant frequency¹¹, the activity under 15 MHz and above 50 MHz is ignored. Now the dominant frequencies are: 22 MHz for phase U, 21 MHz for phase V and 18 MHz for phase W.

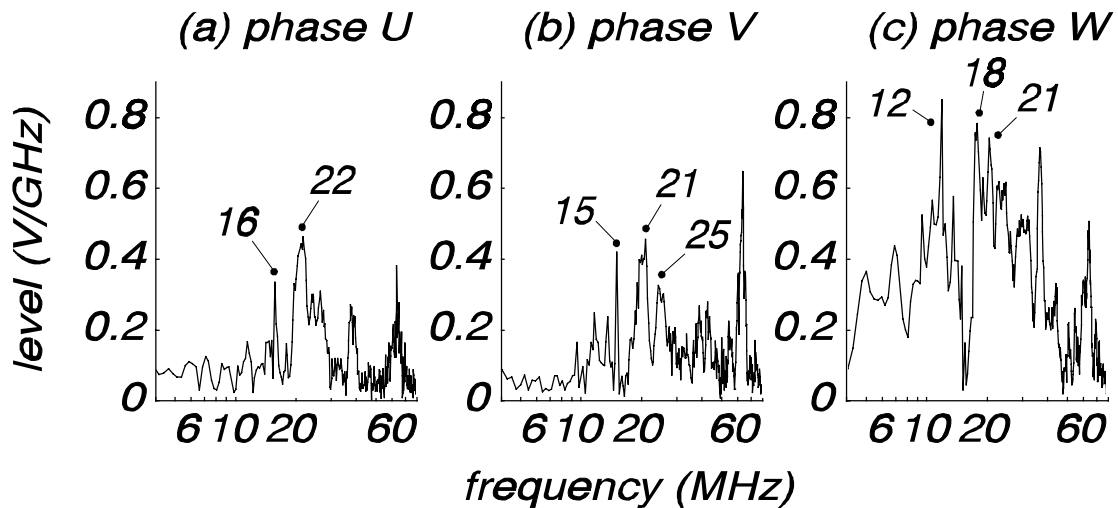


Figure 7.3 Frequency spectra of the signals in Fig. 7.1. The partial discharge occurs in phase W, the signals in the other two phases are caused by cross-talk.

¹¹for an explanation of the 'dominant frequency', see Section 4.2.

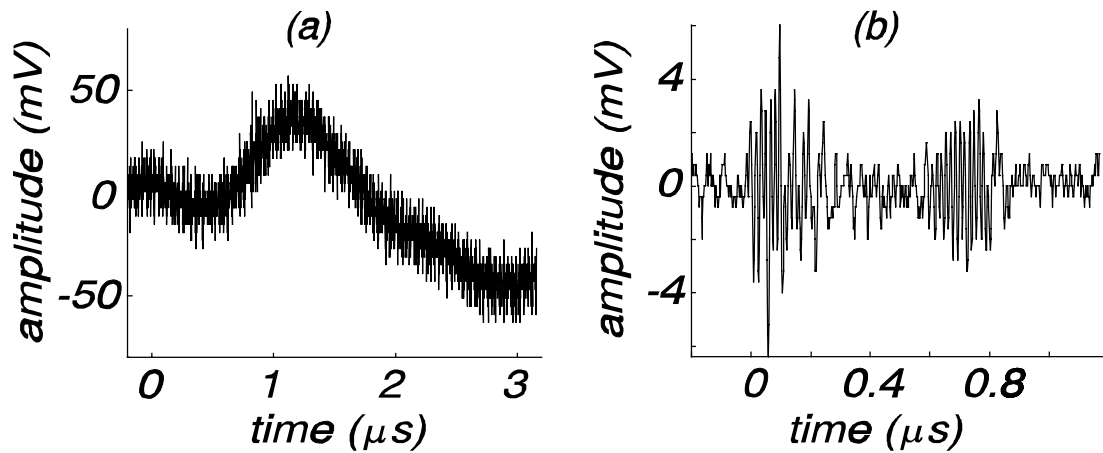


Figure 7.4 Examples of two signals that are considered to be interference. The dominant frequencies are (a) 27 MHz and (b) 24 MHz.

In addition to the PD-signals as in Fig. 7.1, other types of signals were recorded. Two examples are given in Fig. 7.4. The dominant frequencies are respectively 27 MHz and 24 MHz. No structure, such as a clear pulse shape and reflections, can be found, thus they are considered to be interference.

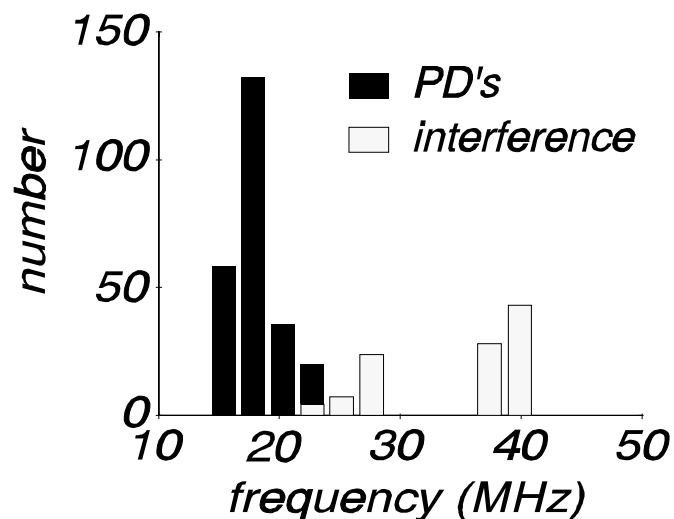


Figure 7.5 Histogram of the dominant frequencies for the measuring session at 2 November 1994. After analysis, 91 of the 336 recorded events are regarded as interference.

A histogram of the dominant frequencies f_d for the measuring session at 2 November 1994 is shown in Fig. 7.5. The automatic classification by the computer is, for this generator, done according to the following criteria:

- if $f_d < 24$ MHz then classify as partial discharge
- if $f_d \geq 24$ MHz then classify as interference.

After the manual confirmation of each classification (see Section 4.2.3), it was found that these criteria are correct for the majority of the recorded signals. However 6 signals which were automatically classified as PD's, had a different shape in the time-domain. Therefore these signals were regarded as interference and the classification had to be corrected. The dominant frequencies for these signals are about 22 MHz, as can be seen in Fig. 7.5 as a small overlap in the histogram at 22 MHz. After analysis, 91 of the 336 recorded events are considered to be interference (or 27 %).

The results of the analysis of all four measuring sessions are given in Table XIII. Especially for the measuring session at 18 October 1995, a large number of interference pulses was recorded. During this session, the generator was running at a reduced load (see Table II), and the average discharge level was about 40 % lower than for the other three sessions (see next Section 7.2.2). Thus the PD signals were very small. Consequently, there was a higher chance to record interference signals. In the case of a dangerous deterioration of the stator winding, the PD levels will rapidly increase and can be expected to be much larger than the interference signals.

Table XIII Results of the analysis for all four measuring sessions. The Table gives the percentage of signals that are identified as interference.

session	2/11/94	8/5/95	18/10/95	8/12/95
% interference signals	27 %	18 %	61 %	46 %

7.2.2 Partial discharge patterns

After analyzing all signals as described in the previous section, the amplitude of all true PD-currents (obtained after numerical integration of the measured PD signal) are plotted versus their position on the actual 50 Hz voltage in their phase. The results are shown in Fig. 7.6. The figure gives the results for all three phases and all four measuring sessions.

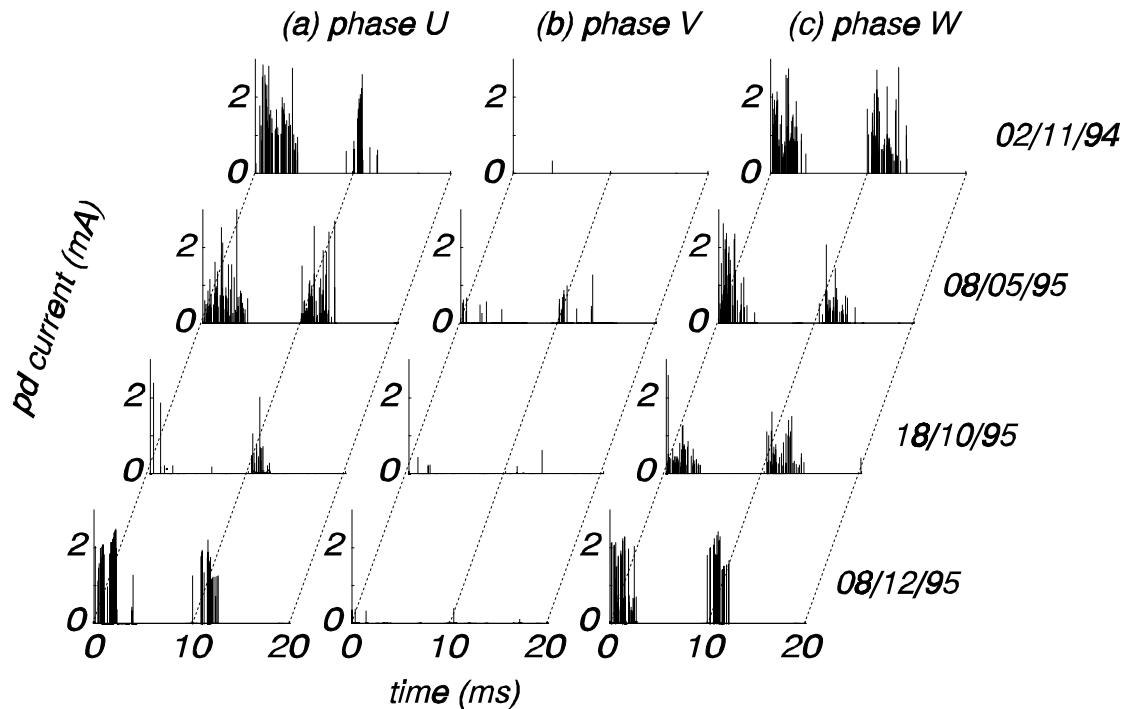


Figure 7.6 *Partial discharge patterns for all three phases and for all four measuring sessions (note: the absolute values of the PD-currents are plotted; the actual current peaks have different polarities for both half-cycles of the 50 Hz voltage).*

The obtained patterns are typical for partial discharges: the discharges are concentrated in the first and third quarter-cycle of the 50 Hz voltage. In addition the discharges have different polarities for both half-cycles of the 50 Hz voltage (not shown in Fig. 7.6). Surprisingly, only a few, small discharges are recorded in phase V.

The operating conditions during the four sessions are given in Table XIV. During three sessions, the generator was operating nearly at full load. The partial discharge patterns for these three sessions are almost identical. During the session at 18 October 1995, the generator was running at a reduced load, and therefore at reduced thermal and mechanical stresses. Now the average discharge level is about 40 % lower than for the other sessions, which indicates that discharges result of combined electrical, thermal and mechanical stresses.

Table XIV *Operating conditions during the four measuring sessions*

	2/11/94	8/5/95	18/10/95	8/12/95
power (MW)	635	645	460	620
reactive power (MVar)	91	158	100	70
winding temperature (°C)	59	60	50	58

7.3 Measurements with the tunable narrow-bandwidth detector

Partial discharges can also be detected by means of a spectrum analyzer (see Section 4.3). We did four measuring sessions, while the generator was running nearly at full load. During each session, we first record a frequency spectrum for each phase, followed by a series of zero-span measurements at 30 different tuning frequencies.

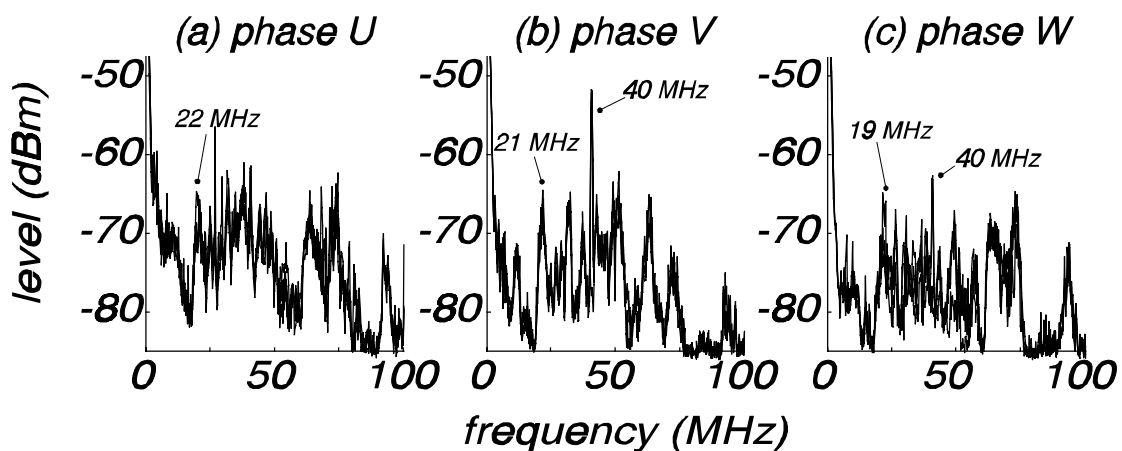


Figure 7.7 Frequency spectra for each phase and all 4 measuring sessions.

The frequency spectra, recorded between 0 and 100 MHz and given in Fig. 7.7, turn out to be similar for all measuring sessions. Also all three phases show similar activity. The spectra show several peaks that are caused by the partial discharges, which excite resonances in the stator windings or cause reflections of the signal in the IPB. The peaks at 40 MHz are caused by a local transmitter in the power plant, which was active part of the time. The positions of the other peaks are nearly similar to the peaks in the calculated frequency spectra of the time-domain measurements (see Fig. 7.3).

Preferably, for discharge measurements the spectrum analyzer should be tuned to a peak where the PD's are strong and no interference or cross-talk is present. To select this frequency, for each phase a series of zero-span measurements is carried out at various tuning frequencies (see Section 4.3.2). The results for phase V are already discussed in Section 4.3.2 (Figure 4.15); the other two phases give comparable results. It turns out that the best tuning frequency is 20 MHz for all three phases. Also the best tuning frequency remained constant for all four measuring sessions in 1996.

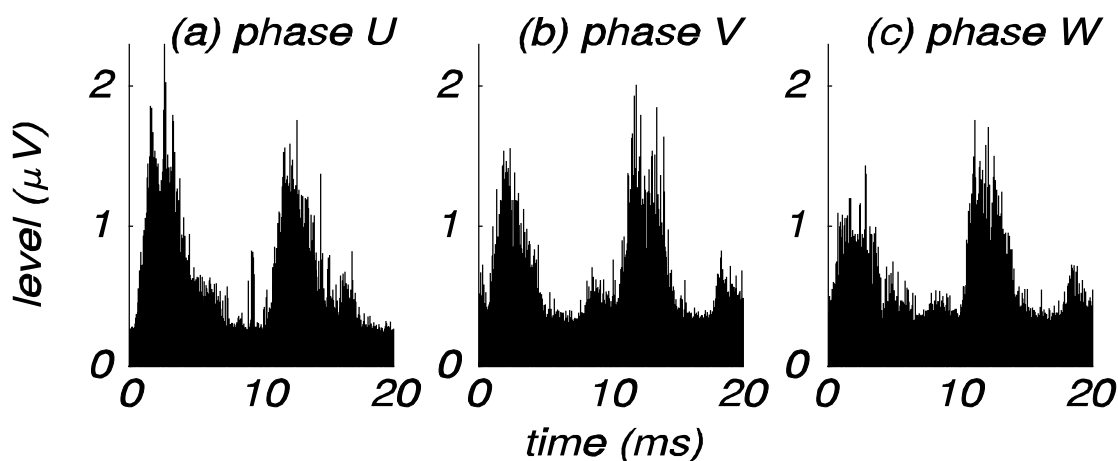


Figure 7.8 *Partial discharge patterns for all three phases, recorded at the optimal tuning frequency of 20 MHz. The timescale is synchronous with the actual high-voltage in each phase.*

Figure 7.8 gives the PD-patterns for all three phases at their best tuning frequency (at 20 MHz), recorded on 28 May 1996. All three phases show nearly similar discharge behavior. This is an indication that the generator is in good condition.

Contrary to the measurements with an oscilloscope (see the previous Section 7.2), discharges are now also observed in phase V. The discharge level is nearly similar to the level in the other two phases. During the measurements with the oscilloscope, very few discharges coming from phase V were recorded. An explanation might be the limited measuring time in comparison with the zero-span measurements. For the latter, all discharges during the measuring time of 60 s are recorded. With the oscilloscope, only 336 recordings are made with a sample-rate of 2 ns/sample and a record-length of 5120 points. Thus the total measuring time is $336 \cdot 2 \cdot 10^{-9} \cdot 5120 = 3.44$ ms. Also the trigger-settings of the oscilloscope can play a role. The signals of the three phases are recorded by means of three different types of plug-in units of the oscilloscope. These three plug-in units have different input- and trigger sensitivity ranges. However the trigger-settings were varied during a measurement: (i) all three phases are set as trigger-source for 1/3 of the measurements, (ii) 50 % of the measurements is recorded with a relatively high trigger-level (in this case 10 mV), all other measurements are done with the trigger-level set to 1 mV.

7.4 Localization of two discharge sources

7.4.1 Sparking near the current sensor in phase U

During the measurements with the spectrum analyzer, in phase U sometimes a large discharge activity was observed. An example is given in Fig. 7.9, which gives the frequency spectra for all phases, as recorded on 13 December 1996.

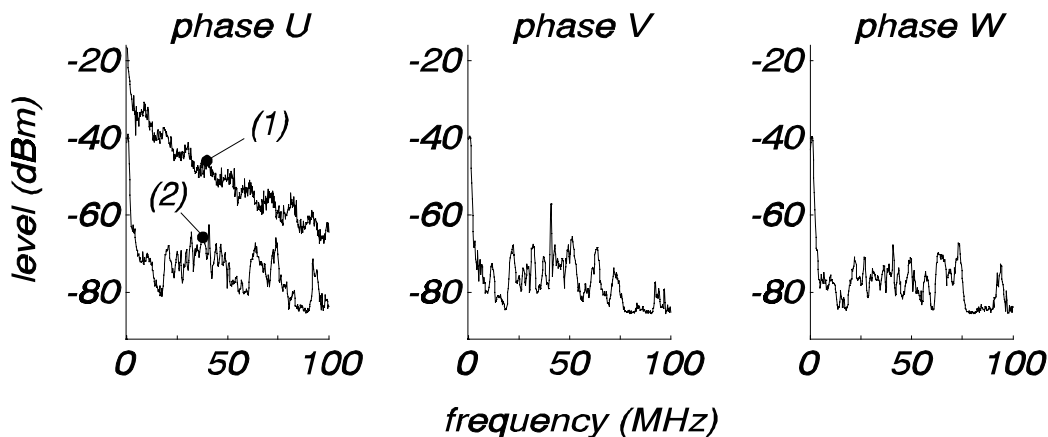


Figure 7.9 Frequency spectra for all three phases at 13 December 1996. Phase U sometimes shows large activity (curve 1).

The extra discharges in phase U have a quite different frequency spectrum. Therefore it was decided to monitor the discharge level in phase U during a longer period. The spectrum analyzer was tuned to the optimal frequency for phase U (20 MHz) and the video-output of the analyzer was recorded by means of a datalogger during 80 hours, with a sample-time of 5 seconds per sample. The result, given in Fig. 7.10 (solid line), indicates the presence of an erratic discharge source with large amplitude.

The location of this discharge source could be determined by simultaneous measurements at each of the four measuring terminals of the inductive current sensor in phase U. A result is given in Fig. 7.11. Only at one terminal (a) a large signal was present. This can only be the case when a local signal-source is present close to this particular measuring terminal. It was found that sparking occurred at a mounting-clamp of the sensor, located near the particular measuring terminal. This sparking was seen during a visual inspection.

As a solution, during a maintenance period of the power plant, the sensors were fully insulated from the generator-housing and the IPB. Now no more sparking took place, which was confirmed by monitoring the discharge level in phase U during 80

hours. The result is shown in Fig. 7.10 (dotted line), which shows a discharge level that slightly varies with the load of the generator. Clearly, the spurious discharges are no longer present.

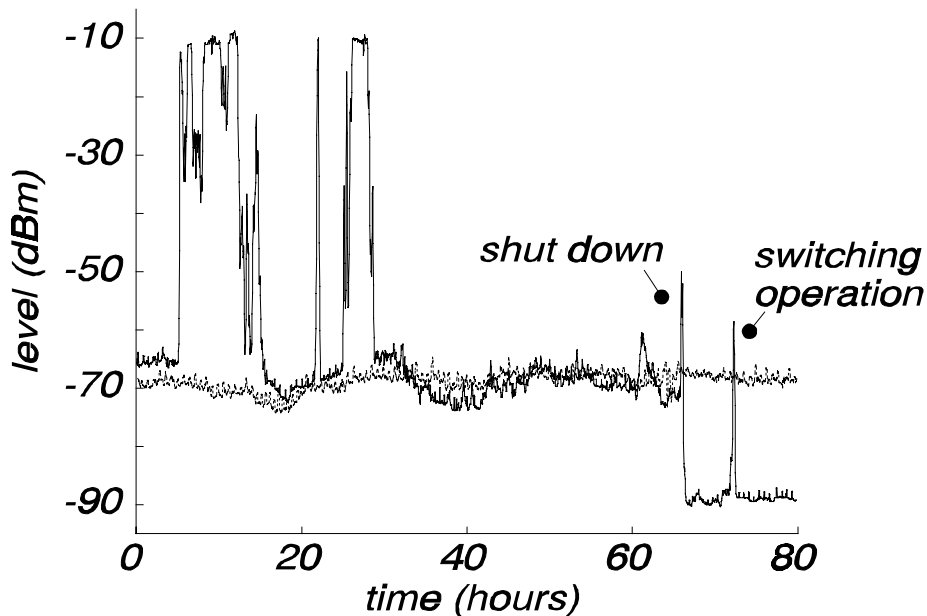


Figure 7.10 Partial discharge level in phase U of generator Hemweg-8, measured during 80 hours at a tuning frequency of 20 MHz. The first recording (solid line) started at 13 December 1996 at 14:00 hour. Note that the generator was shut down after about 65 hours; now it seems that the detection limit of the spectrum analyzer is about -90 dBm. After about 70 hours a peak is recorded due to a switching operation in the 150 kV substation. The second recording (dotted line) started at 21 November 1997 at 11:00 hour.

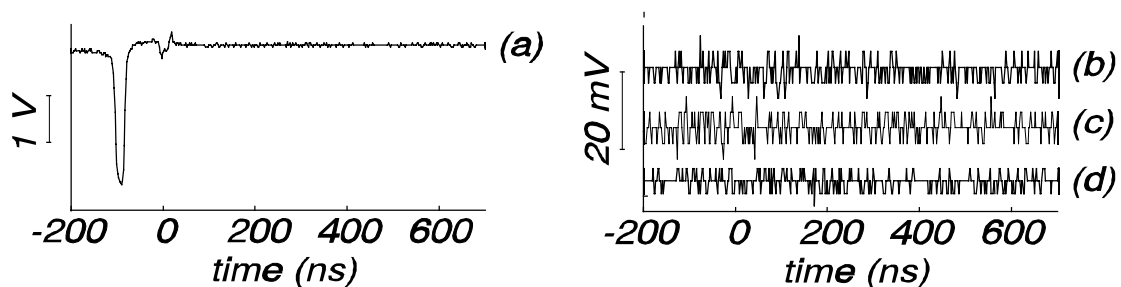


Figure 7.11 Simultaneous measurement at each of the four measuring terminals of the inductive current sensor of phase U.

7.4.2 Sparking inside the step-up transformer

A partial discharge inside the generator manifests itself at its terminals and then propagates along the IPB in the direction of the step-up transformer. An example is given in Fig. 7.12, where a PD in the generator first shows up at the Rogowski-coil at the generator terminal. After a transit-time¹² of 115 ns the signal also shows up at a pick-up loop near the 21 kV bushing of the step-up transformer.

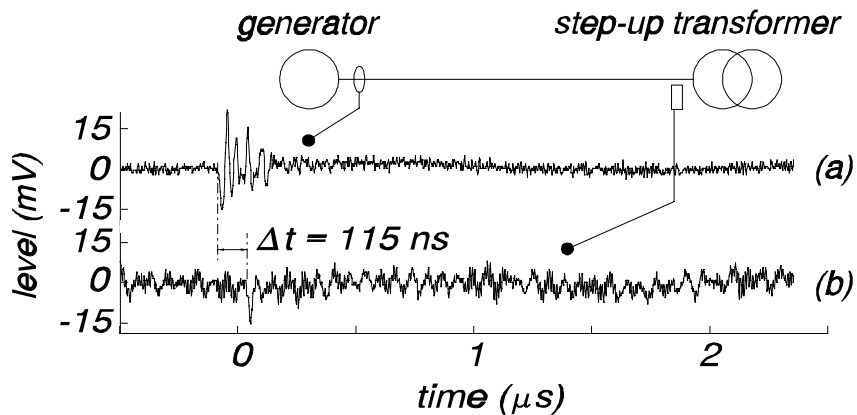


Figure 7.12 Partial discharge inside the generator, observed by means of: (a) a Rogowski-coil around the high-voltage terminal of phase U of the generator, and (b) a pick-up loop near the 21 kV bushing of phase U of the step-up transformer.

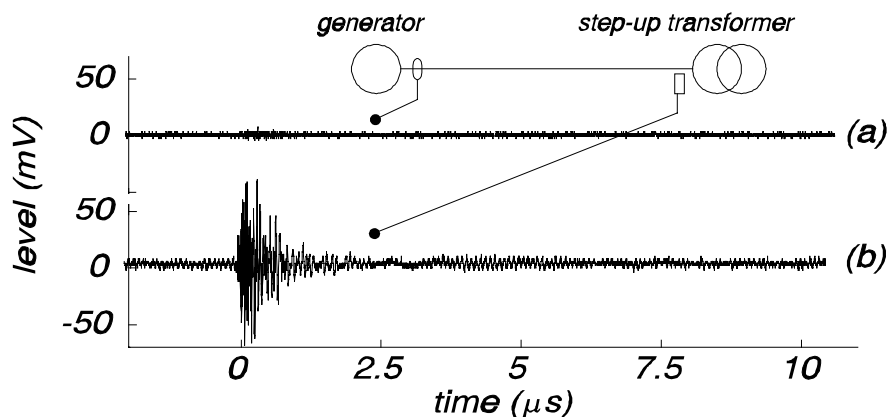


Figure 7.13 Attempt to observe PD's inside the step-up transformer by means of: (a) a Rogowski-coil around the high-voltage terminal of phase U of the generator, and (b) a pick-up loop near the 21 kV bushing of phase U of the step-up transformer.

¹²this transit-time is determined by the transit-time along the IPB ($24 \text{ m} * 3.3 \text{ ns/m} = 79 \text{ ns}$) and the different lengths of measuring cables (7.2 m or 36 ns).

Figure 7.13 shows a signal which first shows up at the transformer side. Due to damping of the IPB or to poor coupling of the signal into the IPB, it cannot be seen at the generator side. During a measuring session at 6 February 1997 about 50 % of the recorded signals were of this type and therefore seem to originate from the step-up transformer.

To verify whether these signals are indeed caused by partial discharges inside the transformer, the PD-patterns were recorded. Therefore both the outputs of the Rogowski-coil near the generator and the pick-up loop near the step-up transformer were connected to a home-built two-channel spectrum analyzer [Vri97]. The tuning frequency was 20 MHz for both channels and the patterns were recorded during 64 cycles of the 50 Hz voltage. The results are shown in Fig. 7.14.

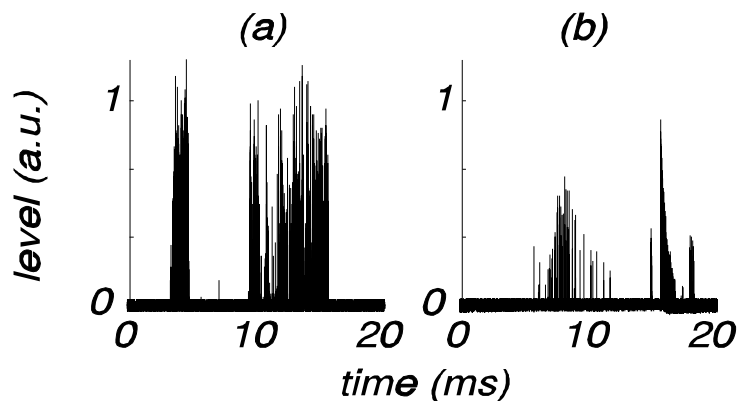


Figure 7.14 PD patterns¹³ measured with (a) a Rogowski-coil near the high-voltage terminal of phase U of the generator, and (b) a pick-up loop near the 21 kV terminal of the step-up transformer. Both patterns are recorded simultaneously by means of a 2-channel spectrum analyzer, tuned to 20 MHz.

Figure 7.14 shows two completely different patterns, although both patterns are recorded at the same busbar. It is fair to assume that the pattern in Fig. 7.14a corresponds with PD's in phase U of the generator, while the pattern of Fig. 7.14b is caused by discharges inside the step-up transformer.

In addition to the partial discharges, the step-up transformer showed a rapid increase of 'gas-in-oil' concentrations, especially of C₂H₆ (ethane) and C₃H₈ (propane) [Via97]. This increase is an indication for the presence of a hot-spot inside the trans-

¹³the time axis is synchronous with the 220 V supply voltage. The phase-angle with respect to the actual high-voltage in phase U is unknown.

former [Kri96]. During an inspection, four hot-spots were found which were caused by short-circuits between sub-conductors of the connection to a 21 kV bushing. One of the fault-locations is shown in Fig. 7.15; the hot-spot is indicated with an arrow. Near the hot-spot, the insulating paper is burned. This degradation of the paper, in combination with the local high temperature, give the increased gas-in-oil concentrations. The short-circuits led to intermittent sparking. This sparking gives signals similar to partial discharges, which were detected with the pick-up loop near the 21 kV terminals of the transformer (Fig. 7.13, Fig 7.14b).

During the next maintenance period, the step-up transformer was repaired by the manufacturer [Bur97]. After this repair, the discharge activity in the transformer had disappeared.

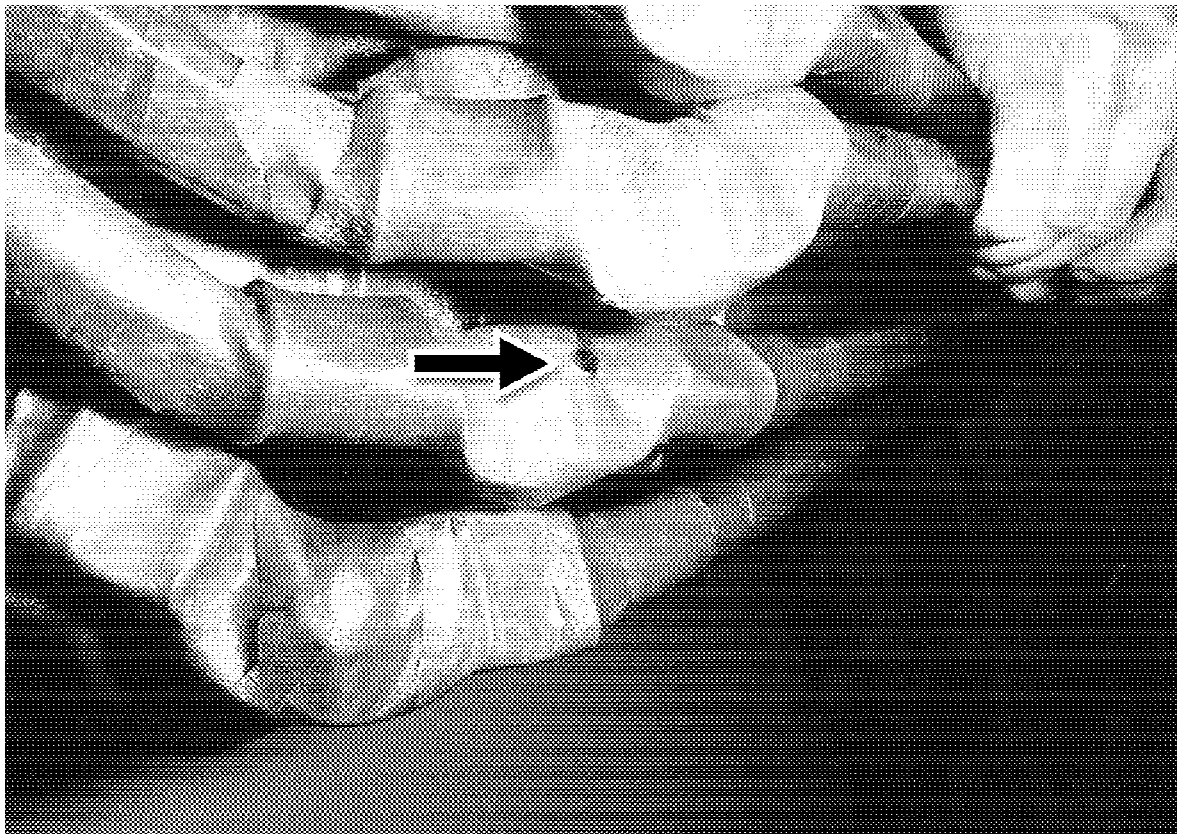


Figure 7.15 *One of the four fault locations in the step-up transformer; the short-circuit is indicated with an arrow. Due to the sparking and the high temperature near the short-circuit, the paper insulation is burned (the small black dot). The sparking results in discharges, while the decomposition of the paper causes increased 'gas-in-oil' concentrations.*

7.5 Conclusions

From time-domain measurements we found that a partial discharge causes a signal in each of the three phases. The signal with the largest amplitude shows up in the phase where the discharge occurs. Due to cross-talk, in the other two phases signals are present with a smaller amplitude. In addition to the PD signals, other types of signals were recorded which were considered to be interference. Discrimination between signals due to partial discharges, cross-talk between the phases and interference is possible by determining the dominant frequency-component in the frequency spectrum between 15 and 50 MHz.

The PD-patterns, which were obtained by means of time-domain measurements, are typical for partial discharges. However only a few discharges are recorded in phase V.

Partial discharges can also be detected by means of a spectrum analyzer in the zero-span mode. It turns out that the best tuning frequency for generator Hemweg-8 is 20 MHz. Contrary to the time-domain measurements, discharges are now also observed in phase V. Only a tentative explanation can be given for this.

During the various measuring sessions, sometimes an unusual discharge behavior was observed. It was found that, besides the normal discharge activity in the generator, two additional discharge sources were present: (i) sparking near the current sensor in phase U, and (ii) sparking inside the step-up transformer. By means of additional measurements, both sources could be located. During a maintenance period both sources were removed, after which the discharge activity was no longer present.

Chapter 8

MEASUREMENTS ON GASTURBINE GENERATOR ROCA-3

8.1 Introduction

The Roca-3 combined-cycle power plant of EZH in Rotterdam has a 169 MW gasturbine generator and a 126 MW steamturbine generator. The power plant has been in operation since June 1996 and both generators have a nominal output voltage of 15 kV. On-line partial discharge measurements have been done on both generators. In this thesis, only the results of measurements on the gasturbine generator will be discussed. The main data of this generator are given in Appendix A.

In each phase, four sensors were available for measurements on this generator: (i) two bus-support-capacitors, one close to the generator and a second one closer to the step-up transformer, (ii) one ring-capacitor, installed close to the bus-support-capacitors at the generator side, and (iii) an overvoltage-capacitor as part of the generator-circuit-breaker. An overview of the installed sensors is given in Fig. 8.1.

During a measurement session on 19 December 1996 both the time-domain measuring technique and the tunable narrow-bandwidth detector were used. The large variety of available sensors gives a unique opportunity for comparing the suitability of the three sensor types for both measuring techniques. The results will be discussed in respectively Section 8.2 and Section 8.3.

8.2 Time-domain measurements

A typical record of a true partial discharge is shown in Fig. 8.2. This signal is measured by means of the three bus-support-capacitors at the generator side. Due to cross-talk between the phases, a signal shows up in all three phases. It is concluded that the discharge occurs in phase W because the signal in this phase has the largest amplitude. The partial discharge signal in phase W starts, in this case, with a fast negative pulse, followed by several other pulses due to reflections in the IPB.

To analyze the reflections, a PD signal in phase W was measured simultaneously by all four sensors in this phase, as shown in Fig. 8.3. The signal first shows up at the ring-sensor and the bus-support-capacitor at the generator side. Both sensors

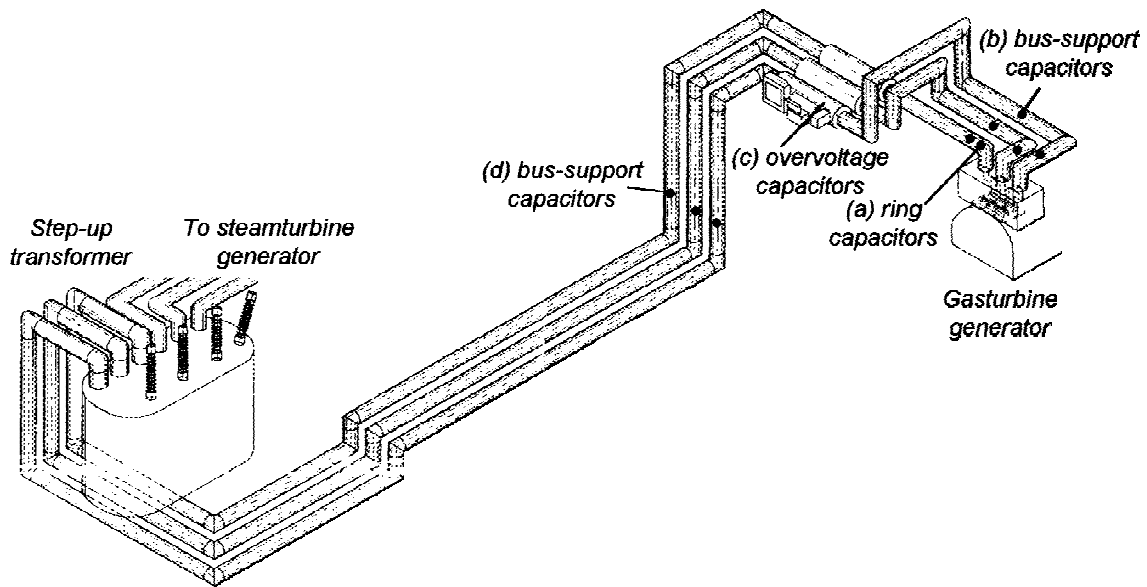


Figure 8.1 Overview of the isolated-phase-bus and the installed sensors of the gasturbine generator Roca-3.

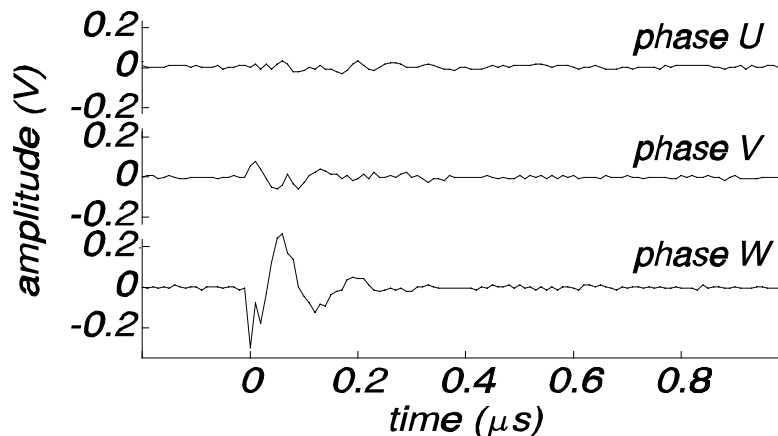


Figure 8.2 A partial discharge in phase W, observed simultaneously in all three phases. Due to cross-talk between the phases, signals also show up in the other two phases.

are close to each other, so no significant transit time can be seen between the two signals. The PD signal propagates with the speed of light along the IPB and arrives, after a transit time $\Delta t_1 = 46$ ns, at the overvoltage-capacitor. Here, part of the signal reflects back towards the generator, resulting in the various reflections that are indicated with arrows in Fig. 8.3. The resulting part of the PD signal continues towards the step-up transformer, and passes the bus-support-capacitor at the transformer side after a transit time $\Delta t_2 = 40$ ns. Both transit times Δt_1 and Δt_2 correspond to the actual distances between the sensors (14 m and 11.5 m respectively).

For a more detailed analysis of the reflections, the results in Fig. 8.3 are plotted in a reflection diagram (Fig. 8.4). The dotted lines show the propagation of the pulse along the IPB. It is clear that at the overvoltage-capacitor (21 m), part of the PD pulse is reflected back towards the generator, resulting in multiple peaks in the various sensor signals.

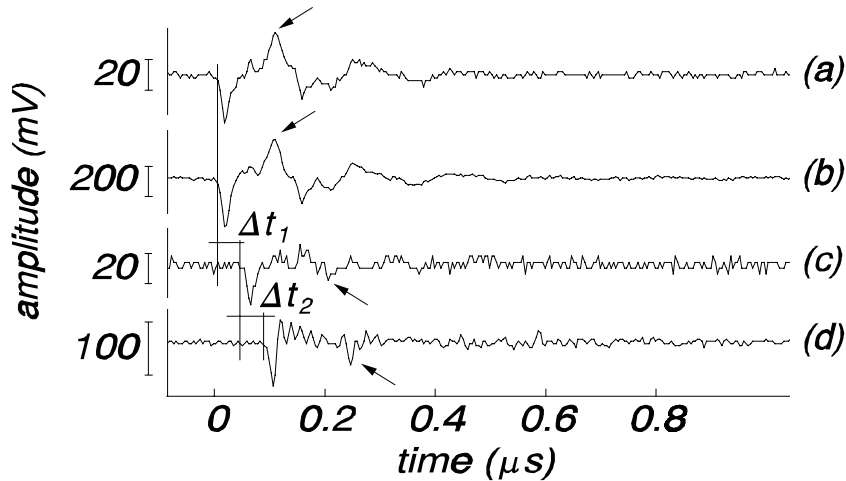


Figure 8.3 A partial discharge in phase W, measured simultaneously by all four sensors in this phase: (a) a ring-capacitor, (b) a bus-support-capacitor at the generator side, (c) an overvoltage capacitor, and (d) a bus-support-capacitor at the transformer side.

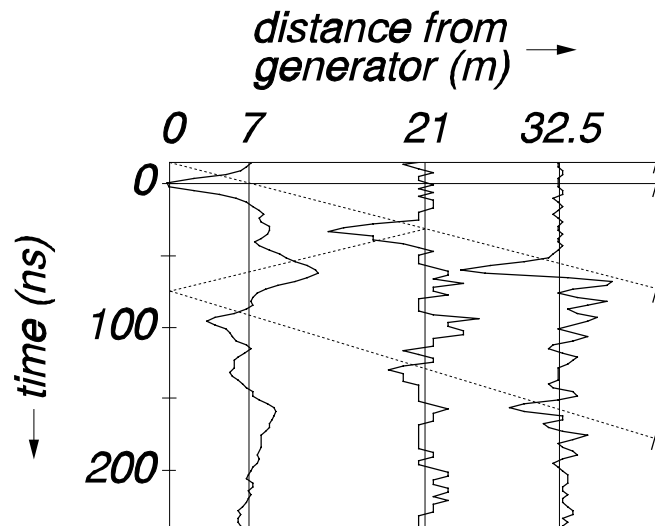


Figure 8.4 Reflection diagram for the signals in Fig. 8.3. The horizontal axis gives the positions of the bus-support-capacitor at the generator side (7 m), the overvoltage-capacitor (21 m) and the bus-support-capacitor at the transformer side (32.5 m).

The calculated frequency spectra of the three signals from Fig. 8.2 are shown in Fig. 8.5. The PD signal in phase W shows strong activity around a dominant frequency f_d of 7.2 MHz. The activity in the other two phases is much weaker. The spectra in Fig. 8.5 are obtained by means of the bus-support-capacitors at the generator side. Due to reflections of the PD signals, different waveshapes show up at the other sensors, resulting in different frequency spectra (see also Fig. 8.12). Nevertheless, all recorded PD-signals had dominant frequencies between 6 and 9 MHz. During the measuring session on 19 December 1996, 672 events were recorded for each sensor type. All events were classified, according to the method described in Section 4.2, as partial discharges inside the generator.

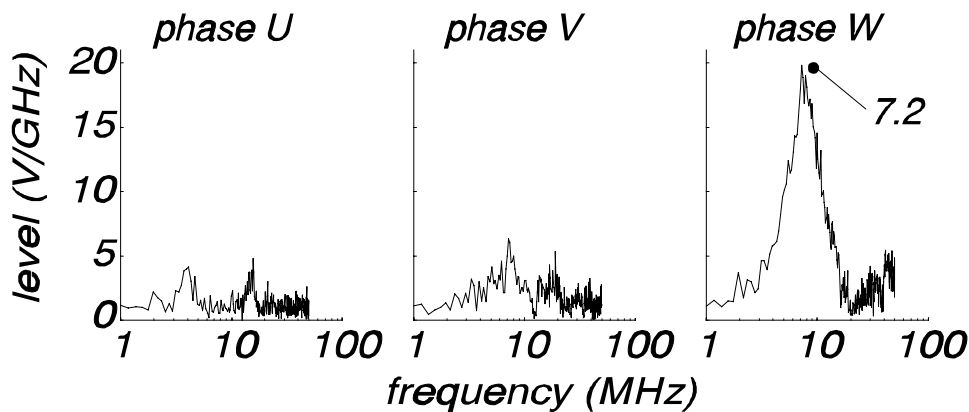


Figure 8.5 Frequency spectra of the signals in Fig. 8.2. The partial discharge occurs in phase W, the signals in the other two phases are caused by cross-talk.

The PD-patterns for phase U, obtained by means of the four different sensors in this phase, are shown in Fig. 8.6. The patterns are almost identical for the four sensors, however the bus-support-capacitor at the generator side gives higher amplitude signals, and thus has a better sensitivity (Fig. 8.6b). Nevertheless, all sensor types give good results. The obtained patterns are typical for partial discharges: the discharges are concentrated in the first and third quarter-cycle of the 50 Hz voltage. In addition the discharges have different polarities for both half-cycles (not shown, since the absolute values of the PD-signals are plotted).

The patterns for the phases V and W are given in Fig. 8.7 and Fig. 8.8 respectively. As for phase U, the patterns are typical for partial discharges, all sensor types give good results and the best sensitivity is obtained with the bus-support-capacitors at the generator side. The patterns for phase W are nearly similar to the patterns for phase U, however for phase V completely different patterns were observed. Not only are the amplitudes of the discharges in phase V roughly a factor two smaller than in the other two phases, but also we see an asymmetry between the two half cycles. During the

positive cycle of the 50 Hz voltage in phase V, the discharges are spread out between 0 and about 6 ms, while they are concentrated between 10 and 13 ms during the negative cycle. Also the discharges during the positive cycle have a smaller amplitude than during the negative cycle. Generally such an asymmetric pattern indicates partial discharges at the interface between the insulation and one of the electrodes. No further analysis could as yet give more certainty on this point.

The rest of this page is intentionally left blank
to facilitate the comparison of the PD-patterns obtained by means of
time-domain measurements (Figs 8.6 to 8.8) and
the tunable narrow-bandwidth detector (Figs 8.9 to 8.11).

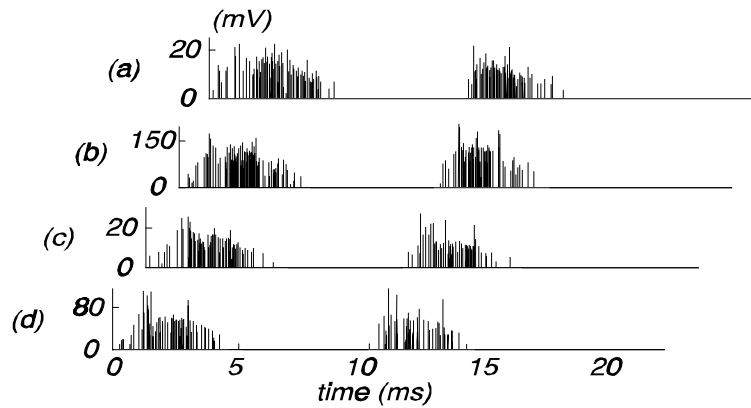


Figure 8.6 PD patterns of phase U of generator Roca-3, obtained by means of time-domain measurements. The patterns are measured with (a) the ring-capacitor, (b) the bus-support-capacitor at the generator side, (c) the overvoltage capacitor, and (d) the bus-support-capacitor closer to the step-up transformer.

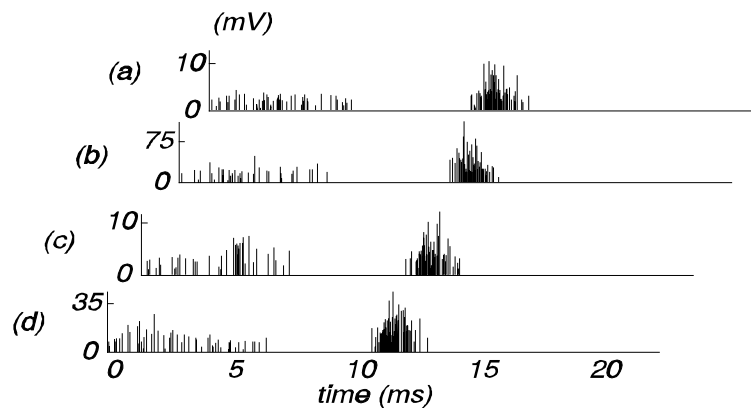


Figure 8.7 As Fig. 8.6, however PD patterns are for phase V.

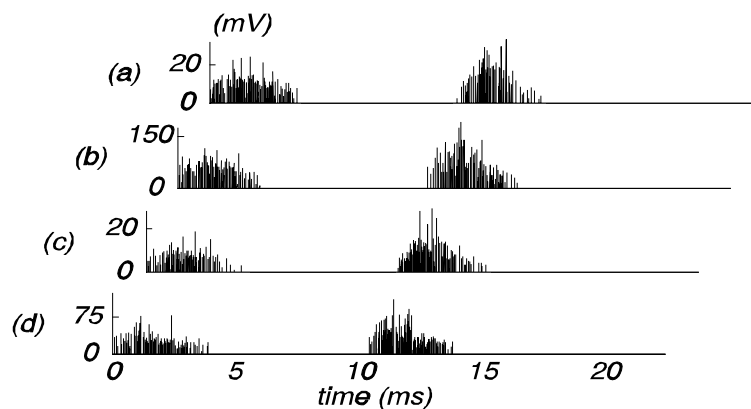


Figure 8.8 As Fig. 8.6, however PD patterns are for phase W.

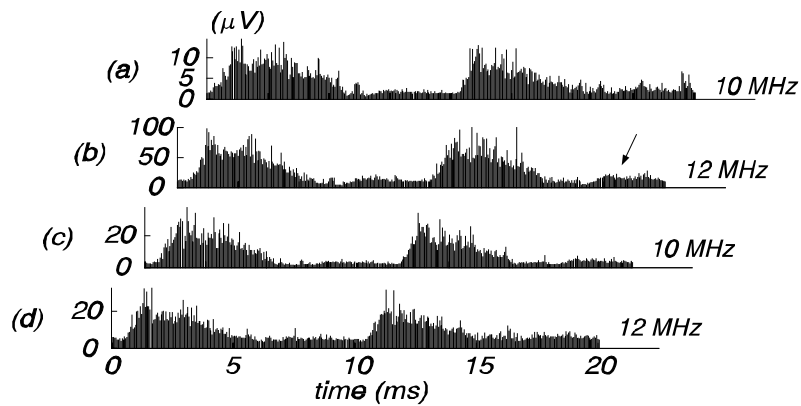


Figure 8.9 PD patterns of phase U of generator Roca-3, obtained by means of a narrow-bandwidth detector tuned to the frequency as indicated in the figure. The graphs labeled (a), (b), (c) and (d) refer to the four sensors, as explained in the caption of Fig. 8.6.

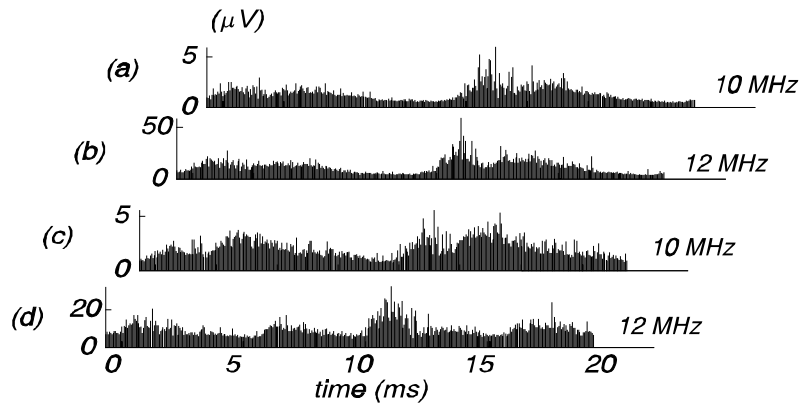


Figure 8.10 As Fig. 8.9, however PD patterns are for phase V.

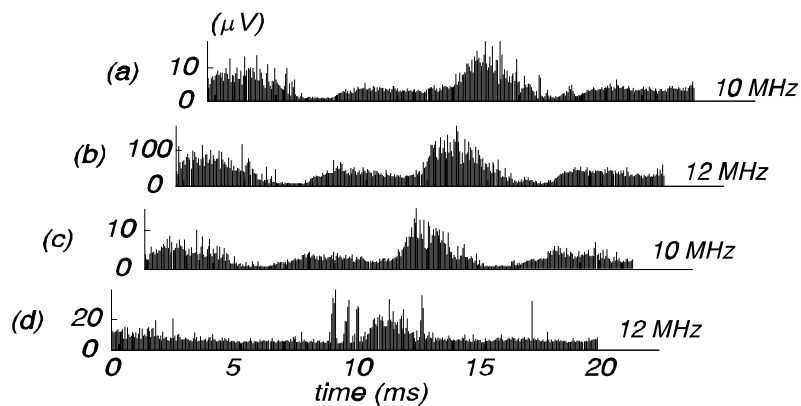


Figure 8.11 As Fig. 8.9, however PD patterns are for phase W.

8.3 Measurements with the tunable narrow-bandwidth detector

Figure 8.12 gives the frequency spectra as recorded in phase W with the bus-support-capacitor near the generator side, the ring-capacitor and the overvoltage-capacitor. The total measuring-time to record each spectrum is 1 minute. Consequently the spectra result from a large number of partial discharges, in contrast to the frequency spectrum for phase W in Fig. 8.5 which is calculated for only one single discharge, recorded by means of the bus-support-capacitor at the generator side. The latter spectrum has its largest level at 7.2 MHz and a minimum at about 20 MHz. These values are comparable to the maximum and minimum values of the 'integrated' frequency spectrum for the bus-support-capacitor in Fig. 8.12, which occur at about 7.5 and 18 MHz respectively.

The frequency spectra for the bus-support-capacitor and the ring-capacitor have different levels but nearly similar shapes, since both sensors are installed close to each other and see identical waveshapes (see Fig. 8.3a and b). It is clear that the bus-support-capacitor at the generator side has the best sensitivity, while the sensitivity of the overvoltage-capacitor is the lowest. Also the bus-support-capacitor and the ring-capacitor are capable of measuring much higher frequencies than the overvoltage-capacitor. The frequency spectrum as measured with the overvoltage-capacitor not only has the lowest level, also the shape differs from the other two spectra. This is not surprising since the behavior of the large overvoltage-capacitors may be dominated by parasitic inductance at high frequencies.

To find the best tuning frequency for the narrow-bandwidth measurements, a series of PD patterns has been recorded at various tuning frequencies for each phase separately. Figure 8.13 gives the patterns for phase U, recorded with the bus-support-capacitor at the generator side. In this case the best choice is 12 MHz, since at this frequency: (i) the largest signal is recorded, (ii) no interference can be recognized (as at 20 MHz), and (iii) little cross-talk takes place (in contrast to at for instance 34 MHz). Between 16 and 20 MHz, no clear PD patterns can be recognized. These frequencies correspond with the dip in the frequency spectrum of Fig. 8.12. Also for the other phases and the other sensors the best tuning frequency turns out to be 10 or 12 MHz.

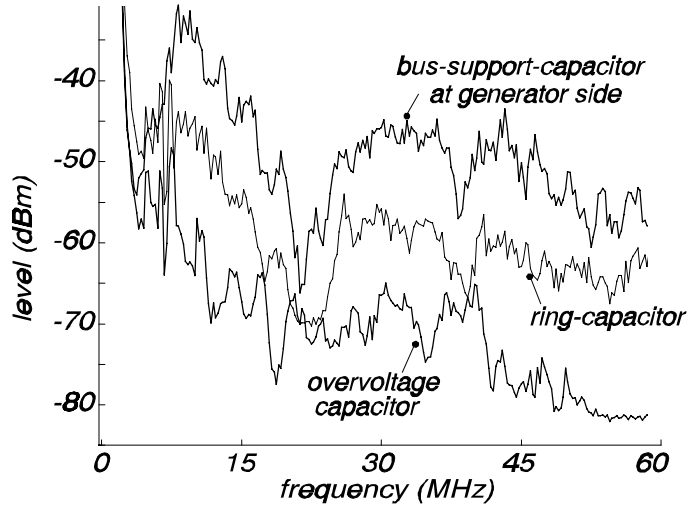


Figure 8.12 Frequency spectra as measured in phase W of generator Roca-3, by means of three different sensors.

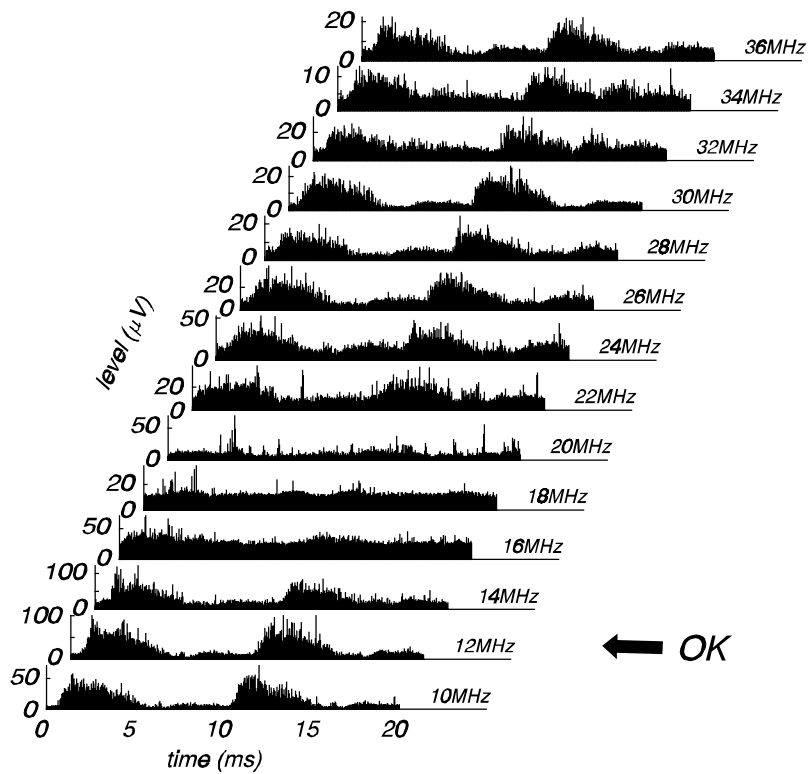


Figure 8.13 Partial discharge patterns for phase U of generator Roca-3, measured at various tuning frequencies and with a bus-support-capacitor near the generator side. Note the difference in vertical scale.

The partial discharge patterns at these optimal frequencies are shown for phase U in Fig. 8.9, for phase V in Fig. 8.10 and for phase W in Fig. 8.11. The results show great similarity to the patterns obtained by means of the time-domain measurements:

- for each phase, the patterns are almost identical for the four different sensors. All sensor types give good results, however the bus-support-capacitor at the generator side has the best sensitivity
- the patterns for phase U and phase W are nearly similar, however for phase V completely different patterns were observed, as was already described in Section 8.2 for the time-domain measurements. In addition, the amplitudes of the discharges in phase V are roughly a factor two smaller than for the other two phases.

All patterns obtained by means of the narrow-bandwidth detector show a weak cross-talk between the phases (indicated with an arrow in Fig. 8.9b). Since for the time-domain measurements each recorded pulse is judged individually, an almost perfect elimination of cross-talk is possible, which becomes clear when we compare the patterns in the Figures 8.6 to 8.11.

8.4 Conclusions

Three different sensor types (bus-support-capacitors, overvoltage-capacitors and ring-capacitors) were compared with each other. All three sensor types give good and comparable results; the best sensitivity is obtained with bus-support-capacitors.

Partial discharges were recorded by means of both time-domain measurements and a tunable narrow-bandwidth detector. Nearly similar partial discharge patterns were obtained with both techniques. The best tuning frequencies for the narrow-bandwidth detector turn out to be 10 and 12 MHz for this generator. Time-domain measurements enable a good discrimination between partial discharges and signals caused by cross-talk. With the tunable narrow-bandwidth detector, a weak cross-talk between the phases is still present.

Chapter 9

LOCALIZATION OF DISCHARGES IN THE MAASVLAKTE POWER PLANT

9.1 Introduction

During measurements on the two generators in the power plants Maasvlakte-1 and Maasvlakte-2 near Rotterdam (Appendix A), abnormal partial discharges were observed. In both cases, efforts were made to locate the source of the discharges in order to take appropriate action.

The localization of the PD's in the Maasvlakte-1 power plant is described in Section 9.2. It was found that the discharges were caused by one of the bus-support-capacitors, which was slightly damaged during transport from the manufacturer to KEMA. All six capacitors were then removed, tested and when necessary repaired. They then had to pass a second commissioning test, after which they were installed in the Maasvlakte-2 power plant.

The large partial discharges, subsequently observed in the Maasvlakte-2 power plant did not occur in the generator but originated from the generator-circuit-breaker, as will be shown in Section 9.3.

9.2 Localization of a PD source at generator Maasvlakte-1

In July 1996 we installed a set of six bus-support-capacitors at the 625 MW Maasvlakte-1 power plant near Rotterdam. During the first on-line measurements, high discharge levels were observed in phase U. Figure 9.1 gives an example of such a large partial discharge, observed simultaneously with two bus-support-capacitors, one at the generator side (Fig. 9.1a) and one at the step-up transformer side (Fig. 9.1b), and by means of a pick-up loop near the generator terminal (Fig. 9.1c).

The signals measured with the bus-support-capacitors show the following characteristics:

- at the transformer side, the amplitude is very high; about 300 V
- the signal first shows up at the transformer side and passes the sensor at the generator side 38 ns later. This transit time corresponds with the distance between the two

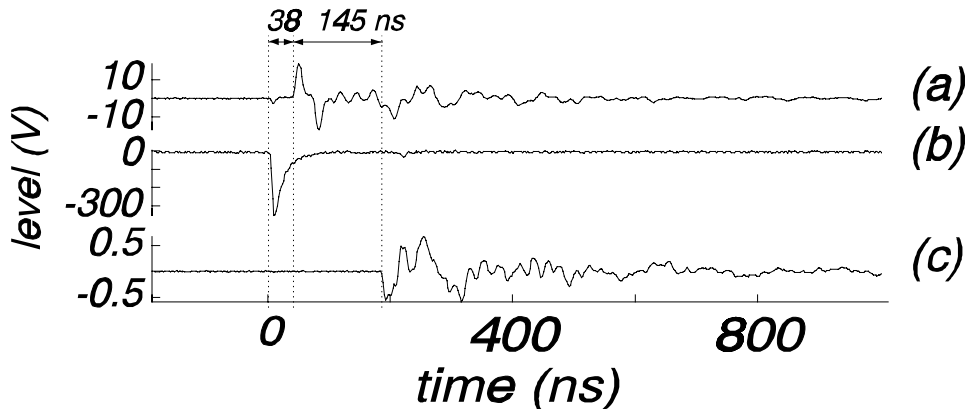


Figure 9.1 A large partial discharge in phase U, measured simultaneously with (a) a bus-support-capacitor near the generator, (b) a bus-support-capacitor near the transformer and (c) a pick-up loop near the generator terminals.

sensors ($11.5 \text{ m} * 3.3 \text{ ns/m} = 38 \text{ ns}$). Thus the signal does not originate from the generator

- both signals have opposite polarity. This is only possible when one of the sensors is the source of the signal, as is shown in Fig. 9.2a. When the signal comes from the generator or from the step-up transformer, the polarity of both signals must be equal, as shown in Fig. 9.2b. Thus it is plausible that the source of these large discharges is the bus-support-capacitor at the transformer side.

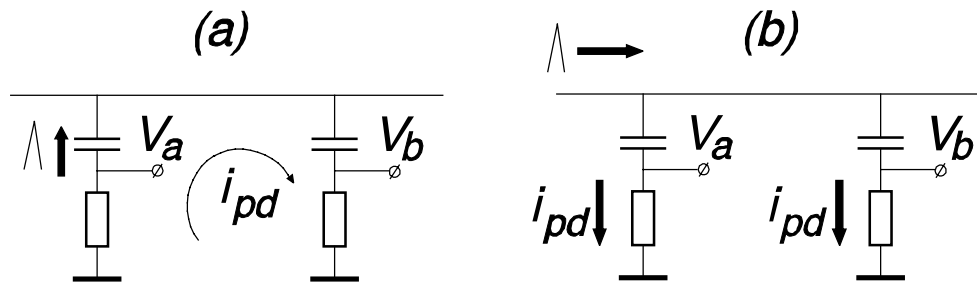


Figure 9.2 Polarity of signals at the bus-support-capacitors for (a) a partial discharge in one of the bus-support-capacitors and (b) a partial discharge in the generator.

In the mean time, after consultation with the plant manager, two immediate actions had been decided:

- as an extra precaution, an oil-sample was taken from the step-up transformer and the two auxiliary transformers. After analysis of the oil-samples by KEMA, no signs of degradation were found [Sto96]. This confirmed that the large partial discharges did not originate in one of the transformers
- as a second priority the source of the discharges had to be located.

This was done by means of a pick-up loop, positioned at various positions: (i) near the generator terminals, (ii) near the terminals of the step-up transformer, and (iii) near the terminals of the two auxiliary transformers. The pick-up loop was always located in regions beyond a short-circuit plate. The output of the pick-up loop was recorded simultaneously with the outputs of both bus-support-capacitors in phase U. Figure 9.3 gives an overview of all measuring positions. An example of a measurement with the pick-up loop near the generator terminals is given in Fig. 9.1. The transit-time between the pick-up loop and the bus-support-capacitor at the generator side is 145 ns, and corresponds to the distance between the bus-support-capacitor and the pick-up loop (6.7 m or 22 ns) and to the difference in lengths of the measuring cables (24.5 m or 123 ns).

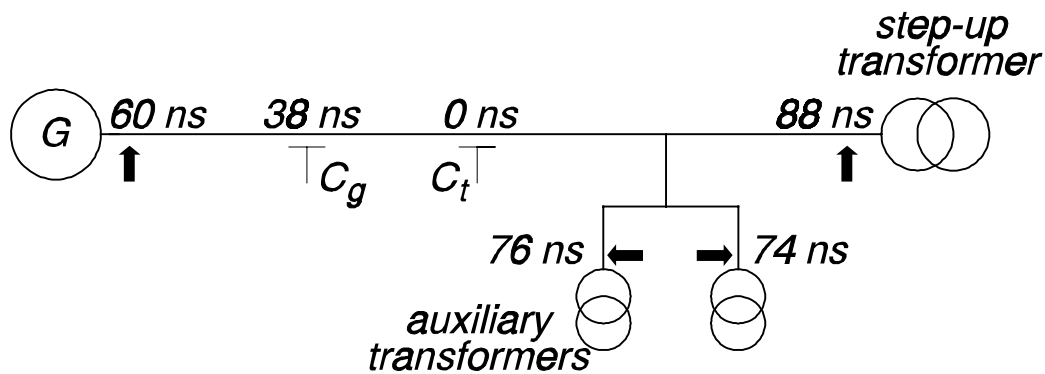


Figure 9.3 Overview of all measuring positions and the measured transit-times with reference to the bus-support-capacitor at the transformer side C_t .

The transit-times for all the measurements at all positions (after correction for different lengths of measuring cables) and with reference to the bus-support-capacitor at the transformer side, are given in Fig. 9.3. All transit-times correspond nicely with the distance between each measuring position and the bus-support-capacitor at the transformer side. This confirms that the discharges are caused by the bus-support-capacitor; consequently it was decided to remove all six capacitors for inspection.

During the inspection of the removed bus-support-capacitor which showed the partial discharges, a loose internal connection from the mica-stack to the top-part of the bus-support-capacitor (see Fig. 9.4) was found to be the cause of the discharges. This loose internal connection must have been the result of several events, which we could reconstruct as follows:

- during the transport from the manufacturer to KEMA, the flexible wire-connection between the top-part of the bus-support-capacitor and the flexible electrode that provides mechanical and electrical contact with the high-voltage rail, was broken

- this had no consequences for the first commissioning tests, since they were carried out without this flexible electrode
- after the commissioning tests, a new flexible wire was soldered to the top-part. Unfortunately, during the soldering the internal connection came loose, which was not noticed at that time
- only after installation in the power plant, during the on-line partial discharge measurements, this damage showed up.

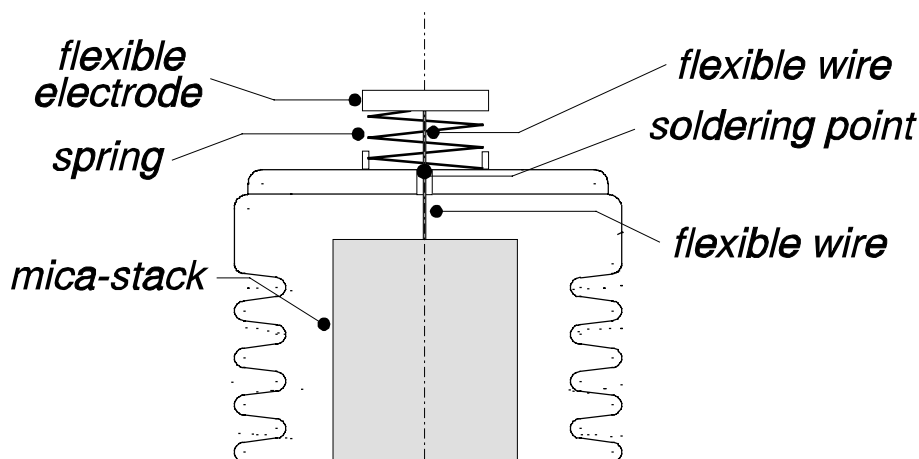


Figure 9.4 *Top-part of a bus-support-capacitor.*

Since the discharges across the interruption had not caused internal damage to the epoxy-resin, it was decided to repair the internal connection. After the repair, all six removed bus-support-capacitors successfully passed a second commissioning test program, after which they were installed in the Maasvlakte-2 power plant (in September 1997).

9.3 Localization of a PD source at the Maasvlakte-2 power plant

During the first measurements on the generator of the Maasvlakte-2 power plant, a large PD level was observed in phase W. This is shown in Fig. 9.5, which gives the PD levels for the three phases, recorded by means of a spectrum analyzer in the zero-span mode, tuned to 24 MHz. The discharges in phase W are about a factor 3 larger than for the other two phases.

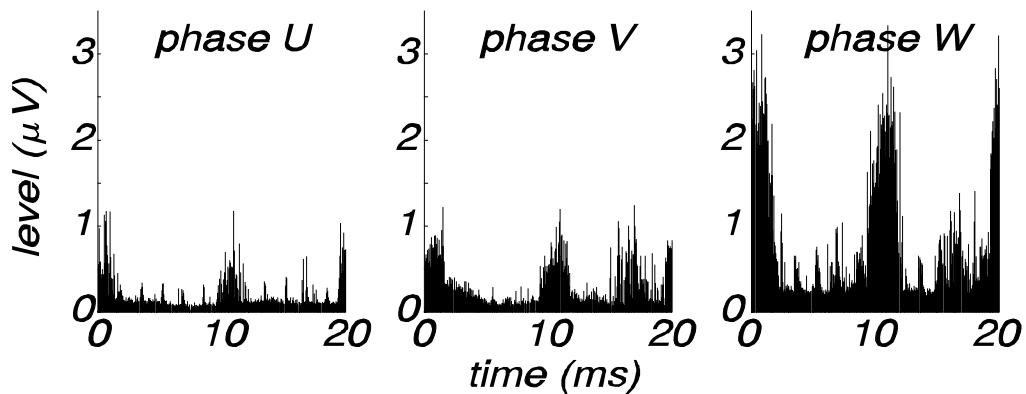


Figure 9.5 PD patterns for the three phases of generator Maasvlakte-2, recorded at a tuning frequency of 24 MHz.

To verify whether the observed activity in phase W is caused by PD's inside the generator or by another source, it was decided to measure the waveshapes of the large PD's. An example is given in Fig. 9.6. As can be seen, the signal first shows up at the sensor near the step-up transformer, which proves that the large PD's do not come from the generator. In case the PD's would come from the transformer, the transit time between both signals in Fig. 9.6 should always be equal to the distance between the sensors times the speed of light (or $11.5 \text{ m} * 3.3 \text{ ns/m} = 38 \text{ ns}$). However, the transit time is much shorter (12 ns), which is only possible if the PD originates between the sensors. Thus we come to the conclusion that the large PD's occur in the generator circuit-breaker.

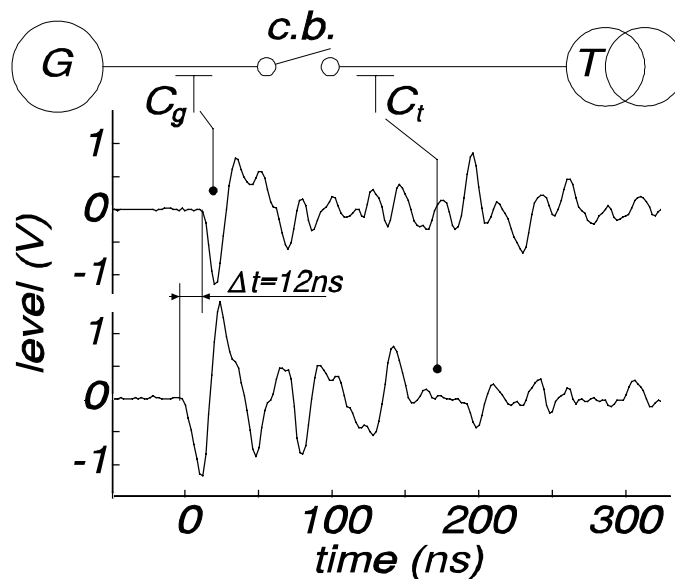


Figure 9.6 A large partial discharge in phase W, measured simultaneously with the two sensors in this phase.

Therefore it was decided to locate the PD source inside the circuit-breaker by means of a Lemke-detector (type LDP 5). This handheld detector has a capacitive probe and can measure EM emission from PD's up to a frequency of 5 MHz. The detector, which is designed to find and locate the position of PD's in medium-voltage sub-stations [Pem99], can normally not be used in a power plant. Due to the relatively low upper detection frequency of 5 MHz, in a power plant only interference from the rotor excitation system will be measured. Nevertheless, the discharge activity in phase W of the Maasvlakte-2 power plant could easily be detected by the Lemke-detector. We scanned the whole circuit-breaker during regular operation; the results are given in Fig. 9.7. It can be seen that the PD's originate from the bleeding resistors at the top of the circuit-breaker.

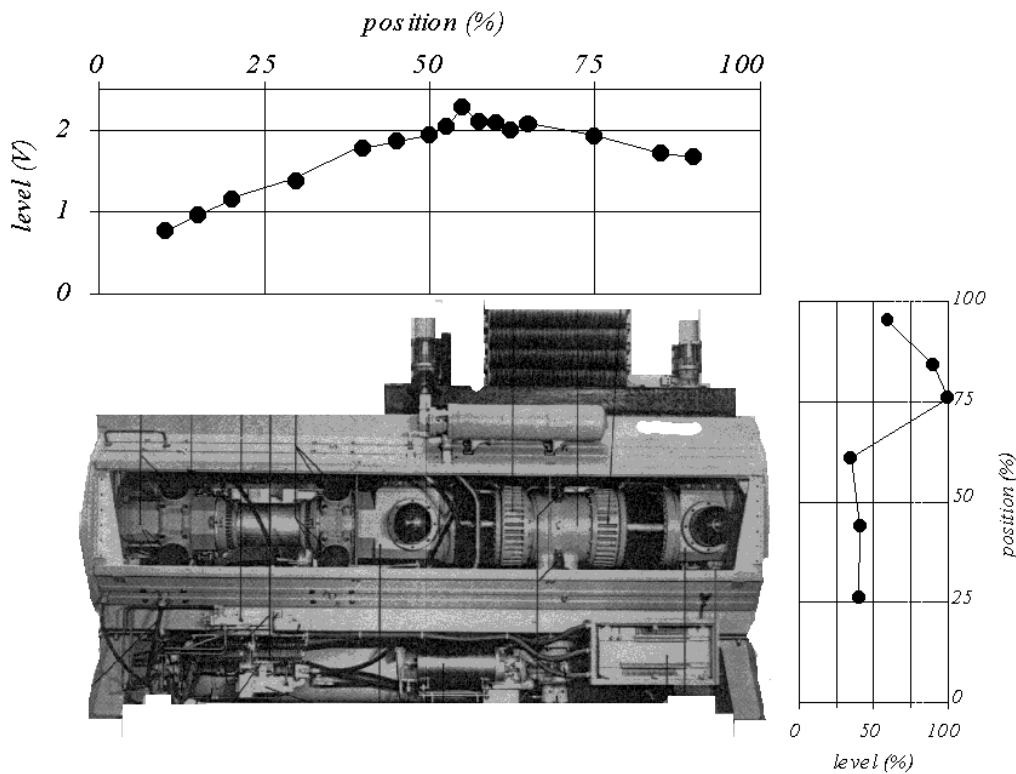


Figure 9.7 PD-levels near the generator circuit-breaker in phase W of the Maasvlakte-2 power plant. The discharges are detected by means of a Lemke-detector, which was moved both horizontally and vertically.

Now that the origin of the discharges is known, appropriate actions can be taken. After consultation with an expert on generator circuit-breakers [Ele98] and the responsible technician of the power plant [Sto98], it was concluded that the PD's will,

on a short term, not lead to serious problems. So it was decided to keep the unit in operation until the next maintenance overhaul, which was planned for December 1998.

During this maintenance overhaul, a visual inspection of the circuit-breaker in phase W was performed by the manufacturer. It was found that the bleeding resistor was installed too close to the grounded frame of the circuit-breaker, thus causing corona discharges. After repair, the generator was taken back in operation and the measurements with the Lemke-detector were repeated. Now, no partial discharge activity could be detected [Lee99].

Chapter 10

CONCLUSIONS

This thesis describes methods to monitor partial discharges (PD's) in stator windings of turbine generators during regular operation. Present methods may easily give false indications as a result of the high levels of electrical interference in a power plant. Two new methods, both employing specially developed sensors, were evaluated under practical conditions in six power plants.

We have succeeded in obtaining interference-free partial discharge patterns:

- interference is rejected to a large extent by applying consistent EMC-methods and by using measuring frequencies above 5 MHz
- remaining interference can be rejected by using an appropriate measuring technique. Two methods have been successfully evaluated: (i) time-domain measurements followed by signal-processing, and (ii) a tunable narrow-bandwidth filter.
- in case of the time-domain measurements, discrimination between PD signals and remaining interference was done by means of the 'dominant frequency'; the frequency where the calculated frequency spectrum has the largest amplitude
- the tunable narrow-bandwidth filter can be tuned to a frequency where PD's are strong and interference is low. Tuning frequencies between 10 and 20 MHz were found to be most suitable.

A partial discharge inside the generator causes a signal in all three phases:

- the signal with the largest amplitude shows up in the phase where the PD occurs
- the signals in the other two phases are caused by cross-talk
- both the time domain measurements and the tunable narrow-bandwidth filter enable a good discrimination between partial discharges and signals caused by cross-talk.

The methods to reject interference and cross-talk were evaluated by means of on-line measured PD patterns: the patterns for signals classified as PD's are indeed typical for partial discharges, while the patterns for signals classified as interference show no phase-related structure.

Both measuring techniques were directly compared in two generators. A good agreement was found in the Roca-3 power plant. However for generator Hemweg-8 inconsistent results were obtained for one phase; the time-domain measuring technique

records not all PD's in this phase. No reasonable explanation can be given for this.

Various sensors have been developed and permanently installed at several generators. A direct comparison of the sensors has been made at two generators. It was found that: (i) all sensor types give good and comparable results, (ii) the best sensitivity is obtained with bus-support capacitors.

For several generators, abnormal partial discharge activity was observed:

- in all cases, the source of these partial discharges could be located
- the transit-time between various sensors and reflections of the PD signal can be used to verify whether discharge activity takes place in the generator or for instance near the step-up transformer
- pick-up loops can be used as additional sensors to locate abnormal PD activity
- abnormal partial discharge activity was observed for the following generators:
 - Amer-9: even after careful checking, only discharges coming from phase V were observed
 - Hemweg-8: (i) sparking near the current sensor in phase V, and (ii) sparking inside the step-up transformer. During a maintenance period both sources were removed, after which the discharge activity was no longer present
 - Maasvlakte-1: large discharges in a slightly damaged bus-support-capacitor
 - Maasvlakte-2: large PD's in the generator circuit-breaker. After repair no more PD activity could be detected.

We studied the propagation of partial discharge pulses in a stator winding and found that:

- a stator winding acts as a transmission line. Therefore a PD signal manifests itself at the generator terminals after a transit time that depends on the origin of the PD
- due to capacitive and inductive couplings in the end-winding region, a second propagation mode is present for higher frequencies. This 'fast mode' manifests itself at the terminals without appreciable time delay
- the capacitive and inductive couplings cause cross-talk between the phases. As a consequence, a signal measured in one phase does not necessarily originate from a discharge in that phase
- the amplitudes of the fast mode and, to a lesser extent, the slow mode (or transmission line mode) are heavily damped when the discharge occurs further away of the measuring terminal. The consequence is that only discharges close to the measuring terminal can be observed, which is expected not to be a serious disadvantage

-
- the total charge at the terminals is only weakly dependent on the origin of the discharge
 - the propagation of a PD signal is not only influenced by the construction of the generator but also by its external connections:
 - at the high-voltage side, the PD signal propagates along the IPB and reflects at the step-up transformer. The signal path is closed via the large parasitic capacitance between the IPB and the generator. The signals in the neighboring phases, caused by cross-talk inside the generator, propagate in a similar manner
 - at the neutral side, the PD signal-path is closed via the other two phases. As a consequence, a signal measured at one of the neutral terminals does not necessarily belong to a PD in that phase.

Bibliography

[ABB87]. ABB document CH-HS 1176 87 E.

[And71]. J.M. Anderson: "*Wide frequency range current transformers*", Review of Scientific Instruments, Vol.42, No.7, July 1971, pp.915-926.

[Bau78]. C.E. Baum, E.L. Breen, J.C. Giles, J. O'Neill, G.D. Sower: "*Sensors for electromagnetic pulse measurements both inside and away from nuclear source regions*", IEEE Transactions on Antennas and Propagation, Vol.AP-26, No.1, January 1978, pp.22-35.

[Bel85]. H. Bellm, A. Kuchler, J. Herold, A.Schwab: "*Rogowski-spulen und Magnetfeldsensoren zur Messung transienter Ströme im Nanosekundenbereich*", Teil 1 und Teil 2, Archiv für Elektrotechnik 68 (1985), pp. 63-74.

[Bin87]. E. Binder: "*Techniques of partial discharge measurements for stator windings of generators*", 1987 CIGRE Session, paper 700-03, Paris, 1987.

[Bin98]. E. Binder, A. Draxler, H. Egger, A. Hummer, M. Muhr, G. Praxl: "*Experience with on-line and off-line PD measurements of generators*", 1998 CIGRE Session, Paris, France, August 1998, paper 15-106.

[Bra94]. R. Brammer, T. Karlsson, D.Rudolfsson, A.Lutz, R. Brutsch: "*Insulating micatapes with increased thermal conductivity*", 1994 CIGRE Session, paper 15-202, Paris, August 1994.

[Bri67]. H. Britsch, R. Schuler: "*Die ganzimprägnierte Statorisolierung Micadur-Compact für Hochspannungsmaschinen*", Brown Boveri Mitteilungen, Band 54, No.9, p.531-538, 1967.

[Bri91]. British Electricity International: "*Modern power station practice, Third Edition, Volume C (Turbines, Generators and Associated Plant), Chapter 6*", Pergamon Press, 1991.

[Bur97]. H.P. Burger, A.W. van Boetzelaer: "*Kwaliteitscontrole tijdens reparatie van machinetransformator Hemweg-8*", KEMA report 60180-T&D 97-103387, 27 May 1997 (in Dutch).

[Cam93]. S.R. Campbell, G.C. Stone, H.G. Sedding, G.S. Klempner, W. McDermid, R.G. Bussey: "*Practical on-line partial discharge tests for turbine generators and motors*", IEEE/PES Summer meeting, paper 93SM353-3EC, Vancouver, Canada, July 1993.

- [Col90]. E. Colombo, G. Tontini: "*ENEL's experience with on-line partial discharge measurements on stator windings of large synchronous hydro generators*", IEEE International Symposium on Electrical Insulation, Toronto, Canada, June 1990.
- [Cul89]. I. Culbert, H.G. Sedding, G.C. Stone: "*A method to estimate the insulation condition of high-voltage stator windings*", Electrical/Electronics Insulation Conference (EEIC), 1989, pp.236-241.
- [Deu93]. A.P.J. van Deursen: "*Electromagnetic Compatibility, Part 5, Installation and Mitigation guidelines, Section 3, Cabling and wiring*", Eindhoven University of Technology Report 93-E-275, July 1993 (prepared for IEC TC77, WG2).
- [Dic88]. E.P. Dick, B.K. Gupta, P. Pillai, A. Narang, D.K. Sharma: "*Practical calculation of switching surges at motor terminals*", IEEE Transactions on Energy Conversion, Vol.3, No.4, December 1988.
- [Dic91]. E.P. Dick, R.W. Cheung, J.W. Porter: "*Generator models for overvoltage simulations*", IEEE Transactions on Power Delivery, Vol.6, No.2, April 1991, pp.728-735.
- [Dol60]. B. Doljak, M. Moravec, O. Wohlfahrt: "*Micadur - eine neue Isolation für Statorwicklungen elektrischer Maschinen*", Brown Boveri Mitteilungen, Band 47, No.5/6, p.352-360, 1960.
- [Dri89]. H. Driesen: "*Koolcomposiet weerstanden; DC-spannings- en stootspanningsvastheid*", Eindhoven University of Technology, High-Voltage and EMC group, report EH.89.S.250, May 1989 (in Dutch).
- [Ele98]. H.J. Eleveld, KEMA, Arnhem, private communication, May 1998.
- [Eme81]. F.T. Emery, B.N. Lenderking, R.D. Couch: "*Turbine generator on-line diagnostics using rf-monitoring*", IEEE Transactions on Power Apparatus and Systems, Vol.PAS-100, No.12, December 1981, pp.4974-4982.
- [Fru90]. B. Fruth, J. Fuhr: "*Partial discharge pattern recognition - a tool for diagnosis and monitoring of aging*", 1990 CIGRE Session, Paris, France, 26 August - 1 September 1990, paper 15/33-12.
- [Fuh93]. J. Fuhr, e.o.: "*Detection and location of internal defects in the insulation of power transformers*", IEEE Transactions on Electrical Insulation, Vol.28, No.6, December 1993.

- [Gla48]. G.N. Glasoe, J.V. Lebacoz: *"Pulse generators, part II the line-type pulser"*, McGraw-Hill, New York/London, 1948, MIT Radiation Laboratory Series, vol.V.
- [Gru94]. P. Grünewald, J. Weidner: *"Possibilities and experience with off- and on-line diagnosis of turbine generator stator winding insulation"*, 1994 CIGRE Session, paper 11-206, Paris, August/September 1994.
- [Gua97]. J.L. Guardado, K.J. Cornick, V. Venegas, J.L. Naredo, E. Melgoza: *"A three-phase model for surge distribution studies in electrical machines"*, IEEE Transactions on Energy Conversion, Vol.12, No.1, March 1997, pp.24-31.
- [Gul91]. E. Gulski: *"Computer-aided recognition of partial discharges using statistical tools"*, Ph.D. Thesis, Delft University Press, October 1990.
- [Gul95]. E. Gulski: *"Digital analysis of partial discharges"*, IEEE Transactions on Dielectrics and Electrical Insulation, Vol.2, No.5, October 1995, pp.822-837.
- [Har79]. R.T. Harrold, F.T. Emery, F.J. Murphy, S.A. Drinkut: *"Radio-frequency sensing of incipient arcing faults within large turbine generators"*, IEEE Transactions on Power Apparatus and Systems, Vol.PAS-98, No.4, July/August 1979, pp.1167-1173.
- [Hef91]. A.D. Heffrick: *"Electrical spectrum and network analysers"*, Academic Press Inc., 1991.
- [Hel95]. M.J.A.M. van Helvoort: *"Grounding structures for the EMC-protection of cabling and wiring"*, Ph.D. Thesis Eindhoven University of Technology, October 1995.
- [Het95]. E. Hetzel, E. Pultrum: *"Diagnostische veldmetingen aan middenspanningstracés, ervaringen en ontwikkelingen in 1995"*, report number 44421-T&D 95-115156, KEMA, Arnhem, December 1995 (in Dutch).
- [Hew67]. Hewlett Packard: *"S-Parameter techniques for faster, more accurate network design"*, Application Note 95-1, 1967.
- [Hor98]. F.B.M. van Horck, A.P.J. van Deursen, P.C.T. van der Laan, P.R. Bruins, B.L.F. Paagmans: *"A rapid method for measuring the transfer impedance of connectors"*, IEEE Transactions on Electromagnetic Compatibility, Vol.40, No.3, August 1998, pp.193-200.
- [Hou90]. M.A. van Houten: *"Electromagnetic compatibility in high-voltage engineering"*, Ph.D. Thesis Eindhoven University of Technology, October 1990.

[Hut92]. W. Hutter: *"Partial discharge detection in rotating electrical machines"*, IEEE Electrical Insulation Magazine, Vol.8, No.3, May/June 1992, pp.21-32.

[IEC81]. IEC Publication 270: *"Partial discharge measurements"*, 2nd edition 1981.

[IEC90a]. *"Characteristics of indoor and outdoor post insulators for systems with nominal voltages greater than 1000 V"*, International Standard IEC273, Third Edition 1990.

[IEC90b]. *"Coupling capacitors and capacitive dividers"*, International Standard IEC358, Second Edition 1990.

[Ito93]. K. Itoh, Y. Kaneda, S. Kitamura, K. Kimura, K. Hayashi, H. Tokura: *"Behavior of noise pulses in a turbine generator"*, Proceedings 8th International Symposium on High-Voltage Engineering (ISH), Yokohama, Japan, 23-27 August 1993, paper 75.04.

[Jac82]. R.J. Jackson, A. Wilson: *"Slot-discharge activity in air-cooled motors and generators"*, IEE Proc., Vol.129, Pt.B, No.3, May 1982, pp.159-167.

[Jam86a]. R.E. James, F.E. Trick, B.T. Phung, P.A. White: *"Interpretation of pd quantities as measured at the terminals of HV power transformers"*, IEEE Transactions on Electrical Insulation, Vol.EI-21, No.4, August 1986.

[Jam86b]. R.E. James, B.T. Phung, R. Miller: *"The effect of end-winding configurations on the transmission of steep pulses through high voltage generator stator windings"*, 5th International Symposium on High-Voltage Engineering (ISH), Braunschweig, Germany, 24-28 August 1986, paper 93.02.

[Jam90]. R.E. James, B.T. Phung, Q. Su: *"Investigation of a low frequency partial discharge location method utilizing a 500 MW/22 kV turbo-generator stator"*, Conference record of the 1990 IEEE International Symposium on Electrical Insulation, Toronto, Canada, 3-6 June 1990, pp.100-105.

[Kee90]. W.W.L. Keerthipala, P.G. McLaren: *"The effects of laminations on steep fronted surge propagation in large AC motor coils"*, IEEE Transactions on Energy conversion, Vol.5, No.1, March 1990, pp.84-90.

[Kem96a]. I.J. Kemp, H. Zhu, H.G. Sedding, J.W. Wood, W.K. Hogg: *"Towards a new partial discharge calibration strategy based on the transfer function of machine stator windings"*, IEE Proceedings Science, Measurements, Technology, Vol.143, No.1, January 1996, pp.57-62.

- [Kem86b]. *KEMA-specificatie voor gesloten schakelinstallaties van 1 tot en met 72.5 kV voor binnenopstelling*", KEMA S4, 1986 (in Dutch).
- [Kim91]. K. Kimura, Y. Kaneda: "*Breakdown voltage and SEM observations on mica insulation systems after thermal and mechanical fatigue*", 7th International Symposium on High-Voltage Engineering, paper 22.13, Dresden, August 1991.
- [Kim93]. K. Kimura: "*Progress of insulation ageing and diagnostics of high-voltage rotating machine windings in Japan*", IEEE Electrical Insulation Magazine, vol.9, no.3, May/June 1993.
- [Kim95]. K. Kimura, Y. Kaneda: "*The role of microscopic defects in multistress aging of micaceous insulation*", IEEE Transactions on Dielectrics and Electrical Insulation, Vol.2, No.3, June 1995, pp.426-432.
- [Kim97]. H.D. Kim, T.W. Kim, J.H. Kim, D.Y. Kang: "*Thermal aging properties of mica/epoxy stator winding insulation*", IEEE Conference on Electrical Insulation and Dielectric Phenomena (CEIDP), Minneapolis, USA, October 19-22, 1997, pp.419-422.
- [Kle91]. H. Kleijer: "*Kortstondige overbelastbaarheid van weerstanden toegepast in elektronische schakelingen*", KEMA report DZO 90-13, Jan. 1991 (in Dutch).
- [Köp95]. U. Köpf, K. Feser: "*Rejection of narrow-band noise and repetitive pulses in on-site PD measurements*", IEEE Transactions on Dielectrics and Electrical Insulation, Vol.2, No.6, December 1995, pp.1180-1191.
- [Kre89]. F.H. Kreuger: "*Partial discharge detection in high-voltage equipment*", Butterworth, 1989.
- [Kri96]. G.P. Krikke: "*Trends in gas-in-oil analyse bij vermogenstransformatoren*", KEMA report 44190-KET/BVA 96-7001, 12 April 1996 (in Dutch).
- [Kur79]. M. Kurtz, J.F. Lyles: "*Generator insulation diagnostic testing*", IEEE Transactions on Power Apparatus and Systems, Vol.PAS-98, No.5, September/October 1979, pp.1596-1603.
- [Kur84]. M. Kurtz, J.F. Lyles, G.C. Stone: "*Application of partial discharge testing to hydro generator maintenance*", IEEE Transactions of Power Apparatus and Systems, Vol.PAS-103, No.8, August 1984, pp.2148-2157.
- [Laa97]. P.C.T. van der Laan, A.P.J. van Deursen: "*Linear EMC-methods applied to power*

systems", Proceedings 10th International Symposium on High-Voltage Engineering (ISH), Montreal, Canada, 25-29 August 1997, keynote address paper.

[Lee99]. W. de Leeuw, KEMA, Arnhem, private communication, May 1999.

[Lyl87]. J.F. Lyles, G.C. Stone, M. Kurtz: *"Experience with PDA diagnostic testing on hydraulic generator"*, IEEE/PES Winter meeting, New York, paper 88WM023-4, February 1987.

[McD90]. W. McDermid: *"Damage resulting from long-term slot discharge activity"*, Conference record of the IEEE International Symposium on Electrical Insulation, Toronto, Canada, 3-6 June 1990, pp. 361-362.

[Mcd99]. W. McDermid, J.C. Bromley: *"Experience with directional couplers for partial discharge measurements on rotating machines in operation"*, IEEE Transactions on Energy Conversion, Vol.14, No.2, June 1999, pp.175-184.

[Mie92]. T.A. Mielke: *"Rewind project rejuvenates 40-year old turbine generator"*, Power, September 1992.

[Mit81]. H. Mitsui, K. Yoshida, Y. Inoue, K. Kawahara: *"Mechanical degradation of high-voltage rotating machine insulation"*, IEEE Transactions on Electrical Insulation, vol.EI-16, No.4, August 1981, pp.351-359.

[Moo93]. J.J.M. Mooren, A.J.M. Pemen: *"Storingsanalyse van turbogeneratoren met inventarisatie van technieken ter voorkoming van dominante storingen"*, KEMA-report 43122-T&D 93-4679, November 1993 (in Dutch).

[Nag93]. V. Nagesh, B.I. Gururaj: *"Evaluation of digital filters for rejecting discrete spectral interference in on-site PD measurements"*, IEEE Transactions on Electrical Insulation, Vol.28, No.1, February 1993, pp.73-85.

[Nar89]. A. Narang, B.K. Gupta, E.P. Dick, D.K. Sharma: *"Measurement and analysis of surge distribution in motor stator windings"*, IEEE Transactions on Energy Conversion, Vol.4, No.1, March 1989, pp.126-134.

[Pee98]. J.J. Peeters, Electron Breda, private communication, October 1998.

[Pem93]. A.J.M. Pemen, P.C.T. van der Laan, P.T.M. Vaessen: *"Sensors for partial discharge monitoring of turbo generators"*, Proceedings 28th UPEC, Staffordshire University, UK,

September 1993, pp.594-597.

[Pem94]. A.J.M. Pemen, P.C.T. van der Laan, P.T.M. Vaessen: "*Partial discharge monitoring of turbine generators; laboratory and live measurements*", Proceedings Conference on Electrical Insulation and Dielectric Phenomena (CEIDP), Arlington, USA, 1994, pp.118-124.

[Pem95]. A.J.M. Pemen, P.T.M. Vaessen, P.C.T. van der Laan: "*On-line monitoring of stator windings using partial discharge measurements*", Proceedings 9th International Symposium on High-Voltage Engineering (ISH), Graz, Austria, August 28 - September 1, 1995, paper 5059.

[Pem96]. A.J.M. Pemen, P.C.T. van der Laan: "*Pitfalls of partial discharge measurements on stator windings of turbine generators*", 7th Conference on Dielectric Materials, Measurements and Applications (DMMA), Bath, UK, 23-26 September 1996, IEE Publication No.430, pp.394-397.

[Pem97a]. A.J.M. Pemen, J.W. Noteboom, P.C.T. van der Laan: "*A diagnostic toolbox for turbine generators*", Cigre/EPRI Colloquium on maintenance and refurbishment of utility turbogenerators, hydrogenerators and large motors, Florence, Italy, 14-16 April 1997.

[Pem97b]. A.J.M. Pemen, W. de Leeuw, P.C.T. van der Laan: "*On-line partial discharge monitoring of stator windings; comparison of different sensors*", Proceedings 10th International Symposium on High-Voltage Engineering (ISH), Montreal, Canada, August 25-29, 1997.

[Pem98]. A.J.M. Pemen, P.C.T. van der Laan: "*On-line detection of partial discharges in stator windings of large turbine generators*", IEE Colloquium on Discharges in Large Machines, IEE Savoy Place, London, UK, 5 March 1998, IEE Digest No: 1998/264, pp. 3/1-3/4 (invited paper and presentation).

[Pem99]. A.J.M. Pemen, W.R. Rutgers, T.J.M. van Rijn, Y.H. Fu: "*On-line partial discharge monitoring of HV-components*", 11th International Symposium on High-Voltage Engineering (ISH), London, UK, August 1999.

[Qui94]. I. Quint, R.H. Schuler, N. Didzen, F. Stobbe: "*Entwicklungsstand der Isolations-technologie bei rotierenden elektrischen Hochspannungs-Maschinen*", Vortrage der ETG-Fachtagung, Würzburg, September 1994, ETG-Fachbericht 53, VDE-Verlag.

[Ram84]. S. Ramo, J.R. Whinnery, T. van Duzer: "*Fields and waves in communication electronics, second edition*", John Wiley & Sons, 1984.

[Ren85]. S. Rengarajan, M.D. Agrawal, R.S. Nema: "*Behavior of high-voltage machine*

insulation system in the presence of thermal and electric stresses", IEEE Transactions on Electrical Insulation, Vol.EI-20, No.1, February 1985, pp.104-110.

[Rog12]. B. Rogowski, W. Steinhaus: "*Die Messung der magnetischen Spannung (Messung des Linienintegrals der magnetischen Feldstärke)*", Archiv für Elektrotechnik, 1.Band, 4.Heft, 1912, pp.141-150.

[Rut97]. W.R. Rutgers, A.J.M. Pemen: "*PD detection sensitivity and E-M wave attenuation in a 400 kV GIS sub-station*", CIGRE Taskforce 15/33.03.05, IWD60, Bedford, USA, August 1997.

[Sch94a]. R.H. Schuler: "*Survey of insulation systems for electrical rotating machines*", proceedings 7th BEAMA International Electrical Insulation Conference, Brighton, UK, 23-26. May 1994.

[Sch94b]. H.H.P. Scheenen: "*Gevoeligheid en selectiviteit van een éénwindings-Rogowski-spoel*", Eindhoven University of Technology, report EH.94.S.311, October 1994 (in Dutch).

[Sed89]. H.G. Sedding, G.C. Stone: "*A discharge locating probe for rotating machines*", IEEE Electrical Insulation Magazine, Vol.5, No.5, September/October 1989, pp.14-17.

[Sed91]. H.G. Sedding, S.R. Campbell, G.C. Stone, G.S. Klempner: "*A new sensor for detecting partial discharges in operating turbine generators*", IEEE Transactions on Energy Conversion, Vol.6, No.1, December 1991, pp.700-706.

[Sed94]. H.G. Sedding, R. Jeffreys, G.S. Klempner, D.J.Wallis, G.Tontini, T.R. Wait: "*The effect of flexible operation on ageing and reliability of generating equipment*", 1994 CIGRE Session, paper 11-203, Paris, August 1994.

[Sed97]. H.G. Sedding, H. Dhirani, G.S. Klempner: "*Application of partial discharge measurements to maintenance of large hydrogen-cooled steam turbine generators*", Cigre/EPRI Colloquium on maintenance and refurbishment of utility turbogenerators, hydrogenerators and large motors, Florence, Italy, 14-16 April 1997.

[Sen83]. J.J. Senff, P.C.T. van der Laan, H. Antonides, L.M.L.F. Hosselet: "*Shielding properties of isolated-phase-bussystems*", IEEE Transactions on Power, Apparatus and Systems, Vol.PAS-102, 1983.

[Sep96]. SEP: "*Elektriciteitsplan 1997-2006*", N.V. Samenwerkende Elektriciteitsbedrijven, July 1996 (in Dutch).

- [Sim95]. J.W.L. Simpson, R.C. Tychsen, Q. Su, T.R. Blackburn, R.E. James: *"Evaluation of partial discharge detection techniques on hydro-generators in the Australian Snowy-Mountains scheme Tumut-1 case study"*, IEEE Transactions on Energy Conversion, Vol.10, No.1, March 1995, pp.18-24.
- [Smu86]. H.W.M. Smulders: *"Het ontwerp van een Rogowskispoel voor een bliksemmeet-systeem"*, Eindhoven University of Technology, report EH.86.S215, 1986 (in Dutch).
- [Ste94]. C.E. Stephan, G. Liptak, R. Schuler: *"An improved insulation system for the newest generation of stator windings"*, 1994 CIGRE Session, paper 11-101, Paris, August 1994.
- [Sto92]. G.C. Stone, H.G. Sedding, N. Fujimoto, J.M. Braun: *"Practical implementation of ultrawideband partial discharge detectors"*, IEEE Transaction on Electrical Insulation, Vol.27, No.1, February 1992, pp.70-81.
- [Sto95]. G.C. Stone, T.E. Goodeve, H.G. Sedding, W. McDermid: *"Unusual PD pulse phase distributions in operating rotating machines"*, IEEE Transactions on Dielectrics and Electrical Insulation, Vol.2, No.4, August 1995, pp.567-577.
- [Sto96]. J.K. Stoutjesdijk, EZH Rotterdam, private communication, November 1996.
- [Sto97]. G.C. Stone: *"Tutorial on rotating machine off-line and on-line partial discharge testing"*, Cigre/EPRI Colloquium on maintenance and refurbishment of utility turbogenerators, hydrogenerators and large motors, Florence, Italy, 14-16 April 1997.
- [Sto98]. J.K. Stoutjesdijk, EZH Rotterdam, private communication, May 1998.
- [Sty82]. W. Stygar, G. Gerdin: *"High frequency Rogowski coil response characteristics"*, IEEE Transactions on Plasma Science, Vol.PS-10, No.1, March 1982, pp. 40-44.
- [Tav87]. P.J. Tavner, J. Penman: *"Condition monitoring of electrical machines"*, Research Studies Press Ltd., Taunton, Somerset, England, 1987.
- [Tav88]. P.J. Tavner, R.J. Jackson: *"Coupling of discharge currents between conductors of electrical machines owing to laminated steel core"*, IEE Proceedings, Vol.135, Pt.B., No.6, November 1988, pp.295-307.
- [Tem62]. H.J. Tempelaar: *"Resultaten van metingen aan de statorisolatie van HV generatoren"*, Elektrotechniek, vol.40, no.8, April 1962 (in Dutch).

- [Tho73]. A.T. Thoeng: "*Detection and location of partial discharges in power transformers*", *Holectechneik* 3 (1973) 2 pp. 52-57.
- [Tim83]. J.E. Timperley: "*Incipient fault identification through neutral rf monitoring of large rotating machines*", *IEEE Transactions on Power Apparatus and Systems*, Vol.PAS-102, No.3, March 1983, pp.693-698.
- [Tim92]. J.E. Timperley, E.K. Chambers: "*Locating defects in large rotating machines and associated electrical systems through EMI diagnostics*", 1992 CIGRE Session, Paris, France, 30 August - 5 September 1992, paper 11-311.
- [Tin93]. P.A.J. Tinnemans: "*Gedrag van een éénwinding-Rogowskispoel*", Eindhoven University of Technology, report EH.93.S.301, October 1993 (in Dutch).
- [Vak94]. B.D. Vakser, B.S. Nindra: "*Insulation problems in high-voltage machines*", *IEEE Transactions on Energy Conversion*, vol.9, no.1, March 1994.
- [Via97]. N.P.J.K.F. Vianden, UNA Amsterdam, private communication, Januari 1997.
- [Vri97]. M.C. de Vries, R. Bijstra: "*Permanent monitorsysteem voor het meten van partiële ontladingen aan turbogeneratoren*", B.Sc. thesis, HTS Groningen, February 1997 (in Dutch).
- [Wic81]. A. Wichman: "*Micalastic high-voltage insulation: design features and experience*", *Proceedings workshop on rotating machine insulation*, EPRI report EL-2211, December 1981.
- [Wic85]. A. Wichmann, P. Grünewald, J. Weidner: "*HF-Störspannungsmessung in Kraftwerkblöcken zur Erkennung von Fehlern in Hochspannungsgeräten*", *Elektrizitätswirtschaft*, Jg.84, H.24, 1985, pp.1009-1012.
- [Wil85]. A. Wilson, R.J. Jackson, N. Wang: "*Discharge detection techniques for stator windings*", *IEE Proceedings*, Vol.132, Pt.B, No.5, September 1985, pp.234-244.
- [Wil90]. A. Wilson: "*High and low intensity slot discharges*", *Conference record of the IEEE International Symposium on Electrical Insulation*, Toronto, Canada, 3-6 June 1990, pp. 363-366.
- [Wil91]. A. Wilson: "*Slot discharge damage in air cooled stator windings*", *IEE Proceedings-A*, Vol.138, No.3, May 1991, pp.153-158.
- [Woo93]. J.W. Wood, H.G. Sedding, W.K. Hogg, I.J. Kemp, H. Zhu: "*Partial discharges in*

HV machines; initial considerations for a PD specification", IEE Proceedings-A, Vol.140, No.5, September 1993, pp.409-416.

[Zhu97]. H. Zhu: "*Analysis of partial discharge calibration difficulties in HV rotating machines*", 10th International Symposium on High-Voltage Engineering (ISH), Montreal, Canada, August 25-29, 1997.

Appendix A

OVERVIEW OF GENERATORS USED FOR THE MEASUREMENTS IN THIS THESIS

Table XV *Overview of the main data of the generators used for the on-line measurements in this thesis*

Generator	Hemweg-6	Amer-9	Hemweg-8	Roca-3 gasturbine	Maasvlakte- 1	Maasvlakte- 2
Location	UNA Amsterdam	EPZ Geer- truidenberg	UNA Amsterdam	EZH Rotterdam	EZH Rotterdam	EZH Rotterdam
Manufactu- rer	Smit/ACEC	ABB	ABB	ABB	BBC	BBC
Power	125 MW	650 MW	650 MW	169 MW	625 MW	625 MW
Line voltage	14 kV	21 kV	21 kV	15 kV	21 kV	21 kV
In operation since	1968 untill dec.1994	1992	1993	1996	1975	1975
Insulation	polyester/ mica	Micadur	Micadur	Micadur	Micadur	Micadur
Cooling	H ₂	H ₂ /water	H ₂ /water	air	H ₂ /water	H ₂ /water

For the measurements in Chapter 2, the stator of an old generator was used (rotor removed). This generator was manufactured by ABB and had the following ratings: power 35 MW, line voltage 10.5 kV, stator insulation is Micadur, air-cooled. The winding diagram of the generator is given in Fig. A.1. In Chapter 2, the individual stator bars are characterized with their phase and number. The numbering method of the bars is given in Fig. A.2. For instance bar U₉ is the 9th bar of phase U, or the bar in slot 41.

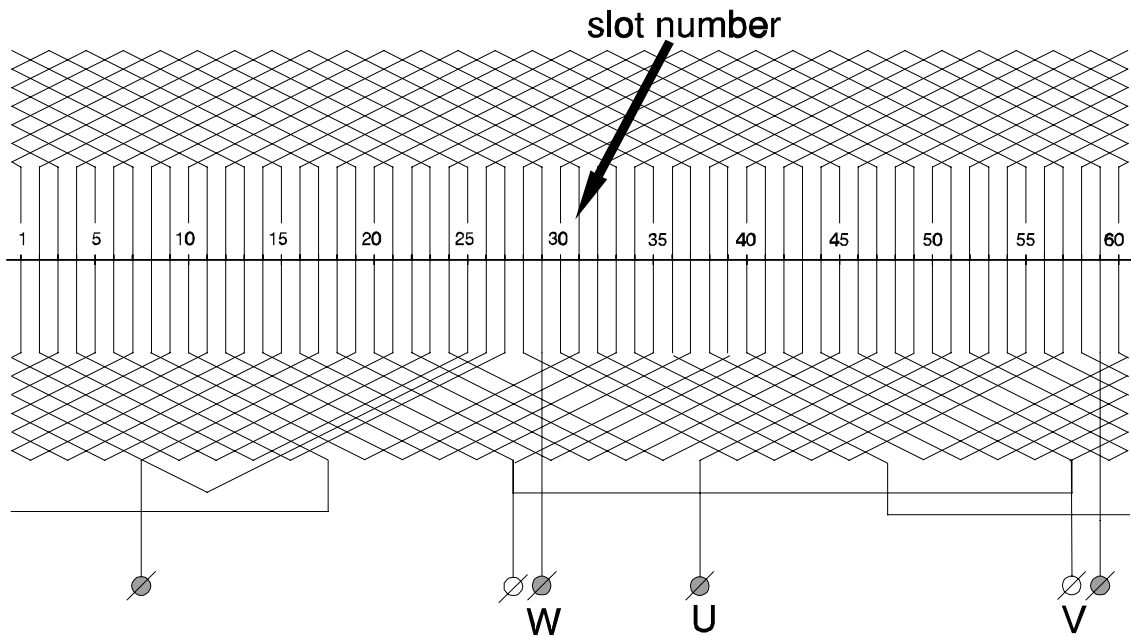


Figure A.1 *Winding diagram.*

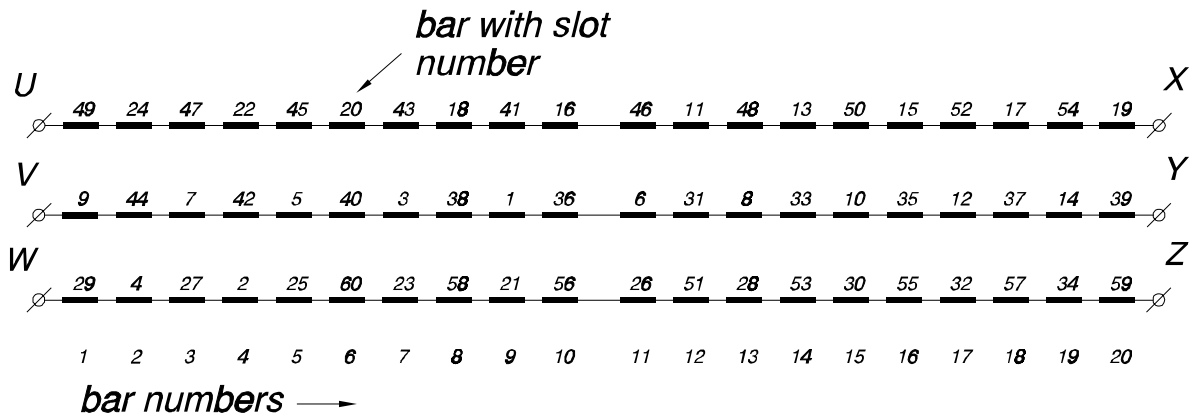


Figure A.2 *Numbering method of the bars.*

Appendix B

CONSTRUCTION OF BUS-SUPPORT-CAPACITORS

B.1 General

A photograph of a bus-support-capacitor, manufactured by MPE in Liverpool, is given in Fig. B.1. A "stacked-mica" capacitor is housed inside the epoxy resin insulator. Mica is chosen for its good high-voltage and high frequency behavior. We use a standard mica-stack of MPE (Muscovite-mica, grade V.4 according to ISO 2185:1972), which is also used in high-power transmitters (e.g. for the Dutch PTT), where it has proven its reliability. To increase the safety factor, the mica-stack is designed for $1.75 U_{rated}$ (so for $U_{rated} = 24$ kV, $U_{design} = 42$ kV).

The mica-stack is placed into a hollow epoxy resin insulator (manufactured by Mekufa, Vroomshoop, The Netherlands; resin by Ciba-Geigy, type Kufalit BXH) which is mounted on an aluminum bottom flange. After the installation of a connector and the $10\text{ k}\Omega$ bleeding resistor, the insulator is filled with epoxy resin and, to prevent voids, cured under vacuum. The connector is a hermetically sealed N-type connector (Huber-Suhner type 22N-50-0-3). The $10\text{ k}\Omega$ is a 2 W coal-composite resistor (Allan-Bradley model 10F395 type RCR42 type HB), tested extensively by KEMA [Kle91] and at the Eindhoven University [Dri89]. Because the resistor and all soldering connections are embedded into the epoxy resin, they are well protected. After the curing, the top flange is mounted and the sensor can be finished. As a quality check, MPE performs a $125\text{ kV}_{dc} / 1$ minute withstand voltage test in the factory.

B.2 Specifications and commissioning testing

The specifications of bus-support-capacitors, given in Table XVI, are based on the standard IEC273 [IEC90a] and the KEMA-specification S4 [Kem86b]. The IEC273 gives specifications for indoor and outdoor post insulators for systems with nominal voltages >1000 V. Since bus-support-capacitors are of a mica/epoxy type and an isolated-phase-bus can be regarded as an indoor installation, Table II of the IEC273 (indoor post insulators of organic material and with internal metal fittings) is relevant. The KEMA-specification S4 is valid for closed, indoor switching-installations with voltages between 1 and 72.5 kV and outlines that partial discharges must be <5 pC at $1.1 U_{rated}$. Another relevant standard is IEC358 (coupling capacitors and capacitor

dividers) [IEC90b]. This standard is less strict than IEC273 and KEMA S4, but gives the procedure for partial discharge testing: the test voltage must be raised to $1.3 U_{rated}$ and be sustained for 10 s. Now the voltage must be decreased to the measuring voltage of $1.1 U_{rated}$ and partial discharge measurements must be done during at least 1 minute.

Table XVI *Specifications for bus-support-capacitors*

rated voltage (kV _{rms})	7.2	10-12	17.5	20-24	30	36
capacitance C_1	80-500 pF					
50 Hz / 1 minute withstand voltage (kV _{rms})	28	38	50	50	70	70
1.2/50 μ s lightning impulse voltage (kV)	60	75	95	125	145	170
partial discharges at $1.1 U_{rated}$	< 5 pC					
loss tangent at $1.1 U_{rated}$ and 20°C	< 0.001					
insulation resistance	> 500 M Ω					
number of ribs	2	3	5	7	10	12
height (mm)	95	130	175	210	270	300
diameter (mm)	60-100	60-105	65-115	65-120	70-130	70-135
temperature range	-40 °C to +80 °C					
parasitic capacitance C_2	< 20 pF					
parasitic inductance	< 200 nH					
resonance frequency	> 80 MHz					

Before installation, each bus-support-capacitor is tested to check its specifications. Especially the high-voltage specifications are extremely important and are tested in the KEMA high-voltage laboratory according to the following protocol:

1. partial discharge measurements. The test voltage is raised to $1.3 U_{rated}$ and sustained for 10 s. Now the voltage is reduced to $1.1 U_{rated}$ and discharges are measured during 1 minute
2. measurement of the loss tangent and capacitance at $1.1 U_{rated}$
3. voltage withstand test at the voltage according to Table XVI, for 1 minute
4. lightning impulse voltage test with a 1.2/50 μ s impulse voltage, with an amplitude according to Table XVI. During the test 15 shots are made with a positive amplitude, followed by 15 shots with a negative amplitude

5. the partial discharge test according to 1. is repeated and the measuring time is increased to 15 minutes
6. the loss tangent and capacitance measurements according to 2. are repeated.

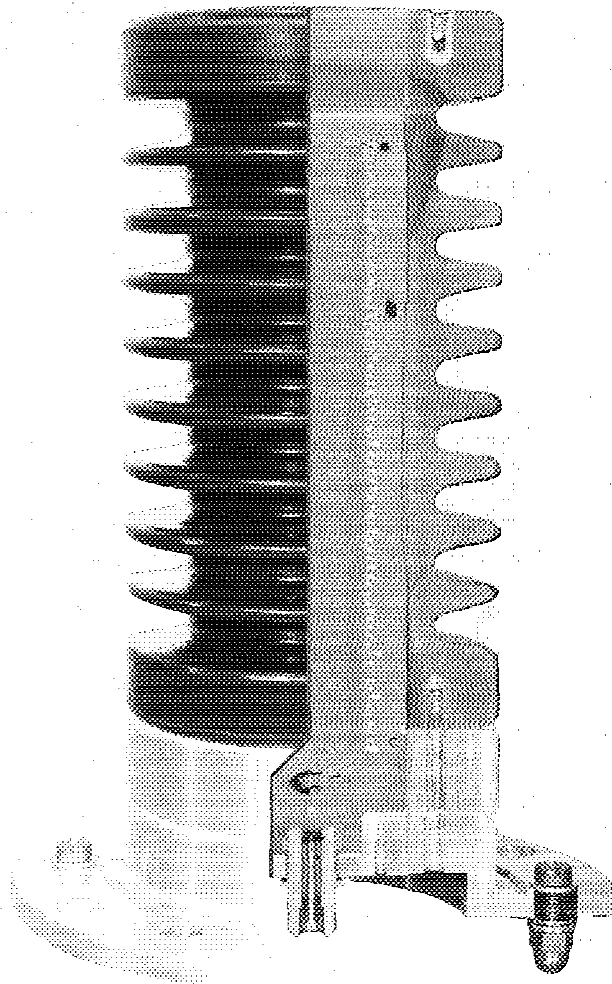


Figure B.1 *Photograph of a cross-section of a bus-support-capacitor*

Appendix C

THE BALUN TRANSFORMER

In Chapter 3, Section 3.3.3, a toroidal single-turn current sensor is described. This sensor has four measuring points which are connected by long measuring cables to resistors R of $50\ \Omega$. A balun¹⁴ transformer (see Fig. 3.14 and Fig. C.1) makes it possible to connect these resistors in series, so that the total output voltage V_{out} of the sensor is increased. The balun transformer must be used otherwise the sensor is short-circuited.

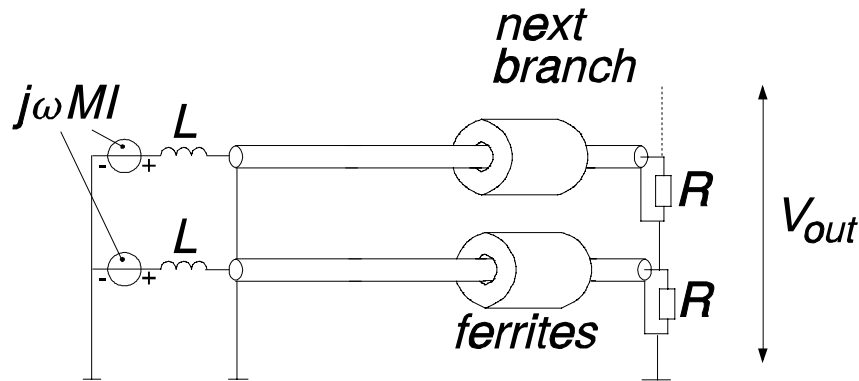


Figure C.1 A toroidal single-turn current sensor, represented by the voltage sources $j\omega MI$ and inductances L , connected to a balun transformer.

In Fig. C.1, each measuring point of the sensor is represented by a voltage source $j\omega MI$ and an inductance L . The voltage source $j\omega MI$ represents the voltage which is induced by the current I , enclosed by the sensor. The inductance L represents the local inductance of the sensor near the measuring point. The balun transformer consists of the coaxial cables, the measuring resistors R (which are connected in series) and the ferrites which prevent that the sensor is short-circuited. For simplicity only 2 branches are shown in Fig. C.1, the system consists of n branches, where n is the number of measuring points (in our case $n = 4$).

The equivalent circuit for this system is given in Fig. C.2. Now each branch of the balun transformer is represented by two coupled inductances L_{fer} with a mutual inductance M_{fer} (with $L_{fer} \approx M_{fer}$). For each branch, two currents are defined: a differential-mode current d_i (with $i = 1, 2, \dots, 4$) and a common-mode current c_i . For instance for the third branch, the differential-mode current d_3 follows the path 1-2-3-4-1, while the

¹⁴balun stands for balanced-unbalanced

common-mode current c_3 follows path gnd-1-4-gnd. The currents in the other three branches are defined in a similar way.

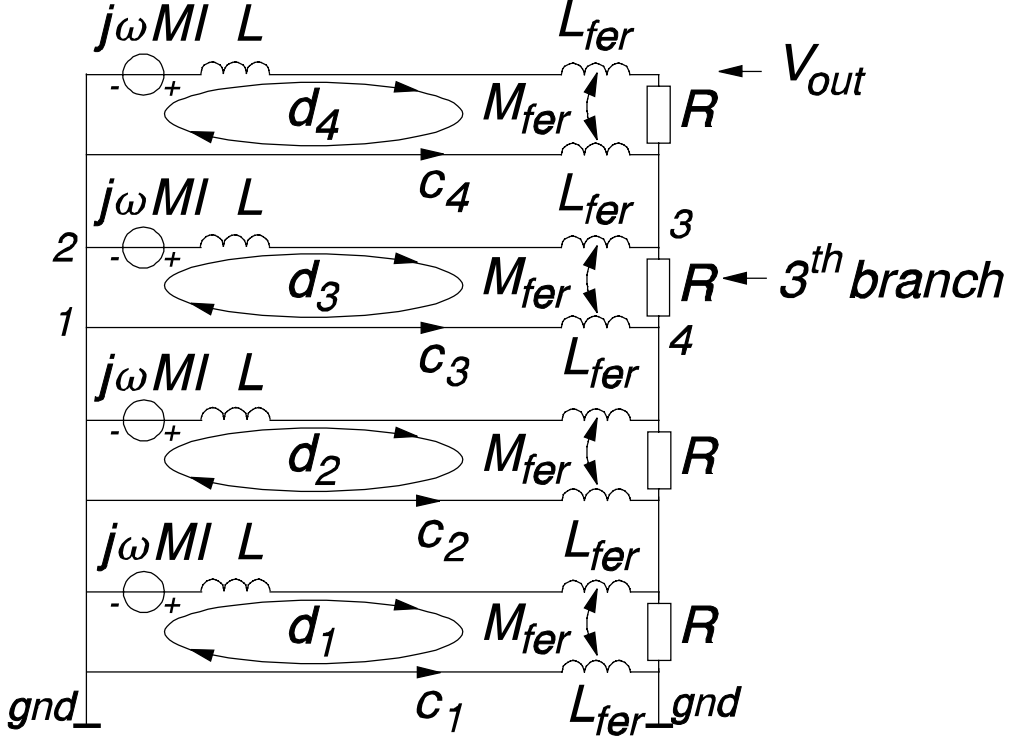


Figure C.2 Equivalent circuit for a toroidal single-turn current sensor with four measuring points, connected to a balun transformer.

The currents $d_1, d_2, d_3, d_4, c_1, c_2, c_3$ and c_4 can be calculated by applying Kirchoff's voltage law for each current-path. The equations for the third branch, which has two current-paths 1-2-3-4-1 and gnd-1-4-gnd, are given in (4).

$$\begin{aligned} j\omega MI &= j\omega L d_3 + j\omega L_{fer} d_3 - j\omega M_{fer} d_3 + R d_3 + j\omega L_{fer} d_3 - j\omega M_{fer} d_3 - j\omega L_{fer} c_3 + j\omega M_{fer} c_3 + R c_4 \\ 0 &= j\omega L_{fer} c_3 - j\omega L_{fer} d_3 + j\omega M_{fer} d_3 + 2R c_3 + 2R c_4 + R c_2 + R d_2 + R d_1 \end{aligned} \quad (4)$$

When we assume that $L_{fer} = M_{fer}$, (4) can be simplified to (5):

$$\begin{aligned} j\omega MI &= (R + j\omega L) d_3 + R c_4 \\ 0 &= j\omega L_{fer} c_3 + R(2c_4 + 2c_3 + c_2 + d_2 + d_1) \end{aligned} \quad (5)$$

The equations for the branches 1, 2 and 4 can be derived in a similar manner. Doing so gives a set of 8 equations. The equation for the path of the common-mode current c_1 in the first branch is given in (6). Since $L_{fer} = M_{fer}$ current c_1 becomes zero.

$$0 = j\omega L_{fer}c_1 - j\omega L_{fer}d_1 + j\omega M_{fer}d_1 \quad (6)$$

The remaining seven equations are written in matrix-form in (7).

$$\begin{array}{c} d_1 \\ d_2 \\ d_3 \\ d_4 \\ c_2 \\ c_3 \\ c_4 \end{array} \begin{vmatrix} 0 & 0 & 0 & R+j\omega L & 0 & 0 & 0 \\ 0 & 0 & R+j\omega L & 0 & 0 & 0 & R \\ 0 & R+j\omega L & 0 & 0 & 0 & R & R \\ R+j\omega L & 0 & 0 & 0 & R & R & R \\ R & R & R & 0 & R & 2R & 3R+j\omega L_{fer} \\ R & R & 0 & 0 & R & 2R+j\omega L_{fer} & 2R \\ R & 0 & 0 & 0 & R+j\omega L_{fer} & R & R \end{vmatrix} = \begin{array}{c} j\omega MI \\ j\omega MI \\ j\omega MI \\ j\omega MI \\ 0 \\ 0 \\ 0 \end{array} \quad (7)$$

The output voltage of the balun transformer V_{out} can be expressed in the differential-mode currents d_1, d_2, d_3, d_4 and the common-mode currents c_2, c_3, c_4 by means of (8):

$$V_{out} = R(d_4 + d_3 + d_2 + d_1) + R(3c_4 + 2c_3 + c_2) \quad (8)$$

The equations (7) and (8) were solved numerically. A result for typical values of R, M, L and L_{fer} (see caption) is given in Fig. C.3. In this case, the output voltage without the balun transformer would be $j\omega MI$, which equals 0.31 V/A at 10 MHz and 3.14 V/A at 100 MHz. Reading the output voltages from Fig. C.3 gives about 1.2 V/A at 10 MHz and 12.2 V/A at 100 MHz. Obviously the total output voltage is increased by a factor 3.9.

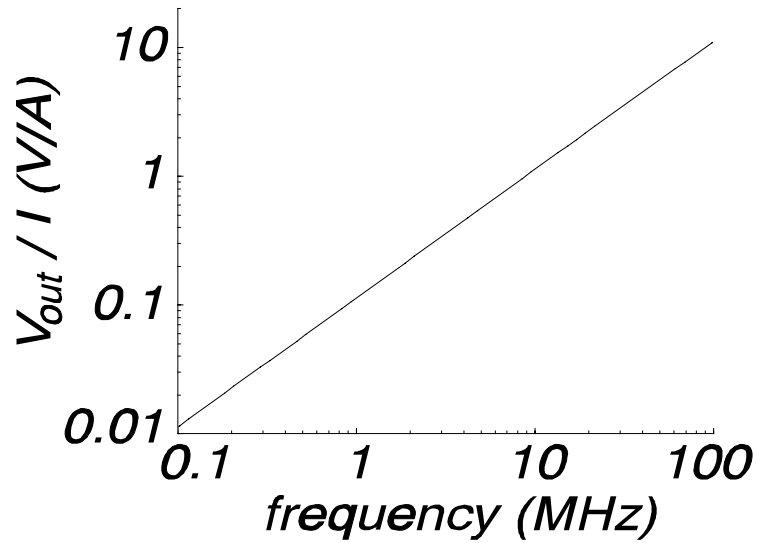


Figure C.3 Calculated transfer of a toroidal single-turn current sensor with four measuring points, connected to a balun transformer, with $R = 50 \Omega$, $M = 5 \text{ nH}$, $L = 20 \text{ nH}$ and $L_{fer} = M_{fer} = 4.6 \mu\text{H}$.

The effectiveness of the balun transformer strongly depends on the inductance L_{fer} of the ferrites. The equations (7) and (8) were solved for various values for L_{fer} , in a frequency range from 30 kHz to 100 MHz. It was found that if $L_{fer} > 4.5 \mu\text{H}$, the total output voltage is increased by a factor >3.8 in this whole frequency range. This value for L_{fer} can be obtained with a reasonable number of standard available ferrite cores.

Appendix D

SHEATH CURRENTS IN AN ISOLATED-PHASE-BUS

D.1 General

Isolated-phase-bus (IPB) systems are used in power plants to connect the generator to the step-up transformer and, when required, also to auxiliary and measuring transformers. The basic layout of an IPB is shown in Fig. D.1. Each of the 3 phase conductors is completely shielded by an aluminum sheath against dust, moisture and accidental contact. At both ends, the sheaths are short-circuited with wide short-circuit plates. This allows the flow of currents in the sheaths (i_1 , i_2 and i_3 in Fig. D.1). These sheath currents tend to be equal and opposite to the conductor currents (I_1 , I_2 and I_3) and largely cancel the magnetic field between the sheaths. Typically the remaining field is 4 % of what it would be without the sheaths. Consequently, the well known advantages of this system are that, even under short-circuit conditions: (i) the residual magnetic fields between the sheaths are small, (ii) the electromagnetic forces between the conductors are strongly reduced, and (iii) eddy-current losses in nearby steel-constructions remain small.

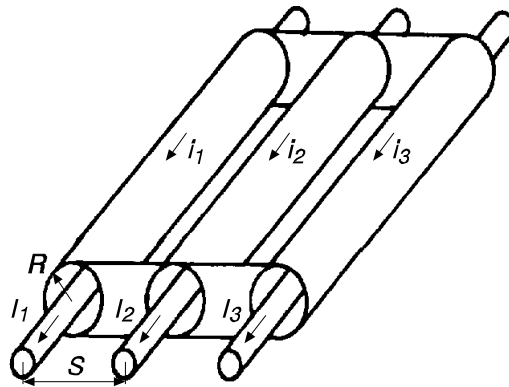


Figure D.1 Basic layout of an isolated-phase-bus system

For some IPB's the sheath currents are lowered by interconnecting the sheaths via coils, as is done in the Hemweg-6 power plant in Amsterdam (Fig. D.2a). To determine the remaining field in this case, the model described in [Sen83] is adapted and measurements were carried out in the Hemweg-6 power plant. The adapted model is given in Section D.2 and the results of the measurements are given in Section D.3. A discussion of the results is given in Section D.4.

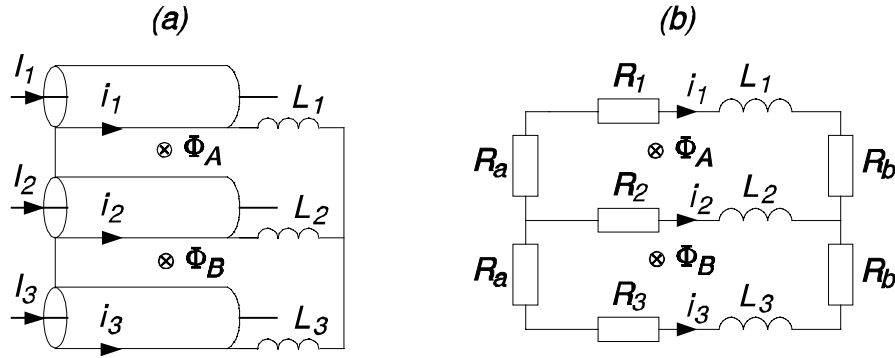


Figure D.2 (A) Layout of the isolated-phase-bus system of the Hemweg-6 power plant, and (b) its electrical equivalent circuit

D.2 Model to calculate sheath currents

To calculate the sheath currents we use the expressions for the fluxes Φ_A and Φ_B threading the two areas between the sheaths (see Fig. D.2a), as given in [Sen83]¹⁵:

$$\begin{aligned}\Phi_A &= LI_1 + MI_3 + (L+2K_e)i_1 + Mi_3 \\ \Phi_B &= -MI_1 - LI_3 - Mi_1 - (L+2K_e)i_3\end{aligned}\quad (9)$$

These two equations are valid when the sums of the three conductor currents and of the three sheath currents are zero ($I_1+I_2+I_3=0$ and $i_1+i_2+i_3=0$), which should be the case. The coefficient K_e accounts for the flux contributions of the short-circuit connections. The physical meaning of the inductances L and M is clarified in Fig. D.3a. The fluxes between the sheaths, at some distance from the ends, can be considered as generated by the residual currents $J=I+i$. Figure D.3a shows the configuration when the residual current J_3 in sheath 3 is zero and thus the residual currents in the other two sheaths are equal but opposite ($J_1=-J_2$). Now the inductance L is defined as $L=\Phi_A/J$ and the inductance M is defined as $M=-\Phi_B/J$.

Values for L and M , including the strong proximity effect, are given in [Sen83] and are shown in Fig. D.3b as a function of the spacing S and the radius R of the sheaths. For the Hemweg-6 power plant $S/R=2.92$ and the average length of the sheaths is 33.4 m, thus $L=12 \mu\text{H}$ and $M=2.3 \mu\text{H}$. To calculate the flux contribution of the short-circuit connections K_e we use equations (26) and (27) of [Sen83]. For Hemweg-6 the factor $K_e=750 \text{ nH}$.

¹⁵we assume that the coils L_1 , L_2 and L_3 do not contribute to Φ_A and Φ_B since all the local magnetic flux is enclosed in the iron cores of the coils

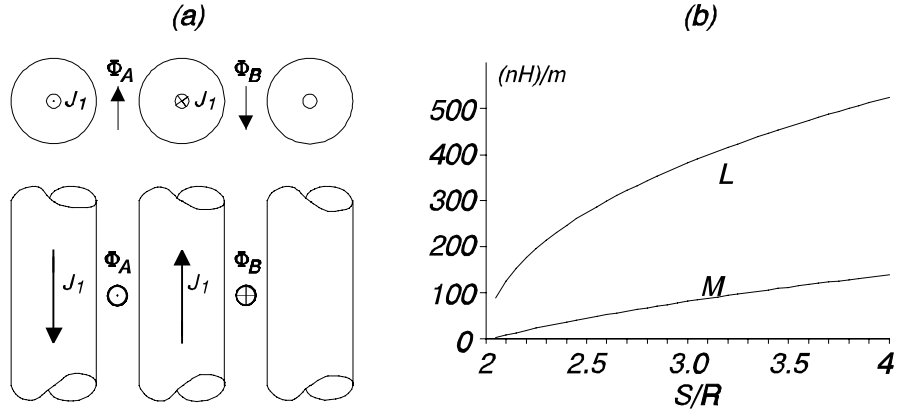


Figure D.3 (A) Current configuration to explain the physical meaning of the inductances L and M , and (b) values for L and M as a function of the spacing S and the radius R of the sheaths, taken from [Sen83]

The equivalent circuit of the Hemweg-6 IPB is given in Fig. D.2. The sheath resistances are represented as R_1 , R_2 and R_3 . The resistances of the end-connections are represented as R_a and R_b . By applying the induction law to contours around the fluxes Φ_A and Φ_B we find:

$$\begin{aligned} i_1(R_1 + R_a + R_b + j\omega L_1) - i_2(R_2 + j\omega L_2) &= -j\omega \Phi_A \\ i_2(R_2 + j\omega L_2) - i_3(R_3 + R_a + R_b + j\omega L_3) &= -j\omega \Phi_B \end{aligned} \quad (10)$$

Combining equations (9) and (10) we obtain the solutions for the sheath currents:

$$\begin{aligned} i_1 &= \frac{-CD - BE}{B^2 - AC} \\ i_2 &= \frac{CD + BE - AE - BD}{B^2 - AC} \\ i_3 &= \frac{AE + BD}{B^2 - AC} \end{aligned} \quad (11)$$

The terms A , B , C , D and E in equation (11) are:

$$\begin{aligned} A &= R_1 + R_2 + R_a + R_b + j\omega(L_1 + L_2 + L + 2K_e) \\ B &= R_2 + j\omega(L_2 + M) \\ C &= R_2 + R_3 + R_a + R_b + j\omega(L_2 + L_3 + L + 2K_e) \\ D &= -j\omega(LI_1 + MI_3) \\ E &= j\omega(MI_1 + LI_3) \end{aligned} \quad (12)$$

D.3 Measurements at the IPB of the Hemweg-6 power plant

Since for the IPB in the Hemweg-6 power plant the sheaths are interconnected via coils, a considerable remaining magnetic field is expected between the sheaths. To determine the remaining field in this case, we measured the 50 Hz conductor-, sheath- and residual currents. The currents were measured by means of a flexible Rogowski-coil, which can easily be wrapped around the conductors and sheaths of the IPB, see Fig. D.4. A Rogowski-coil measures the time derivative of the enclosed current I . The original current must be obtained by integration, according to:

$$V_{rog} = M \frac{dI}{dt} \rightarrow \text{after integration: } V_{out} = \frac{M}{\tau} I \quad (13)$$

- with:
- mutual inductance of the Rogowski-coil M (we used a Rogowski-coil with a length of 5 m, a cross-section of $3.53 \times 10^{-3} \text{ m}^2$, 173 windings per meter and a mutual inductance M of 0.7 μH)
 - time constant of the integrator τ (a Walker Scientific, type MI-3D, with time constant $\tau = 3.7 \text{ ms}$)
 - output voltage of the Rogowski-coil V_{rog}
 - output voltage of the integrator V_{out} .

The output of the integrator is recorded by a digital oscilloscope. To determine the relative phase angles of the currents, a 50 Hz reference voltage is recorded simultaneously. To prevent interference, both the integrator and the oscilloscope are placed in an EMC-cabinet.

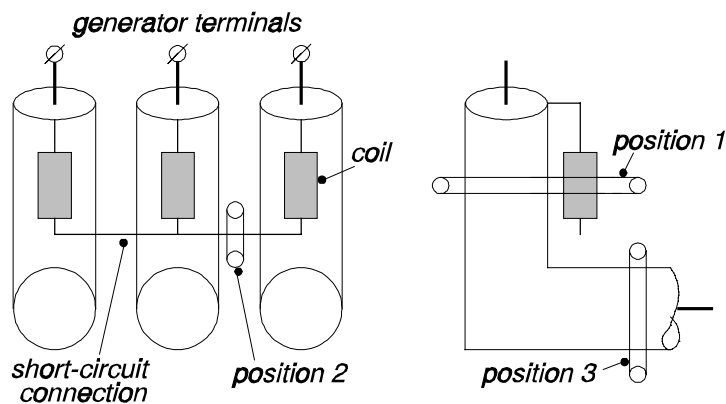


Figure D.4 Various measuring positions

Figure D.4 shows how the various currents are measured. A conductor current is measured at position 1 (the Rogowski-coil now encloses $I_{conductor} + i_{sheath} - i_{sheath}$). A sheath current can be measured at position 2. The sheath currents can be measured for two phases. At position 3, a residual current is measured (the Rogowski-coil encloses $I_{conductor} + i_{sheath}$).

The results are shown in Table XVII. In this Table also the sum of the three conductor currents is given. This 'zero-sequence' current must be the result of measuring errors or changes in the generator output during the measuring period (the measurements took about half an hour, while the generator output varied with about 5 %). To correct for this erroneous zero-sequence current, and to obtain balanced three-phase currents as input for the model, one third of the observed zero-sequence current is subtracted from each of the three currents. The same is done for the residual currents. Now the three sheath currents are calculated from the conductor- and the residual currents. The results of these calculations is given in Table XVIII.

Table XVII *Measured 50 Hz currents in the Hemweg-6 IPB*

phase	conductor currents I	sheath currents i	residual currents J
U	5920 A 0°	2432 A 180°	3594 A 355°
V	6089 A 239°	2776 A 48°	3806 A 239°
W	6089 A 115°		3933 A 117°
sum	366 A 55°		180 A 203°

Table XVIII *50 Hz currents in the Hemweg-6 IPB, after correction*

phase	conductor currents I	sheath currents i	residual currents J
U	5851 A 359°	2222 A 185°	3647 A 355°
V	6211 A 239°	2454 A 58°	3757 A 240°
W	6029 A 116°	2100 A 296°	3930 A 116°

It turns out that the sheath currents are nearly opposite to the conductor currents. However, their amplitude is only about 40 % of the amplitude of the conductor currents. Thus the remaining magnetic field between the sheaths is about 60 % of what it would be without the sheaths, instead of the 4 % for an IPB system without coils.

D.4 Calculations and discussion

Table IXX gives an overview of the input-values into the model of Section D.2, used to calculate the sheath currents for the IPB Hemweg-6. We use as inputs the conductor currents after correction for the zero-sequence current. The calculated sheath currents are given in Table XX. The calculated sheath currents show good agreement with the measured currents; the deviation is less than 10 %.

Table IXX *Input values for the calculation of the sheath currents for the IPB Hemweg-6*

$R_1 = 238 \mu\Omega$	$L_1 = 16 \mu\text{H}$	$R_a = 19.7 \mu\Omega$	$I_u = 5851 \text{ A} / 359^\circ$
$R_2 = 179 \mu\Omega$	$L_2 = 10 \mu\text{H}$	$R_b = 16.9 \mu\Omega$	$I_v = 6211 \text{ A} / 239^\circ$
$R_3 = 208 \mu\Omega$	$L_3 = 9 \mu\text{H}$	$K_e = 750 \text{ nH}$	$I_w = 6029 \text{ A} / 116^\circ$
$L = 12 \mu\text{H}$	$M = 2.3 \mu\text{H}$		

Table XX *Sheath currents for the IPB Hemweg-6 and for two hypothetical cases without extra inductances*

phase	measured	calculated	calculated without inductances ($L_1=L_2=L_3=0$)	
			$K_e = 750 \text{ nH}$	$K_e = 80 \text{ nH}$
U	2222 A 185°	2093 A 189°	5252 A 183°	5808 A 185°
V	2454 A 58°	2529 A 56°	5287 A 64°	5936 A 64°
W	2100 A 296°	1896 A 290°	5365 A 304°	5845 A 304°

The sheaths of the Hemweg-6 IPB are interconnected via coils. For the hypothetical case that these coils are not present, the sheath currents turn out to be almost equal and opposite to the conductor currents, as can be seen in Table XX (column for $K_e=750 \text{ nH}$). As a consequence, the magnetic field between the sheaths is reduced to about 14 %.

Nevertheless, still a considerable amount of magnetic field is present. This is caused by the relatively large flux-contribution of the short-circuit connections. For the Hemweg-6 IPB these short-circuit connections are relatively thin copper strips. As a

consequence the short-circuit connections tend to couple more flux into the region between the sheaths, which corresponds to a relatively large value for $K_e=750$ nH.

In [Sen83] it is shown that for IPB-systems as in the Amer-8 power plant the remaining field is in the order of 4 %. This is to be expected, since at the Amer-8 IPB the sheaths are short-circuited with wide short-circuiting plates (see Fig. D.1). The flux contribution K_e of these short-circuit connections is quite low, about 80 nH. The effect of the flux-contribution of the short-circuit connections is shown in Table XX, which gives the calculated sheath currents for $K_e=750$ nH and for $K_e=80$ nH. As expected, a lower value for K_e results in larger sheath currents and thus in a lower remaining field.

At the higher frequencies of partial discharge signals, one may question how effective the iron cores of the coils are. However the relatively thin copper bars, connecting the sheaths via the coils, introduce already inductance, which can be expressed as a large value for K_e . Therefore, even if the iron cores are not effective, we may expect high frequency flux between the sheaths. For IPB systems without coils and with a low value for K_e , as in the Amer-8 power plant, no significant high frequency flux can exist in the region between the sheaths. In these IPB's measurements with pick-up loops outside the short-circuiting plates remain meaningful (see for instance Chapter 9).

Dankwoord

Vele mensen hebben bijgedragen aan de totstandkoming van dit proefschrift. Graag wil ik bedanken:

Mijn promotor Piet van der Laan voor de begeleiding gedurende de loop van dit onderzoek. Hij heeft mij gebracht tot dit proefschrift. Ik denk met heel veel plezier terug aan onze vele motiverende discussies. Ondanks de reorganisatie-onrust was de capaciteitsgroep Elektrische Energietechniek voor mij een eiland van rust, waar ik onbelemmerd aan mijn proefschrift kon werken.

Alle (oud)collega's van de capaciteitsgroep Elektrische Energietechniek.

Medewerkers van KEMA T&D Power en KEMA Power Generation. Dankzij Peter Vaessen heb ik een andere kijk gekregen op het uitoefenen van mijn vak. Wout de Leeuw heeft voortreffelijk werk gedaan gedurende de vele metingen in centrales.

Mijn 21 afstudeerders en stagiaires die allemaal leuke banen hebben gevonden.

Dit onderzoek werd gesteund door de Nederlandse electriciteitsproductiebedrijven EPON, EPZ, EZH en UNA. Met plezier denk ik terug aan de vele metingen die ik in hun centrales heb verricht. Graag dank ik alle medewerkers van deze centrales voor hun medewerking en gastvrijheid. Een belangrijke bijdrage is geleverd door de werkgroep Generatorrailsystemen.

De firma's MPE te Liverpool en Alpatron te Rotterdam voor hun bijdrage aan de ontwikkeling van de bus-support-capacitors.

De Stichting Professor Gelissen-fonds voor gegeven steun.

En mijn vrienden, mijn ouders en Marie-José voor hun steun.

Curriculum vitae

Geboren op 3 april 1961 te Breda.

1973 - 1981 MAVO te Zundert en daarna MTS Elektrotechniek te Breda.

1981 - 1986 HTS Elektrotechniek te Breda, afstudeerrichting Elektrische Energietechniek.

1987 Ericsson, Gilze-Rijen. Opzetten van kwaliteitscontroles voor componenten van telefoontoestellen.

1987 - 1994 Vakgroep Hoogspanningstechniek & EMC, Technische Universiteit Eindhoven. Onderzoeksmedewerker voor onderzoek naar partiële ontladingen, hoogspanningsmeetsystemen, toepassingen van gepulste corona en vacuüm-isolatie.

1994 - 1998 KEMA T&D Power te Arnhem. Contractonderzoek naar methoden voor conditiebewaking en levensduur-management van hoogspanningscomponenten, waaronder turbogeneratoren. Analyse en onderzoek van schades aan generatoren. Advisering met betrekking tot bedrijfsvoering en onderhoud van generatoren. Oprichter van een kenniscentrum voor generatoren.

1998 - heden Capaciteitsgroep Elektrische Energietechniek, Technische Universiteit Eindhoven. Onderzoek naar biogasreiniging met behulp van gepulste elektrische ontladingen (corona's).

Lid van IEEE Power Engineering Society, IEEE Dielectrics and Electrical Insulation Society, IEEE Nuclear and Plasma Science Society.